PHYSICAL REVIEW B **92**, 014506 (2015)

Superconductor-insulator transitions: Phase diagram and magnetoresistance

I. S. Burmistrov,[1,2] I. V. Gornyi,[3,4,5,1] and A. D. Mirlin[3,4,6,1]

[1]*L.D. Landau Institute for Theoretical Physics, Kosygina street 2, 119334 Moscow, Russia*

[2]*Moscow Institute of Physics and Technology, 141700 Moscow, Russia*

[3]*Institut für Nanotechnologie, Karlsruhe Institute of Technology, 76021 Karlsruhe, Germany*

[4]*Institut für Theorie der kondensierten Materie, Karlsruhe Institute of Technology, 76128 Karlsruhe, Germany*

[5]*A.F. Ioffe Physico-Technical Institute, 194021 St. Petersburg, Russia*

[6]*Petersburg Nuclear Physics Institute, 188300 St. Petersburg, Russia*

(Received 22 March 2015; published 13 July 2015)

The influence of the disorder-induced Anderson localization and electron-electron interaction on the superconductivity in two-dimensional systems is explored. We determine the superconducting transition temperature T_c, the temperature dependence of the resistivity, the phase diagram, and the magnetoresistance. The analysis is based on the renormalization group (RG) for a nonlinear sigma model. The derived RG equations are valid to the lowest order in disorder but for an arbitrary electron-electron interaction strength in a particle-hole and the Cooper channels. Systems with preserved and broken spin-rotational symmetry are considered, with both short-range and long-range (Coulomb) interactions. In the case of short-range interaction, we identify parameter regions where the superconductivity is enhanced by localization effects. Our RG analysis indicates that the superconductor-insulator transition is controlled by a fixed point with a resistivity R_c of the order of the quantum resistance $R_q = h/4e^2$. When a transverse magnetic field is applied, we find a strong nonmonotonous magnetoresistance for temperatures below T_c.

DOI: 10.1103/PhysRevB.92.014506 PACS number(s): 72.15.Rn, 71.30.+h, 74.78.−w, 74.62.−c

I. INTRODUCTION

Superconductivity [1,2] and Anderson localization [3] are among the most important and fundamental quantum phenomena in condensed matter physics. These two phenomena are in a sense antagonists: in the case of superconductivity, the Cooper interaction creates a collective state with vanishing resistivity, while the Anderson localization resulting from disorder-induced quantum interference drives the system into a state with zero conductivity. Therefore, when both interaction and disorder are present, a competition between the superconductivity and localization naturally arises. This competition is of particular interest in two-dimensional (2D) geometry, where even a weak disorder makes the system an Anderson insulator. Thus a 2D system may be expected to undergo a direct quantum phase transition (QPT) between the insulating and superconducting states, the superconductor-insulator transition (SIT).

Experimentally, SIT has been studied in a variety of 2D structures, including amorphous Bi and Pb [4,5], MoC [6], MoGe [7], Ta [8], InO [9–11], NbN [12], and TiN films [13,14], see also the reviews [15]. In recent years, there has been also a growing experimental activity on SIT in novel 2D materials and nanostructures, such as $LaAlO_3/SrTiO_3$ interfaces [16,17], $SrTiO_3$ surfaces [18,19], MoS_2 flakes [20,21], FeSe thin films [22], LaSrCuO surfaces [23], and Li_xZrNCl layered materials [24]. Characteristic for many of the novel structures is a strong screening of the Coulomb interaction due to a large dielectric constant of the substrate (such as $SrTiO_3$). In addition, strong spin-orbit coupling is present in many of the novel materials (MoS_2, $LaAlO_3/SrTiO_3$, $SrTiO_3$).

To drive the system through SIT, one changes a parameter (film thickness, gate voltage, doping) controlling the high-temperature sheet resistivity. With lowering temperature, systems with lower resistivity become superconducting (resistivity drops to zero), while those with higher resistivity get insulating (resistivity becomes exponentially large). The most salient observations common to the majority of the above experiments are as follows.

(i) Most of the experiments are interpreted as supporting a direct transition between the superconducting and insulating phases, although some of them suggest a possibility of existence of an intermediate metallic phase. The critical resistivity R_c (the low-temperature limit of the separatrix curve separating the temperature dependence of resistivity in the insulating and superconducting phases) is of the order of the quantum resistance $R_q = h/4e^2 \simeq 6.5\,\mathrm{k}\Omega$. However, the precise value of R_c varies from one experiment to another, roughly in the range between $R_q/2$ and $3R_q$.

(ii) For those systems that are superconducting (at low temperature T and magnetic field H), a nonmonotonous dependence of resistivity on T and H is observed. In particular, a giant nonmonotonous magnetoresistance is found in such systems at very low temperatures, $T \ll T_c$.

(iii) The temperature dependence of resistivity on the insulating side is very fast (activation or even stronger).

The theoretical investigation of the interplay of interaction and disorder in systems with Cooper attraction has a long history. Soon after the development of the microscopic theory of superconductivity by Bardeen, Cooper, and Schrieffer (BCS) [2], the question of influence of disorder on superconductivity attracted a great deal of attention. It was found [25,26] that the diffusive motion of electrons does not affect essentially the temperature T_c of superconducting transition, i.e., the mean free path does not enter the expression for T_c. This statement is conventionally called "the Anderson theorem."

The effects of disorder-induced Anderson localization [3] on superconductivity were considered in Refs. [27,28]. It was found that, within the BCS approach, the superconductivity in a disordered system persists up to the localization threshold

and even in the localized regime near the Anderson transition. Furthermore, Refs. [27,28] came to the conclusion that the mean-field transition temperature T_c in these regimes remains unaffected by disorder (i.e., the Anderson theorem holds). In a parallel line of research, it was discovered [29–31] that an interplay of the long-range $(1/r)$ Coulomb interaction and disorder leads to suppression of T_c. These ideas were put on a solid basis by Finkelstein [32] who developed the nonlinear sigma model (NLSM) renormalization-group (RG) formalism.

An alternative approach to the SIT known as the "bosonic mechanism" was proposed in Refs. [33]. It takes into account the superconducting phase fluctuations and discards completely all other degrees of freedom, in particular, the localization effects. It was also proposed that an intermediate "Bose metal" phase may separate the superconductor and insulator [34]. A relation between the bosonic and fermionic mechanisms as well as a status of the Bose metal conjecture remain quite obscure.

Recently, Feigelman *et al.* [35,36] found that the eigenfunction multifractality near the localization threshold in three dimensions strongly affects the properties of a superconductor. Their remarkable finding is that T_c is dramatically enhanced: its dependence on the coupling constant is no longer exponential (as in the conventional BCS solution) but rather of a power-law type. This result was obtained on the basis of the BCS-type self-consistency equation, with Cooper attraction being the only interaction included.

In a preceding work by the present authors [37] the influence of disorder-induced Anderson localization on the temperature of the superconducting transition T_c was studied within the field-theoretical framework. The electron-electron interaction in particle-hole and Cooper channels was taken into account. The focus was put on the case of a weak short-range interaction (which is relevant to materials with a large dielectric constant, as well to cold atom systems). Two-dimensional systems in the weak localization and antilocalization regime, as well as systems near the mobility edge were investigated. A systematic analytical approach to the problem was developed in the framework of the interacting NLSM and its RG treatment. The approach took into account the mutual renormalization of disorder and all interaction constants (that, in particular, leads to mixing of different interaction channels). This methodology allows us to explore both the cases of a long-range (Coulomb) interaction previously studied by Finkelstein [32] and of a weak short-range interaction within a unified formalism. More specifically, in the case of short-range interactions a system of coupled RG equations for the problem was derived in the lowest order in disorder and three interaction couplings (singlet, triplet, and Cooper channels).

The analysis of RG equations for the weak short-range interaction showed a behavior which is *exactly opposite* to that predicted by Ref. [32] for the Coulomb interaction. It was found that the interplay of such interactions and the Anderson localization leads to *strong enhancement* of superconductivity in a broad range of parameters in dirty 2D systems, as well as in three-dimensional (3D) systems near the Anderson transition (in contrast to the *suppression* in the Coulomb case). In the latter case (vicinity of the Anderson transition), the microscopic theory of Ref. [37] justified previous theoretical results obtained from the self-consistency equation [35,36].

This result of Ref. [37] is of fundamental importance and represents unexpected physics (enhancement of superconductivity by localization, which is naively its exact "antagonist"). Indeed, remarkably, the localization physics, responsible for the increase of resistivity and thus driving the system towards an insulating state, favors at the same time the superconductivity. The key condition is a suppression of the long-range component of the Coulomb interaction (see also Ref. [38]). This opens a new way for searching novel materials exhibiting high-temperature superconductivity: one needs the combination of a large dielectric background constant and disorder in layered structures.

In this paper, we extend the formalism of Ref. [37] by deriving the RG equations to the lowest order in disorder but, formally, for arbitrary interaction couplings. We use this framework to explore systematically the interplay of superconductivity, interaction, and localization in 2D systems, with a focus on the SIT in thin films. More specifically, (i) we evaluate the temperature dependence of the resistivity $\rho(T)$ for given bare (high-temperature) couplings down to the temperature T_c at which the finite expectation value of the superconducting order parameter emerges, or else, down to the temperature where the system enters the insulating regime.

(ii) We use the RG equations to determine the structure of the phase diagram. In particular, we identify parameter regions where the superconductivity is enhanced by localization. Our results also indicate that in some cases the phase diagram may include a critical-metal phase.

(iii) We study the magnetoresistance near the SIT within a two-step RG approach. Since the magnetic field suppresses both superconductivity and localization, a nonmonotonous magnetoresistance arises, as observed experimentally. Furthermore, this magnetoresistance becomes very strong at low temperatures, again in agreement with experiments. Both orbital and Zeeman effects of the magnetic field are incorporated in the unifying RG scheme. All the above analysis is performed for the cases of the short-ranged and long-ranged Coulomb interactions, both with and without spin-orbit interaction.

The structure of the article is as follows. In Sec. II, we introduce the NLSM formalism. The corresponding RG equations (valid to the lowest order in disorder and for arbitrary interaction strength) are presented in Sec. III. The RG equations are used in Sec. IV to analyze the phase diagram in zero magnetic field. The temperature dependence of resistivity in zero magnetic field is discussed in Sec. V. In Sec. VI, this analysis is extended to calculate the magnetoresistance in a transverse and in a parallel magnetic field. Section VII contains a discussion of the obtained results, their implications, limitations, possible extensions, and a comparison with numerical and experimental results. Finally, our results and conclusions are summarized in Sec. VIII. Several appendices contain technical details of the derivation of RG equations and of their analysis.

II. FORMALISM

A. NLSM action

The action of the NLSM is given as a sum of the noninteracting part S_σ, and contributions arising from the

interactions in the particle-hole singlet $S^{(\rho)}_{\rm int}$, particle-hole triplet $S^{(\sigma)}_{\rm int}$, and particle-particle (Cooper) $S^{(c)}_{\rm int}$ channels (see Refs. [32,39] for review):

$$S = S_\sigma + S^{(\rho)}_{\rm int} + S^{(\sigma)}_{\rm int} + S^{(c)}_{\rm int}, \tag{1}$$

where

$$S_\sigma = -\frac{g}{32}\int d\boldsymbol{r}\,{\rm Tr}(\nabla Q)^2 + 4\pi T Z_\omega \int d\boldsymbol{r}\,{\rm Tr}\,\eta Q,$$

$$S^{(\rho)}_{\rm int} = -\frac{\pi T}{4}\Gamma_s \sum_{\alpha,n}\sum_{r=0,3}\int d\boldsymbol{r}\,{\rm Tr}\left[I^\alpha_n t_{r0} Q\right]{\rm Tr}\left[I^\alpha_{-n} t_{r0} Q\right],$$

$$S^{(\sigma)}_{\rm int} = -\frac{\pi T}{4}\Gamma_t \sum_{\alpha,n}\sum_{r=0,3}\sum_{j=1}^{3}\int d\boldsymbol{r}\,{\rm Tr}\left[I^\alpha_n \boldsymbol{t}_{\boldsymbol{r}} Q\right]{\rm Tr}\left[I^\alpha_{-n} \boldsymbol{t}_{\boldsymbol{r}} Q\right],$$

$$S^{(c)}_{\rm int} = -\frac{\pi T}{2}\Gamma_c \sum_{\alpha,n}\sum_{r=0,3}(-1)^r\int d\boldsymbol{r}\,{\rm Tr}\left[I^\alpha_n t_{r0} Q I^\alpha_n t_{r0} Q\right].$$

Here, g is the total Drude conductivity (in units e^2/h and including spin), $\boldsymbol{t}_{\boldsymbol{r}} = \{t_{r1}, t_{r2}, t_{r3}\}$, and we use the following matrices:

$$\Lambda^{\alpha\beta}_{nm} = {\rm sgn}\, n\, \delta_{nm}\delta^{\alpha\beta} t_{00},$$
$$\eta^{\alpha\beta}_{nm} = n\,\delta_{nm}\delta^{\alpha\beta} t_{00}, \tag{2}$$
$$\left(I^\gamma_k\right)^{\alpha\beta}_{nm} = \delta_{n-m,k}\delta^{\alpha\beta}\delta^{\alpha\gamma} t_{00},$$

with $\alpha,\beta = 1,\ldots,N_r$ standing for replica indices and n,m corresponding to the Matsubara fermionic energies $\varepsilon_n = \pi T(2n+1)$. The sixteen matrices,

$$t_{rj} = \tau_r \otimes s_j, \quad r,j = 0,1,2,3, \tag{3}$$

operate in the particle-hole (subscript r) and spin (subsrcipt j) spaces with the corresponding Pauli matrices denoted by

$$\tau_1 = \begin{pmatrix} 0 & 1 \\ 1 & 0 \end{pmatrix}, \quad \tau_2 = \begin{pmatrix} 0 & -i \\ i & 0 \end{pmatrix}, \quad \tau_3 = \begin{pmatrix} 1 & 0 \\ 0 & -1 \end{pmatrix}, \tag{4}$$

$$s_1 = \begin{pmatrix} 0 & 1 \\ 1 & 0 \end{pmatrix}, \quad s_2 = \begin{pmatrix} 0 & -i \\ i & 0 \end{pmatrix}, \quad s_3 = \begin{pmatrix} 1 & 0 \\ 0 & -1 \end{pmatrix}. \tag{5}$$

Matrices τ_0 and s_0 stand for the 2×2 unit matrices. The matrix field $Q(\boldsymbol{r})$ (as well as the trace Tr) acts in the replica, Matsubara, spin, and particle-hole spaces. It obeys the following constraints:

$$Q^2 = 1, \quad {\rm Tr}\, Q = 0, \quad Q^\dagger = C^T Q^T C. \tag{6}$$

The charge conjugation matrix $C = it_{12}$ satisfies the following relation $C^T = -C$. Matrix Q can be parameterized as $Q = T^{-1}\Lambda T$ where the matrices T obey (symbol $*$ denotes the complex conjugation)

$$CT^* = TC, \quad (T^{-1})^* C = CT^{-1}. \tag{7}$$

In order to avoid notational confusion, it is instructive to compare our notation with that of the reviews [32] and [39]. In both references, a different definition of Pauli matrices in the particle-hole space has been used, namely, $i\tau_j$ instead of τ_j for $j = 1,2,3$. In Ref. [32], the Pauli matrices in the spin space coincide with our definition (5). In Ref. [39], the spin-space Pauli matrices $-is_j$ (for $j = 1,2,3$) were used instead of our definition (5). The interaction terms $S^{(\rho)}_{\rm int}$, $S^{(\sigma)}_{\rm int}$, and $S^{(c)}_{\rm int}$ coincide with terms in Eqs. (3.9a), (3.9b), and (3.9b) of Ref. [32] provided the following relations between the couplings Γ_s, Γ_t, and Γ_c in $S^{(\rho)}_{\rm int}$, $S^{(\sigma)}_{\rm int}$, and $S^{(c)}_{\rm int}$ and Z, Γ_2, and Γ_c in Ref. [32] hold: $\Gamma_s \equiv -(\pi\nu/4)Z$, $\Gamma_t \equiv (\pi\nu/4)\Gamma_2$, and $\Gamma_c \equiv (\pi\nu/4)\Gamma_c$. Here, the thermodynamic density of states ν includes the spin-degeneracy factor. Note that Ref. [32] focuses on the case of unscreened (long-ranged) Coulomb interaction. Hence the interaction amplitude Γ_s in the singlet particle-hole channel is expressed through the frequency renormalization factor Z there. We consider both long-ranged (Coulomb) and short-ranged interactions. In the latter case, the quantities Γ_s and Z_ω are independent variables. The interaction terms $S^{(\rho)}_{\rm int}$, $S^{(\sigma)}_{\rm int}$, and $S^{(c)}_{\rm int}$ coincide with the terms in Eqs. (3.92d), (3.92e), and (3.92f) of Ref. [39] provided $\Gamma_s \equiv K^{(1)}$, $\Gamma_t \equiv K^{(2)}$, and $\Gamma_c \equiv K^{(3)}/2$. The parameters g and Z_ω in S_σ are related to the corresponding quantities D, Z, ν of Ref. [32] as $g = 4\pi\nu D$ and $Z_\omega = (\pi\nu/4)Z$ and to the parameters G and H in Ref. [39] as $g = 16/G$ and $Z_\omega = H/2$.

B. Interaction in the Cooper channel

The Cooper-channel interaction term can be rewritten as

$$S^{(c)}_{\rm int} = -\frac{\pi T}{4}\Gamma_c \sum_{\alpha,n}\sum_{r=1,2}\sum_{j=0}^{3}\int d\boldsymbol{r}\,{\rm Tr}\left[t_{rj} L^\alpha_n Q\right]{\rm Tr}\left[t_{rj} L^\alpha_n Q\right]. \tag{8}$$

Here the matrix L^α_n is defined as

$$\left(L^\alpha_n\right)^{\beta\gamma}_{km} = \delta_{k+m,n}\delta^{\alpha\beta}\delta^{\alpha\gamma} t_{00}. \tag{9}$$

However, for $j = 1,2,3$, we find

$${\rm Tr}\left[t_{rj} L^\alpha_n Q\right] = -{\rm Tr}\left[C t^T_{rj} C L^\alpha_n Q\right] = -{\rm Tr}\left[t_{rj} L^\alpha_n Q\right] = 0. \tag{10}$$

Therefore the term $S^{(c)}_{\rm int}$ describing the interaction in the Cooper channel is fully determined by the Cooper-singlet channel:

$$S^{(c)}_{\rm int} = -\frac{\pi T}{4}\Gamma_c \sum_{\alpha,n}\sum_{r=1,2}\int d\boldsymbol{r}\,{\rm Tr}\left[t_{r0} L^\alpha_n Q\right]{\rm Tr}\left[t_{r0} L^\alpha_n Q\right]. \tag{11}$$

C. Relation with the BCS Hamiltonian

In general, bare values of the interaction parameters Γ_s, Γ_t, and Γ_c can be estimated for a given electron-electron interaction $U(\boldsymbol{r}-\boldsymbol{r}')$ in a microscopic Hamiltonian. It is convenient to introduce the dimensionless parameters $\gamma_{s,t,c} = \Gamma_{s,t,c}/Z_\omega$. Then their bare values can be written as

$$\gamma_{s0} = -\frac{F_s}{1+F_s}, \quad \gamma_{t0} = -\frac{F_t}{1+F_t}, \quad \gamma_{c0} = -F_c, \tag{12}$$

where $F_s = \nu U(q) + F_t$,

$$F_t = -\frac{\nu}{2}\langle U_{\rm scr}(2k_F\sin(\theta/2))\rangle_{\rm FS},$$
$$F_c = \frac{F_t}{2} - \frac{\nu}{4}\langle U_{\rm scr}(2k_F\cos(\theta/2))\rangle_{\rm FS}. \tag{13}$$

Here, $U_{\rm scr}(q)$ stands for the statically screened interaction and $\langle\ldots\rangle_{\rm FS}$ denotes averaging over the Fermi surface. In the

BCS case (for example, for a weak short-range attraction mediated by phonons), the interaction can be written as $U(\boldsymbol{r}) = -(\lambda/\nu)\delta(\boldsymbol{r})$ where $0 < \lambda \ll 1$. Neglecting screening in this case, we find

$$F_s \approx -\lambda/2, \quad F_t \approx \lambda/2, \quad F_c \approx \lambda/2. \tag{14}$$

Thus, for the BCS case (i.e., when neither screened nor unscreened Coulomb repulsion is taken into account), we get the following interaction parameters at the ultraviolet scale (which is given by Debye frequency ω_D in the case of phonon-induced superconductivity):

$$-\gamma_{s0} \approx \gamma_{t0} \approx \gamma_{c0} \approx -\lambda/2. \tag{15}$$

If disorder is strong, $\omega_D\tau \ll 1$, the relations (15) determine the initial values of the interaction parameters for the action (1). In what follows, we will refer to the line determined by the relations $-\gamma_s = \gamma_t = \gamma_c$ as the "BCS line." When the disorder is weak, $\omega_D\tau \gg 1$, the relations (15) hold at the scale corresponding to the Debye frequency ω_D. Then the Cooper interaction constant is renormalized at ballistic scales (between ω_D and $1/\tau$) such that

$$\begin{aligned} -\gamma_{s0} &= \gamma_{t0} = -\lambda/2, \\ \gamma_{c0} &= -\frac{\lambda/2}{1-(\lambda/2)\ln\omega_D\tau} = \frac{1}{\ln T_c^{\mathrm{BCS}}\tau}. \end{aligned} \tag{16}$$

where $T_c^{\mathrm{BCS}} = \omega_D \exp(-2/\lambda)$.

D. $\mathcal{F}$ algebra and $\mathcal{F}$ invariance

The NLSM action (1) involves the matrices that are formally defined in the infinite Matsubara frequency space. To perform calculations with these matrices, it is convenient to introduce an ultraviolet cutoff N'_M for the Matsubara frequencies. In addition, it is useful to introduce another cutoff $N_M < N'_M$ indicating the size of a nontrivial part of the Q matrix (beyond which the Q matrix equals Λ). At the end of calculations, both cutoffs should be sent to infinity.

Global rotations of the Q matrix with any matrix of the type $\exp(i\hat{\chi})$, where $\hat{\chi} = \sum_{\alpha,n} \chi_n^\alpha I_n^\alpha t_{00}$, play an important role [40,41]. In the limit $N_M, N'_M \to \infty$ and $N_M/N'_M \to 0$, the set of rules known as $\mathcal{F}$ algebra [40] allows one to establish the following relations (for $r = 0,3$ and $j = 0,1,2,3$):

$$\begin{aligned} \mathrm{Tr}\, I_n^\alpha t_{rj} e^{i\hat{\chi}} Q e^{-i\hat{\chi}} &= \mathrm{Tr}\, I_n^\alpha t_{rj} e^{i\chi_0} Q e^{-i\chi_0} \\ &\quad + 8in\chi_{-n}^\alpha \delta_{r0}\delta_{j0}, \\ \mathrm{Tr}\, \eta e^{i\hat{\chi}} Q e^{-i\hat{\chi}} &= \mathrm{Tr}\, \eta Q + \sum_{\alpha,n} in\chi_n^\alpha\, \mathrm{Tr}\, I_n^\alpha t_{00} Q \\ &\quad - 4\sum_{\alpha,n} n^2 \chi_n^\alpha \chi_{-n}^\alpha, \\ \mathrm{Tr}\left[I_n^\alpha t_{r0} e^{i\hat{\chi}} Q e^{-i\hat{\chi}}\right]^2 &= \mathrm{Tr}\left[I_n^\alpha t_{r0} Q\right]^2. \end{aligned} \tag{17}$$

Using Eqs. (17), one can check that, provided $\Gamma_s = -Z_\omega$, the action (1) is invariant under global rotations of the matrix Q with the matrix $\exp(i\hat{\chi})$ (so-called $\mathcal{F}$ invariance). The constraint $\Gamma_s = -Z_\omega$ corresponds to the case of the Coulomb interaction [32]. Since the relation $\Gamma_s = -Z_\omega$ is dictated by the symmetry of the action (1), it should remain fulfilled under the RG flow.

III. ONE-LOOP RENORMALIZATION-GROUP EQUATIONS

A. Preserved spin-rotational symmetry

To derive RG equations in the one-loop approximation (i.e., to the lowest order in disorder strength), we employ the background-field method and apply it to the renormalization of the NLSM action (1). Details of the derivation can be found in Appendix A. In $d = 2$ dimensions, the one-loop RG equations read [$t = 2/(\pi g)$]

$$\frac{dt}{dy} = t^2[1 + f(\gamma_s) + 3f(\gamma_t) - \gamma_c], \tag{18}$$

$$\frac{d\gamma_s}{dy} = -\frac{t}{2}(1+\gamma_s)\left(\gamma_s + 3\gamma_t + 2\gamma_c + 4\gamma_c^2\right), \tag{19}$$

$$\frac{d\gamma_t}{dy} = -\tfrac{t}{2}(1+\gamma_t)[\gamma_s - \gamma_t - 2\gamma_c(1+2\gamma_t - 2\gamma_c)], \tag{20}$$

$$\begin{aligned} \frac{d\gamma_c}{dy} &= -2\gamma_c^2 - \frac{t}{2}\big[(1+\gamma_c)(\gamma_s - 3\gamma_t) - 2\gamma_c^2 + 4\gamma_c^3 \\ &\quad + 6\gamma_c(\gamma_t - \ln(1+\gamma_t))\big], \end{aligned} \tag{21}$$

$$\frac{d\ln Z_\omega}{dy} = \frac{t}{2}\left(\gamma_s + 3\gamma_t + 2\gamma_c + 4\gamma_c^2\right), \tag{22}$$

where $y = \ln(L/l)$ (l denotes the mean free path) and $f(x) = 1 - (1+1/x)\ln(1+x)$. These RG equations describe the evolution of the system with spin-rotational and time-reversal symmetries upon changing the characteristic length scale L. We stress that the RG equations (18)–(22) satisfy the particle number conservation since $d(Z_\omega + \Gamma_s)/dy = 0$. Further, it is worth emphasizing that the right-hand sides of the equations are nonsingular in the limit of the Coulomb interaction, $\gamma_s = -1$.

The ultraviolet value of the NLSM coupling t that describes the disorder strength is given by the dimensionless Drude resistivity. The renormalization of t at larger scales involves the contributions to the resistivity induced by interference effects and by virtual (elastic) processes due to interactions in the particle-hole singlet (γ_s) and triplet (γ_t), as well as in the Cooper channel (γ_c).

We emphasize that Eqs. (18)–(22) are obtained in the lowest order in t but they are formally exact in interactions $\gamma_{s,t,c}$. It is worth noting that the Cooper-interaction coupling γ_c enters all the RG equations only in a polynomial way. Interestingly, the contribution of the Cooper channel to the renormalization of t is fully described by the linear term only, thus rendering Eq. (18) for arbitrary γ_c the same as in the weak-coupling limit [42], $|\gamma_c| \ll 1$.

The first term in Eq. (21) describes the standard BCS instability; in accordance with the Anderson theorem this term is not affected by disorder. Moreover, the Anderson theorem manifests itself in Eq. (21) through the absence of the terms $t\mathcal{O}(\gamma_c)$ on the right-hand side. To the lowest order in interaction couplings, the effect of disorder on the renormalization of γ_c is solely due to the presence of the interaction in the particle-hole channels.

Somewhat counterintuitively, Eq. (18) suggests an insulating behavior (an increase of the resistivity with increasing L) for $\gamma_c \to -\infty$. We note, however, that the (dimensionless)

physical resistivity ρ is not exactly equal to the NLSM coupling t because of the inelastic contribution to the conductivity governed by superconducting fluctuations, see Sec. V below for details. Near the superconducting instability (for large $|\gamma_c| \gg 1$), this antilocalizing inelastic contribution to the conductivity becomes large.

Furthermore, towards the superconducting instability, $\gamma_c \to -\infty$, the disorder-induced renormalization of γ_c in Eq. (21) is dominated by the term $-2t\gamma_c^3$, which tends to impede a development of the superconducting instability. Thus, if Eqs. (18)–(22) would constitute the ultimate truth, the superconducting instability would not, strictly speaking, develop. An explanation for this apparent paradox is as follows. It turns out that the one-loop RG equations become insufficient in the vicinity of the superconducting instability, namely, on scales larger than L_X where $|\gamma_c|$ reaches a value $\sim 1/t \gg 1$. In other words, the weak-disorder condition of validity of the one-loop RG, $t \ll 1$, should in fact be supplemented by the condition $t|\gamma_c| \ll 1$.

The emergence of the latter condition (and thus of the scale L_X) becomes evident from a comparison of the terms of the zeroth and the first order in t in Eq. (21). This scale L_X arises also in the calculation of the conductivity (see Sec. V): at this scale, the inelastic contribution to the conductivity reaches in magnitude the elastic one. We expect that in the vicinity of the superconducting instability higher-loop terms of the type $t(t\gamma_c)^k$ in the beta-function for t and $\gamma_c^2(t\gamma_c)^k$ in the equation governing the renormalization of γ_c should emerge. Upon resummation, they are expected to restore the divergence of γ_c at a scale L_c slightly larger than L_X. At the same time, since the second-loop ($k = 2$) terms are similar to those describing the mesoscopic fluctuations of the superconducting order parameter [44,45], we expect for $|\gamma_c|t > 1$ (i.e., for temperatures slightly above the transition) strong spatial fluctuations of the observables (in particular, of the local tunneling density of states [45,46], as observed in experiments, see, e.g., Ref. [11]).

To the lowest order in γ_c, Eqs. (18)–(22) coincide with the results obtained by Finkelstein long ago [42]. Recently, one-loop RG equations beyond the lowest order in interactions were reported in Ref. [43] for the case of preserved spin-rotational and time-reversal symmetries. It should be stressed, however, that our RG equations (18)–(22) differ from those of Ref. [43]. It is instructive to highlight the difference. First of all, the right-hand side of the RG equation for γ_s in Ref. [43] [see Eq. (A12) there] contains a term proportional to $t\gamma_c^2$ rather than to $t(1+\gamma_s)\gamma_c^2$ as in our Eq. (19). Since the quantity $Z_\omega + \Gamma_s = Z_\omega(1+\gamma_s)$ should have no renormalization by virtue of the particle number conservation, this would imply the presence of a term proportional to $t\gamma_c^2/(1+\gamma_s)$ in the RG equation for Z_ω. Being divergent for the case of the Coulomb interaction, $\gamma_s = -1$, such a term would, however, violate the $\mathcal{F}$ invariance of the NLSM action (1) and is thus not allowed. Second, the RG equation for γ_t reported in Ref. [43] does not contain the term proportional to $t\gamma_c^2$, in contrast to our Eq. (20). Finally, the RG equation for γ_c reported in Ref. [43] contains an additional term proportional to $t\gamma_c \ln(1+\gamma_s)$ as compared to our Eq. (21). We note that a similar term was reported by Belitz and Kirkpatrick in Ref. [39] [see Eq. (6.8g) there]. In our opinion, such terms, divergent for the case of the Coulomb interaction, $\gamma_s = -1$, cannot appear in the course of renormalization of $\mathcal{F}$-invariant operators, including S_c. In Ref. [47], the appearance of a term proportional to $t\gamma_c \ln(1+\gamma_s)$ in the RG equation for γ_c of Ref. [39] was attributed to an improper treatment of the gauge invariance. In our background-field RG calculations, terms proportional to $\ln(1+\gamma_s)$ do appear in the course of renormalization of Γ_c at intermediate steps but cancel each other in the final results, in agreement with the $\mathcal{F}$ invariance, see Appendix A.

B. General case

The RG equations (18)–(22) have been derived for the case of preserved spin-rotational symmetry. We are now going to generalize them to systems with spin-rotational symmetry broken (partly or fully) due to spin-orbit coupling and/or spin-orbit impurity scattering. Both these symmetry-breaking mechanisms induce finite relaxation rates $(1/\tau_s^x, 1/\tau_s^y, 1/\tau_s^z)$ for the corresponding components of the electron spin. The relaxation rates determine the mass of the corresponding triplet modes (diffusons and cooperons). As an example, the mode corresponding to the spin component S_x acquires a mass proportional to $1/\tau_s^y + 1/\tau_s^z$. This mode thus becomes effectively frozen and drops out of RG equations at length scales $L \gg L_s^x \sim [1/(D\tau_s^y) + 1/(D\tau_s^z)]^{-1/2}$.

In the presence of spin-orbit coupling, spin relaxation due to the D'yakonov-Perel' mechanism takes place. The corresponding relaxation rates are given by $1/\tau_s^{x,y,z} \sim \Delta_{\rm so}^2\tau$, where $\Delta_{\rm so}$ denotes the spin-orbit splitting [48]. Therefore all triplet modes (both for diffusons and cooperons) are suppressed at the length scales $L \gg L_{\rm so} = v_F/\Delta_{\rm so}$, i.e., the number of triplet modes contributing to the RG equations is $n = 0$. In the case of a 2D electron system with the spin-orbit impurity scattering but without spin-orbit coupling, the spin relaxation is anisotropic: $1/\tau_s^z = 1/\tau_{\rm so}$, $1/\tau_s^{x,y} = 0$, where $1/\tau_{\rm so}$ denotes the skew scattering rate [49]. Thus, for $L \gg L_s = \sqrt{D\tau_{\rm so}}$, the triplet modes corresponding to the total spin component S_z remain massless. Therefore, in this case, $n = 1$ triplet mode still contributes to the RG equations.

If the spin-orbit coupling and spin-orbit scattering are both present, then different regimes with $n = 3$, $n = 1$, and $n = 0$ can be realized depending on the relations between L, $L_{\rm so}$, and L_s. For all three cases, the one-loop RG equations can be written as

$$\frac{dt}{dy} = t^2\left[\frac{n-1}{2} + f(\gamma_s) + nf(\gamma_t) - \gamma_c\right], \tag{23}$$

$$\frac{d\gamma_s}{dy} = -\frac{t}{2}(1+\gamma_s)\big(\gamma_s + n\gamma_t + 2\gamma_c + 4\gamma_c^2\big), \tag{24}$$

$$\frac{d\gamma_t}{dy} = -\frac{t}{2}(1+\gamma_t)[\gamma_s - (n-2)\gamma_t - 2\gamma_c(1+2\gamma_t - 2\gamma_c)], \tag{25}$$

$$\frac{d\gamma_c}{dy} = -2\gamma_c^2 - \frac{t}{2}\big[(1+\gamma_c)(\gamma_s - n\gamma_t) - 2\gamma_c^2 + 4\gamma_c^3 + 2n\gamma_c(\gamma_t - \ln(1+\gamma_t))\big], \tag{26}$$

$$\frac{d\ln Z_\omega}{dy} = \frac{t}{2}\big(\gamma_s + n\gamma_t + 2\gamma_c + 4\gamma_c^2\big). \tag{27}$$

In the case $n = 0$, Eq. (25) should be omitted. The RG equations (23)–(26) constitute one of the main results of the paper. In the rest of the paper, we will analyze these equations to investigate phase diagrams and observables for the cases of preserved and broken spin-rotational symmetry.

The system of RG equations (23)–(26) has the fixed plane $\gamma_s = -1$ corresponding to the case of the long-ranged Coulomb interaction. In fact, this statement is not restricted to the one-loop RG equations. The existence of such a fixed plane is a consequence of the particle-number conservation and of the $\mathcal{F}$ invariance of the NLSM action (1). Due to the charge conservation, RG equations for γ_s and z are related to all orders in t:

$$\frac{d\gamma_s}{dy} = -(1+\gamma_s)\zeta_z, \quad \frac{dZ_\omega}{dy} = Z_\omega \zeta_z. \tag{28}$$

The value ζ_z^* of the anomalous dimension ζ_z at a fixed point determines the dynamical critical exponent $z = d + \zeta_z^*$. The latter controls the temperature behavior of the specific heat, $c_v \sim T^{d/z}$ [50]. Typically, one expects that $z \leq d$ ($\zeta_z^* < 0$), which implies the instability of the fixed point in the plane $\gamma_s = -1$ with respect to the increase of γ_s.

It is worth reminding the reader that RG equations (23)–(27) are of one-loop order with respect to diffusive modes (i.e., are derived by expansion of the right-hand side to the lowest nontrivial order in t) but are exact in the interaction. Typically, one expects that one-loop RG equations are valid until entering the insulating (strong-disorder) phase, i.e., for $t \lesssim 1$. This requires a tacit assumption that in the expansion of the right-hand side of RG equations in powers of t, all coefficients (which are functions of interaction amplitudes) are of the order of unity. In the case of superconducting instability, γ_c diverges at some scale L_c, so that the coefficients of the expansion in powers of t become much larger than unity. As discussed in Sec. III A, near the superconducting instability (i.e., at $|\gamma_c| \gg 1$), the general condition of validity of the one-loop approximation $t \lesssim 1$ becomes more restrictive: $t|\gamma_c| \lesssim 1$. Similarly, near the Stoner instability (which corresponds to the divergence of γ_t) the two-loop analysis [51,52] demonstrates that expansion in t is justified for $t \lesssim 1/\gamma_t \ll 1$.

Up to now, we have discussed the renormalization as a flow of couplings with the length scale. In practice, one usually has a sufficiently large system and the infrared cutoff is controlled not by the system size but rather by the temperature T. In this situation, the renormalization due to the contributions to RG equations (23)–(27) induced by interactions should be stopped at the length scale L_T, which is determined as follows [see Eq. (A15)]:

$$T = \frac{1}{\tau}\left(\frac{l}{L_T}\right)^2 \frac{t_0 Z_{\omega 0}}{t(L_T) Z_\omega(L_T)}, \tag{29}$$

where $t_0 = t(l)$ and $Z_{\omega 0} = Z_\omega(l)$. This transformation of temperature into the length scale [53] allows us to investigate the temperature dependence of observables. In particular, the electrical resistivity in the absence of magnetic field is addressed in Sec. V. The inclusion of magnetic field induces two additional length scales, l_H and l_Z, related to the orbital and Zeeman effect of the magnetic field and leading to the magnetoresistivity, Sec. VI.

IV. PHASE DIAGRAM AT ZERO MAGNETIC FIELD

A. Preserved spin-rotational symmetry

We start our analysis of RG equations (23)–(27) from the case in which spin-rotational and time reversal symmetries are preserved, i.e., there are $n = 3$ triplet modes. We note that in the notations of Ref. [39] this case is termed as G(LR) for the Coulomb interaction and G(SR) for the short-ranged interaction.

1. Coulomb interaction

For the case of the Coulomb interaction, $\gamma_s = -1$, which is the fixed plane of Eqs. (23)–(26), the RG equations can be simplified as (we set $n = 3$)

$$\frac{dt}{dy} = t^2[2 + 3f(\gamma_t) - \gamma_c], \tag{30}$$

$$\frac{d\gamma_t}{dy} = \frac{t}{2}(1+\gamma_t)(1+\gamma_t+2\gamma_c(1+2\gamma_t-2\gamma_c)), \tag{31}$$

$$\frac{d\gamma_c}{dy} = -2\gamma_c^2 + \frac{t}{2}\big[(1+\gamma_c)(1+3\gamma_t) + 2\gamma_c^2(1-2\gamma_c) - 6\gamma_c(\gamma_t - \ln(1+\gamma_t))\big]. \tag{32}$$

Let us now analyze fixed points of Eqs. (30)–(32). It turns out that the structure of the set of fixed points and of the three-dimensional phase diagram is very rich. Specifically, (1) there is a marginally unstable line of fixed points at $t = \gamma_c = 0$ (with arbitrary γ_t). These fixed points describe a conventional *clean Fermi liquid* without the Cooper-channel attraction. (2) There is a line of fixed points at $t = 0$ and $\gamma_c = -\infty$ (with arbitrary γ_t) corresponding to the *superconducting* (SC) phase. (3) Further, Eqs. (30)–(32) contain also the attractive line of fixed points at $\gamma_t = \infty$ and $\gamma_c = 1$. The divergence of γ_t corresponds to a *ferromagnetic* instability. (4) Formally, in Eqs. (30)–(32), there exists also a fixed point at $\gamma_t = -1$, $\gamma_c = 0$, and $t = \infty$. While the range of $t \gtrsim 1$ is beyond the accuracy of the one-loop RG, it is expected on general grounds that full RG equations should contain an attractive fixed point (or a family of fixed points) with $t = \infty$ describing the *insulating* phase.

(5) Within Eqs. (30)–(32), there is a possibility at some length scale to enter the phase with $\gamma_t = -1$. At this length scale, there are finite values $\gamma_c < 0$ and t. We note that $\gamma_t = -1$ corresponds to the infinitely strong attraction in the triplet particle-hole channel indicating a possibility of *exciton condensation*. Since the value $\gamma_t = -1$ is reached at a length scale close to L_X, full RG equations are needed to study a competition of exciton condensation in the spin channel and superconductivity in the Cooper channel. We leave this as a prospect for future research and do not discuss a possibility of exciton condensation in the rest of the paper.

(6) Going beyond the one-loop RG equations (30)–(32), we expect a fixed point at $\gamma_c = -\infty$, $t \sim 1$, and a certain value of γ_t governing the *transition between the superconductor and insulator phases*. The corresponding phase boundary is a critical surface with a flow towards this SIT fixed point originating at the trivial fixed point with $t = \gamma_c = \gamma_t = 0$. We will discuss the SIT fixed point in more detail in Sec. VII below.

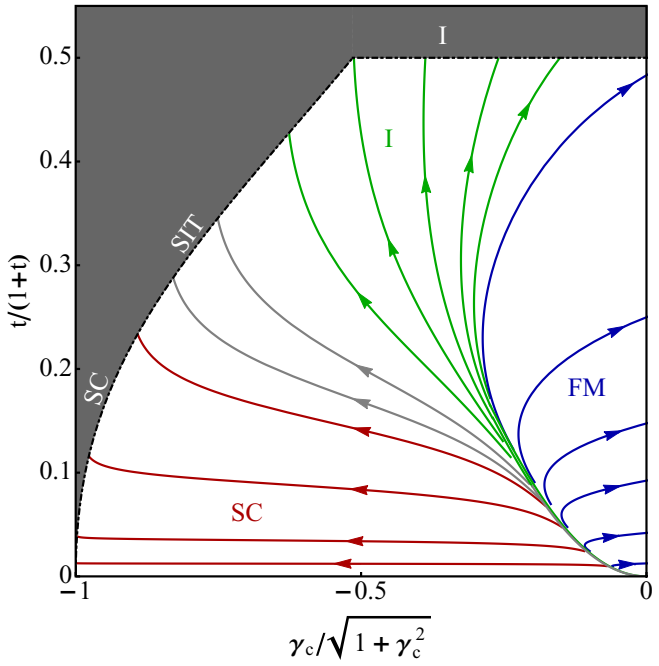

FIG. 1. (Color online) The case of preserved spin-rotational symmetry with the Coulomb interaction, $\gamma_s = -1$: the RG flow obtained from a numerical solution of Eqs. (30)–(32). The initial condition fixes $\gamma_{t0} = 0.2$. The arrows indicate the flow towards the infrared. The gray region indicates the part of the phase diagram that is not accessible within one-loop RG equations. The lines describing the flow to the superconducting (SC), insulating (I), and ferromagnetic (F) phases are shown in red, green, and blue, correspondingly. Gray flow lines correspond to the region of superconductor-insulator transition (SIT).

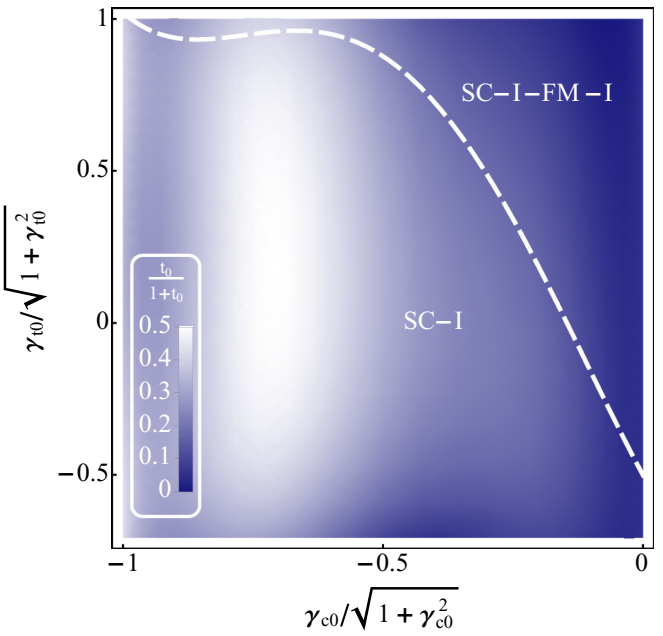

FIG. 2. (Color online) The case of preserved spin-rotational symmetry with the Coulomb interaction, $\gamma_s = -1$: a projection of the phase diagram on the $\gamma_{t0} - \gamma_{c0}$ plane. The color indicates the value of the Drude resistivity t_0 at which the quantum phase transition from SC to I occurs. Above the dashed line, the FM phase appears in addition to SC and I phases. The figure is obtained from numerical solutions of RG Eqs. (30)–(32).

(7) Similarly, we expect strong-coupling fixed points that control the ferromagnet-insulator and the ferromagnet-superconductor transitions. We will not discuss these fixed points in the present paper [55].

Let us now discuss the properties of the emerging phases (see Figs. 1 and 2) and corresponding fixed points, in more detail.

Superconducting phase. We first note that within the RG equations (30)–(32) the superconducting line of fixed points at $t = 0$ and $\gamma_c = -\infty$ is unstable, which makes the superconducting phase formally unreachable. As we have already discussed, this indicates a failure of the one-loop (lowest order in t) RG equations near the superconducting instability. In the absence of disorder (i.e., at $t = 0$), Eq. (32) describes the usual BCS-type scenario. The Cooper-channel interaction γ_c diverges at some finite length scale L_c as $\gamma_c(L \to L_c) \sim -1/(L_c - L)$. To estimate the length scale L_c in the case of finite disorder, we shall use the scale L_X defined by the condition $|\gamma_c(L_X)| = 1/t(L_X) \gg 1$. Assuming that the divergence of γ_c is of the BCS type, we get an estimate $(L_c - L_X)/L_X \sim t(L_X) \ll 1$. Thus, while the one-loop RG is not sufficient to follow the flow up to the singularity scale L_c, it works up to a scale L_X which is only slightly smaller than L_c.

Insulating phase and superconductor-insulator transition. On general grounds, we assume that once the RG flow reaches $t \sim 1$, the system is in the insulating phase, i.e., it flows into the insulating (I) fixed point with $t = \infty$. On the other hand, as discussed above, if t remains small when $|\gamma_c|$ reaches a value $1/t$, the system flows into a superconducting fixed point. There should be thus a fixed point at $t \sim 1$ (i.e., with a resistivity of the order of quantum resistance R_q) and certain values of γ_c and γ_t that controls the quantum phase transition between superconductor and insulator, see Sec. VII for further discussion. At small values of t and $\gamma_c < 0$, $\gamma_t > 0$, the separatrix surface between the two phases is parametrized by the following equation: $t = 4\gamma_c^2/(1 + 3\gamma_t)$.

"Ferromagnetic" phase. For the attractive line of fixed points at $\gamma_t = \infty$ and $\gamma_c = 1$, the value $\gamma_c = 1$ is fixed by a cancellation of terms in the right-hand side of Eq. (32), which are proportional to $\gamma_t \gg 1$. The divergence of γ_t occurs at some finite length scale $L_{\rm FM}$. Due to a delocalizing effect of the interaction (Altshuler-Aronov) contribution to the renormalization of the resistance at large γ_t, the fixed point value $t(L_{\rm FM})$ remains finite and is nonuniversal (i.e., determined by the initial conditions). Therefore Eqs. (30)–(32) predict a ferromagnetic metallic phase with a nonuniversal resistivity. Strictly speaking, one-loop equations are insufficient to describe accurately the regime $t\gamma_t \gtrsim 1$ (see Refs. [51,52]) but this is not expected to modify essentially the emergence of instability.

However, since the emergent fixed points are characterized by a finite value of dimensionless resistivity $t(L_{\rm FM})$, the diffusive RG continues at larger scales. Specifically, to describe properly the system at scales larger than $L_{\rm FM}$, one needs to take into account breaking of spin-rotational symmetry and derive a new set of RG equations. In this case, all triplet diffusive modes

in the particle-hole channel and singlet and triplet modes in the Cooper channel are suppressed. One can thus assume that the system at $L > L_{\rm FM}$ is described by RG equations (23) with $n = 0$, $\gamma_c = 0$, and $\gamma_s = -1$, which results in insulating behavior at large length scales. Moreover, due to enhanced spin fluctuations near the Stoner instability, the system at $L > L_{\rm FM}$ can demonstrate a spin-glass behavior [62]. In what follows, we shall term this phase ferromagnetic (FM) for simplicity.

Overall RG flow and phase diagram. A part of the RG flow for Eqs. (30)–(32) is shown in Fig. 1. In general, a projection of the flow in a three-dimensional parameter space onto a 2D plane, as in Fig. 1, depends on the initial conditions for the couplings. For the plot shown in Fig. 1, we have assumed a realistic relation between the triplet (third axis) and Cooper amplitudes, which has allowed us to avoid intersections in the projected flows. Furthermore, the RG flow is shown only in the region of validity of the one-loop approximation: $t \max\{1, |\gamma_c|\} \lesssim 1$. The flows towards the superconducting, insulating, and ferromagnetic phases are plotted in red, green, and blue, correspondingly. The grey part of the flow describes the vicinity of the SIT. One of the grey curves is the separatrix between the superconducting and insulator phases. However, the one-loop precision is insufficient to determine the separatrix in the region $t \max\{1, |\gamma_c|\} \gtrsim 1$. At small values of γ_c, the separatrix is parametrized by $t = 4\gamma_c^2/(1 + 3\gamma_t)$.

The phase diagram expected on the basis of the RG equations (30)–(32) is shown in Fig. 2 in the plane of bare interaction couplings γ_{c0} and γ_{t0}. For $\gamma_{c0} < 0$, the superconducting phase exists at small values of t_0. For given γ_{c0} and γ_{t0}, the quantum phase transition from superconductor to insulator occurs with increase of t_0. In addition, for a sufficiently large γ_{t0} (above the dashed line) a ferromagnetic phase emerges. In this part of the γ_{c0}-γ_{t0} plane, a sequence of transitions S–I–FM–I takes place with increasing bare resistivity t_0. For $\gamma_{c0} > 0$, there is no superconducting phase; changing t_0 drives a transition from the ferromagnetic to the insulator phase.

The dependence of the NLSM coupling t on the length scale L across the quantum phase transition from the superconducting to insulating phase (in the part of the phase diagram in Fig. 2 where FM phase does not occur) is shown in Fig. 3. This dependence dominates the corresponding evolution of the total electrical resistivity ρ (apart from a narrow region close to the superconducting instability, where the inelastic contributions due to fluctuating Cooper pairs becomes dominant, see Sec. V for details).

In Fig. 4, we choose the values of γ_{c0} and γ_{t0} such that the FM phase exists in addition to the SC and I ones. We thus show the length dependence of t across the quantum phase transitions from SC to I and from I to FM phases. We note that within the RG equations (30)–(32), the insulating phase (between SC and FM phases) exists in a very narrow interval of t_0, see Fig. 4. As one can see, the scale L_X (at which red curves in Fig. 4 are stopped), which yields approximately the superconducting coherence length, is larger than the BCS coherence length $L_c^{\rm BCS} = l \exp(-1/2\gamma_{c0})$. In the ferromagnetic phase, the corresponding length scale $L_{\rm FM}$ (where blue curves end) is still larger than L_X.

At finite temperature, the interaction contributions to the RG equations (30)–(32) are stopped at the length scale L_T.

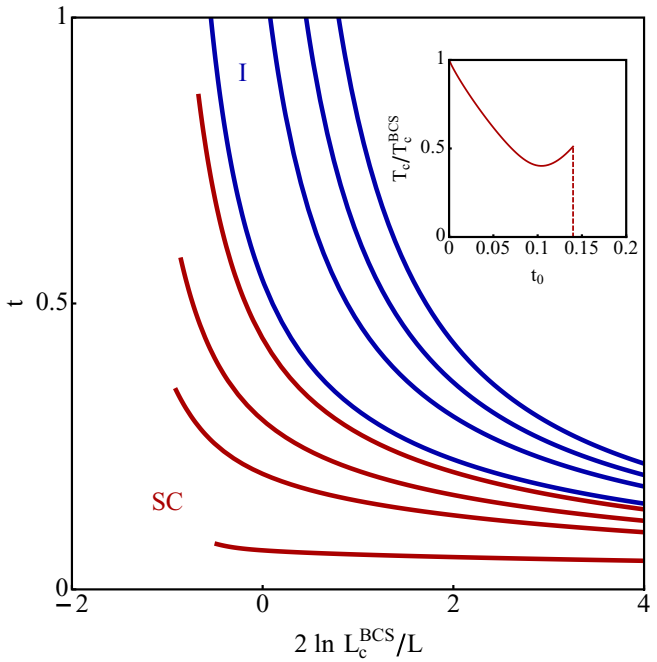

FIG. 3. (Color online) The case of preserved spin-rotational symmetry with the Coulomb interaction, $\gamma_s = -1$: dependence of t ("renormalized Drude resistivity") on the length scale across the quantum phase transition between the superconducting (SC, red curves) and insulating (I, blue curves) phases. The curves are obtained from numerical solutions of RG equations (30)–(32) for $\gamma_{c0} = -0.25$, $\gamma_{t0} = 0.01$, and $t_0 = 0.05, 0.1, 0.12, 0.14, 0.15, 0.18, 0.2, 0.22$ (from the bottom to the top).

Neglecting the difference between L_T and the temperature-induced dephasing length L_ϕ (which cuts off the localization corrections), we can stop the whole RG at L_T. Then the transition temperatures to superconducting (T_c) and ferromagnetic phases ($T_{\rm FM}$) is estimated as follows (see also a discussion in the end of Sec. III): $T_c \approx (1/\tau)(l/L_X)^2$ and $T_{\rm FM} \approx (1/\tau)(l/L_{\rm FM})^2$. A typical dependence of T_c and $T_{\rm FM}$ on t_0 is shown in the insets to Figs. 3 and 4. The effect of disorder on T_c depends on the sign of the term in the square brackets in the right-hand side of Eq. (32). It occurs that for $\gamma_c < 0$ and $\gamma_t > -1$ this term is always positive, except for a small region at small negative values of γ_c and $-1 < \gamma_t < -1/3$. Therefore, as was first found by Finkelstein [32], disorder in the presence of the Coulomb interaction suppresses the superconducting phase (i.e., lowers T_c). At the same time, disorder induces the ferromagnetic phase that exists in an intermediate range of disorder. This implies a nonmonotonous dependence of $T_{\rm FM}$ on t_0.

We note that T_c evaluated from the RG equations (30)–(32) is in fact somewhat larger than the true superconducting [Berezinskii-Kosterlitz-Thouless (BKT)] transition temperature $T_{\rm BKT}$ due to the presence of phase fluctuations of the order parameter at temperatures below T_c, see Sec. V for more detail. The relative difference between T_c and $T_{\rm BKT}$ is, however, small for weak disorder, and thus does not essentially affect the much stronger variation of T_c with disorder explored in this paper.

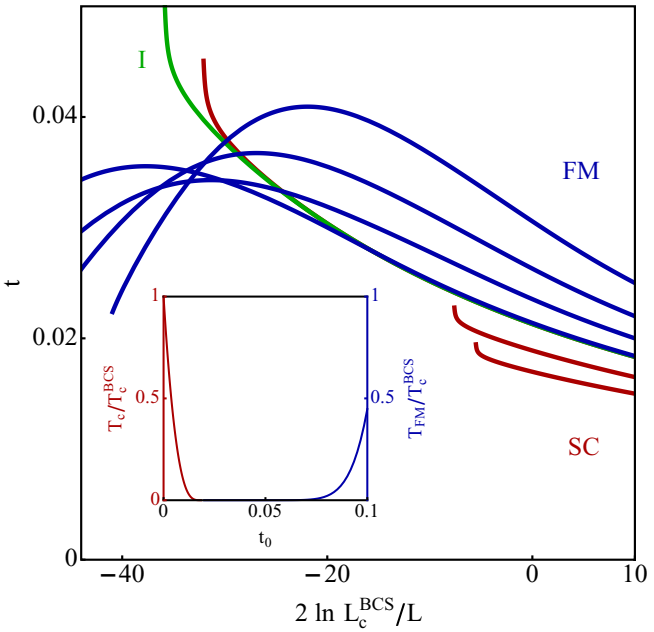

FIG. 4. (Color online) The case of preserved spin-rotational symmetry with the Coulomb interaction, $\gamma_s = -1$: dependence of t on the length scale across the quantum phase transition between superconducting (SC, red curves), insulating (I, green curve), and ferromagnetic (FM, blue curves) phases. The curves are obtained from numerical solutions of RG equations (30)–(32) for $\gamma_{c0} = -0.1$, $\gamma_{t0} = 0.4$ and $t_0 = 0.015, 0.0165, 0.18325, 0.18326, 0.184, 0.02, 0.022, 0.025$ (from the bottom to the top). For higher values of t_0, another insulating phase (not shown on this scale) emerges. Inset: dependence of $T_c/T_c^{\rm BCS}$ and $T_{\rm FM}/T_c^{\rm BCS}$ on t_0.

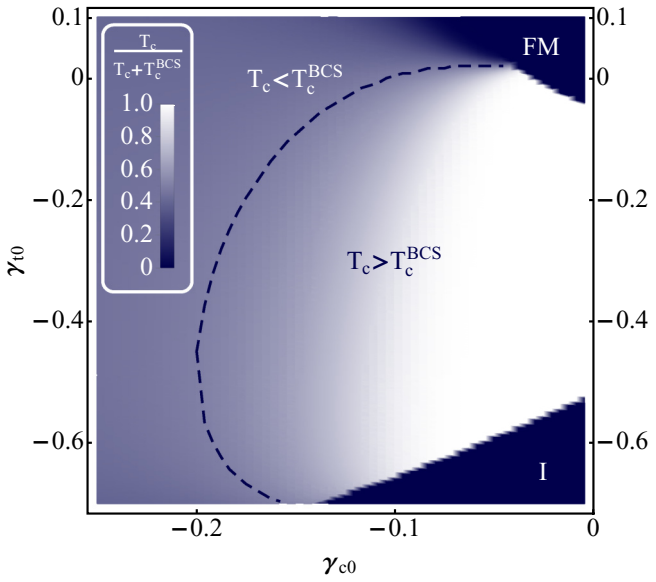

FIG. 5. (Color online) The case of preserved spin-rotational symmetry with the short-ranged interaction, $\gamma_{s0} = -0.05$: a projection of the phase diagram on the $\gamma_{t0} - \gamma_{c0}$ plane. The color indicates the ratio of $T_c/(T_c + T_c^{\rm BCS})$ for $t_0 = 0.06$. The dashed curve separates the regions with $T_c < T_c^{\rm BCS}$ and with $T_c > T_c^{\rm BCS}$. The figure is obtained from numerical solutions of RG equations (33)–(36).

2. Short-ranged interaction

In the case of short-ranged interaction, RG equations (23)–(26) with $n = 3$ read

$$\frac{dt}{dy} = t^2[1 + f(\gamma_s) + 3f(\gamma_t) - \gamma_c], \tag{33}$$

$$\frac{d\gamma_s}{dy} = -\frac{t}{2}(1+\gamma_s)\left(\gamma_s + 3\gamma_t + 2\gamma_c + 4\gamma_c^2\right), \tag{34}$$

$$\frac{d\gamma_t}{dy} = \frac{t}{2}(1+\gamma_t)[-\gamma_s + \gamma_t + 2\gamma_c(1 + 2\gamma_t - 2\gamma_c)], \tag{35}$$

$$\frac{d\gamma_c}{dy} = -2\gamma_c^2 + \frac{t}{2}\big[(1+\gamma_c)(-\gamma_s + 3\gamma_t) + 2\gamma_c^2(1 - 2\gamma_c) - 6\gamma_c(\gamma_t - \ln(1+\gamma_t))\big]. \tag{36}$$

Contrary to the Coulomb-interaction case (where we had $\gamma_s = -1$), the singlet particle-hole amplitude γ_s is not fixed now, so that the RG flow occurs in the four-dimensional parameter space. However, the structure of the set of attractive fixed points (quantum phases) and of fixed points describing quantum phase transitions between them remains qualitatively the same as in the Coulomb case. Specifically, the fixed points of the RG flow for the short-ranged interaction are as follows [55]. (1) There is a surface of clean-Fermi-liquid fixed points at $t = \gamma_c = 0$ (with arbitrary γ_t and γ_s). (2) The fixed-point surface at $t = 0$ and $\gamma_c = -\infty$ corresponds to the superconducting phase. (3) The line of fixed points with $\gamma_s = -1$, $\gamma_t = \infty$, $\gamma_c = 1$, and arbitrary t, is attractive in the γ_s direction. Therefore the RG equations (33)–(36) lead to the same ferromagnetic phase that exists in the case of the Coulomb interaction. (4) Exactly as in the Coulomb case, there should be a fixed point (or a family of fixed points) with $t = \infty$ describing the insulating phase. (5) For the same token as in the Coulomb case, a SIT fixed point with $t \sim 1$ should separate the superconducting and insulating phases.

The phase diagram for a given $\gamma_{s0} > -1$ is similar to that for the case of the Coulomb interaction, $\gamma_{s0} = -1$ (shown in Fig. 2). With increase of γ_{s0}, the destruction of the superconducting phase gets shifted towards larger values of t_0. The crucial difference between the cases of the short-ranged and Coulomb interactions is the existence of a large region of the phase diagram with $L_X < L_c^{\rm BCS}$ (and thus $T_c > T_c^{\rm BCS}$). In the case of a bare repulsion in the particle-hole channel, $\gamma_{s0} < 0$ and $\gamma_{t0} > 0$, the superconducting transition temperature is typically lower than the clean BCS result, $T_c < T_c^{\rm BCS}$ (see Fig. 5). However, the situation changes if the bare interaction in the triplet particle-hole channel is attractive, $\gamma_{t0} < 0$. As illustrated in Fig. 5, a significant part of the phase diagram is occupied by a superconductor with $T_c > T_c^{\rm BCS}$. It should be emphasized that the superconducting phase with enhanced T_c exists also for $\gamma_{t0} > 0$. However, it occurs only in a small region of $\gamma_{t0}, |\gamma_{c0}|, |\gamma_{s0}| \ll 1$ (see Fig. 5). Typical RG evolution of the resistance t in this region of initial values of interactions is shown in Fig. 6. Being initially suppressed by disorder, T_c can be significantly (several orders of magnitude) enhanced with respect to $T_c^{\rm BCS}$ near the superconductor-insulator quantum phase transition, as illustrated in the inset to Fig. 6. This is in agreement with the conclusion of our work [37] where RG equations (18)–(21)

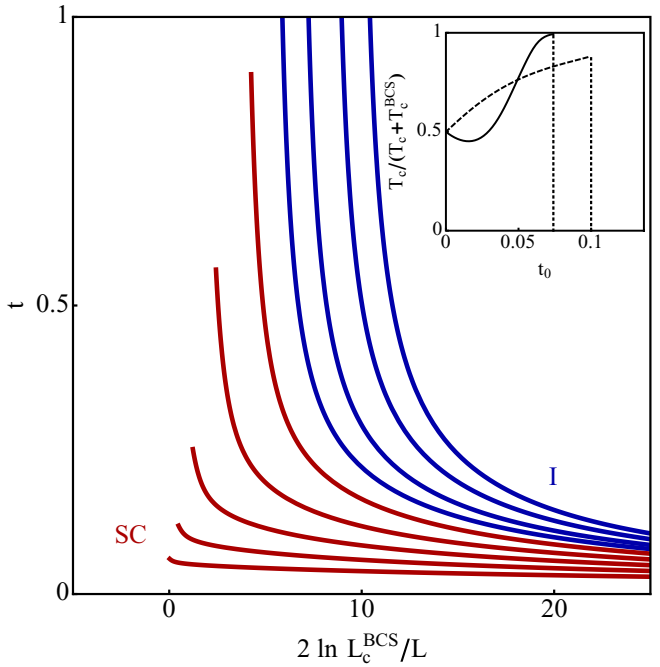

FIG. 6. (Color online) The case of preserved spin-rotational symmetry with the short-ranged interaction, $\gamma_{s0} = -0.05$: dependence of t on the length scale across the quantum phase transition between superconducting (SC, red curves) and insulating (I, blue curves) phases. The curves are obtained from the numerical solution of RG equations (33)–(36) for $\gamma_{c0} = -0.04$, $\gamma_{t0} = 0.005$, and $t_0 = 0.01, 0.03, 0.05, 0.06, 0.07, 0.078, 0.085, 0.095, 0.105$ (from bottom to top). For higher values of t_0, an insulating phase (not shown on this scale) emerges. The dependencies of $T_c/(T_c + T_c^{\rm BCS})$ on t_0 for $\gamma_{c0} = -0.04$, $\gamma_{t0} = 0.005$, and $\gamma_{s0} = -0.05$ (solid curve) and for $\gamma_{c0} = -\gamma_{s0} = \gamma_{t0} = -0.1$ (dashed curve) are shown in the inset.

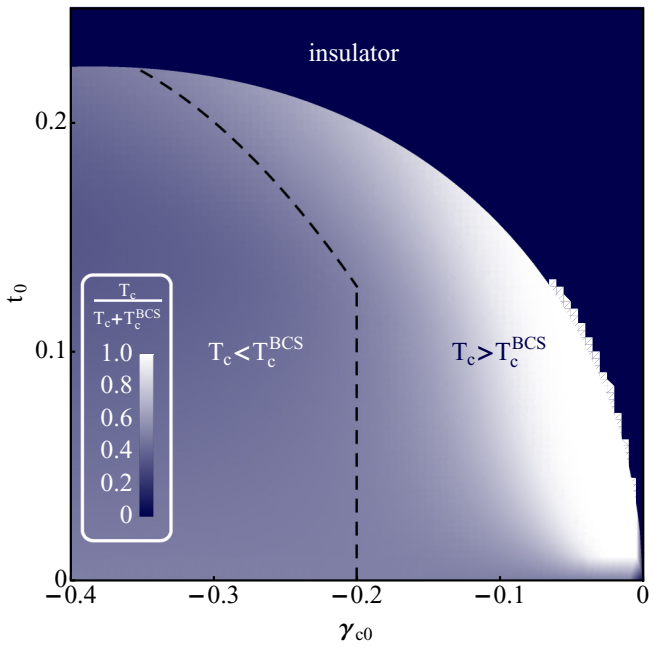

FIG. 7. (Color online) The case of preserved spin-rotational symmetry with the short-ranged interaction on the BCS line: the color density plot for the ratio $T_c/(T_c + T_c^{\rm BCS})$ in the $t_0 - \gamma_{c0}$ plane. The dashed black lines separate the regions with $T_c > T_c^{\rm BCS}$ and $T_c < T_c^{\rm BCS}$.

with the right-hand sides expanded to the lowest nontrivial order in γ_s, γ_t, and γ_c were analyzed.

The mechanism of enhancement of the transition temperature is as follows. For small initial values of interaction parameters $|\gamma_{s0}|, |\gamma_{t0}|, |\gamma_{c0}| \ll t_0 \ll 1$, the renormalization of the Cooper interaction amplitude occurs in two distinct steps. At the first step of the RG flow, the interaction is renormalized due to the presence of disorder (the terms proportional to t), while at the second step the standard BCS-type renormalization (the term $-2\gamma_c^2$) takes place. At the first step of renormalization, we can linearize the RG equations (33)–(36) in interaction parameters and neglect the term $-2\gamma_c^2$. Then, in the course of RG flow, the interaction amplitudes approach the BCS line $\gamma_s = \gamma_t = -\gamma_c$, converting the repulsion in singlet and triplet particle-hole channels into attraction. This is the consequence of the (weak) multifractality of the noninteracting fixed point. At some scale L_1 such that $\ln L_1/l = 1/t_0 - 1/t$, the interaction couplings become of the order of the resistance: $|\gamma_{s,t,c}| \sim t$. Provided $|\gamma_{s0}|, |\gamma_{t0}|, |\gamma_{c0}| \gg t_0^2$, the resistance at this scale $t(L_1) \sim t_0^2/\max\{|\gamma_{s0}|, |\gamma_{t0}|, |\gamma_{c0}|\} \ll 1$ and all interaction parameters are still much smaller than unity. After the length scale L_1 the second step of RG flow starts, where in Eq. (21) one can neglect terms proportional to t compared to the disorder-independent term $-2\gamma_c^2$. Thus the Cooper interaction γ_c flows according to the standard BCS RG equation for a clean system with the initial value $\gamma_c(L_1) \sim t(L_1)$ rather than γ_{c0}. Hence we find the following rough estimate for the transition temperature: $T_c \sim (1/\tau)(l/L_1)^2 \exp(-1/|\gamma_c(L_1)|) \sim (1/\tau)\exp(-2/t_0) \gg T_c^{\rm BCS}$ (see Appendix B for details).

In short, the role of the noninteracting disorder-induced multifractality is to enhance the interaction in the Cooper channel such that it becomes comparable to the resistance. After that, the divergence in the Cooper channel is driven by the standard mechanism (the same as in a clean system). The enhancement of T_c occurs in an intermediate range of disorder (t_0 between $|\gamma_{i0}|$ and $|\gamma_{i0}|^{1/2}$). For a weaker disorder $t_0 \lesssim \max\{|\gamma_{c0}|, |\gamma_{t0}|, |\gamma_{s0}|\}$, one can find a suppression of the transition temperature instead of enhancement, see the solid curve in the inset to Fig. 6.

If the disorder scattering rate $1/\tau$ exceeds the Debye frequency ω_D, the starting point of the RG flow will be likely located not far from the BCS line, $\gamma_{s0} = -\gamma_{t0} = -\gamma_{c0}$ (see Sec. II C). For such initial conditions, the dependence of $T_c/(T_c + T_c^{\rm BSC})$ on t_0 is shown in the inset to Fig. 6 by the dashed curve. It is worth stressing that in the case of initial interaction parameters on the BCS line there is no initial decrease of the transition temperature with increase of t_0. This is because the second term in the right-hand side of Eq. (36) is negative on the BCS line for $0 > \gamma_c > -0.41$. The dependence of $T_c/T_c^{\rm BSC}$ on γ_{c0} and t_0 on the BCS line is shown in Fig. 7.

Let us now turn to the region in the phase diagram, Fig. 5, where the ferromagnetic (FM) phase emerges. Figure 8 shows typical dependencies of resistance t on the length scale L across the transition from SC to FM phases with increasing t_0. The inset presents dependencies of both critical temperatures (T_c and $T_{\rm FM}$) on t_0.

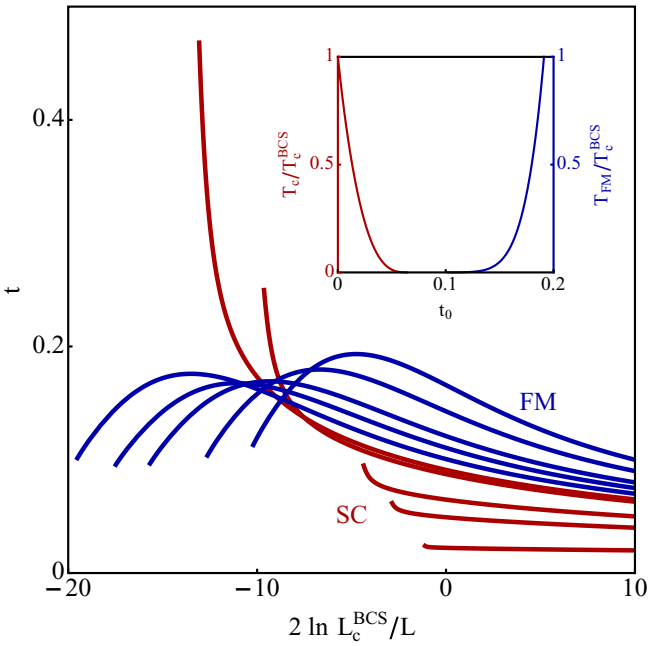

FIG. 8. (Color online) The case of preserved spin-rotational symmetry with the short-ranged interaction, $\gamma_{s0} = -0.05$: dependence of t on the length scale across the quantum phase transition between superconducting (SC, red curves) and ferromagnetic (FM, blue curves) phases. The curves are obtained from the numerical solution of RG equations (33)–(36) for $\gamma_{c0} = -0.1$, $\gamma_{t0} = 0.2$, and $t_0 = 0.02,\ 0.04,\ 0.05,\ 0.063,\ 0.065,\ 0.07,\ 0.075,\ 0.08,\ 0.09,\ 0.1$ (from bottom to top). The dependencies of $T_c/T_c^{\rm BCS}$ and $T_{\rm FM}/T_c^{\rm BCS}$ on t_0 are shown in the inset.

B. Broken spin-rotational symmetry

In the presence of spin-orbit coupling and/or spin-orbit scattering, the spin-rotational symmetry is broken. At length scales $L \gg \max\{L_{\rm so}, L_s\}$, the spin-rotational symmetry is completely broken and all triplet modes are suppressed such that $n = 0$. In Ref. [39], this case is referred to as SO(LR) for the Coulomb interaction and SO(SR) for the short-ranged interaction [57].

1. Coulomb interaction

For $n = 0$ and for the case of the Coulomb interaction, $\gamma_s = -1$, the one-loop RG equations, Eqs. (23)–(26), take the form

$$\frac{dt}{dy} = t^2\left(\frac{1}{2} - \gamma_c\right), \tag{37}$$

$$\frac{d\gamma_c}{dy} = -2\gamma_c^2 + \frac{t}{2}\left[1 + \gamma_c + 2\gamma_c^2(1 - 2\gamma_c)\right]. \tag{38}$$

The first, perturbative study of the effect of interaction on the conductivity of a disordered system in the presence of spin-orbit scattering has been performed in Ref. [63]. To the lowest order in γ_c, Eqs. (37) and (38) coincide with the one-loop RG equations derived in Refs. [64–66].

Since the spin-orbit interaction kills the contribution of the triplet channel, while the particle-hole singlet amplitude remains fixed, $\gamma_s = -1$, the RG flow now occurs in a 2D parameter space, t and γ_c. The structure of the phase diagram is governed by the following fixed points. (1) Equations (37) and (38) possess a clean-Fermi-liquid fixed point at $t = \gamma_c = 0$, which is marginally unstable. (2) There is the fixed point at $t = 0$ and $\gamma_c = -\infty$ corresponding to the superconducting (SC) phase. (3) As in all other symmetry classes, there should be the insulating (I) phase with $t = \infty$. It is, however, not reachable within the one-loop RG equations.

(4) There is a stable nontrivial fixed point at $\gamma_c^* = 1/2$ and $t^* = 2/3$ describing the critical metallic (CM) phase. This fixed point appears at the borderline of applicability of one-loop RG equations, $t^* \sim 1$, so that we do not have a rigorous argument in favor of existence of the CM phase. We find, however, very plausible that the attractive character of this fixed point is not destroyed by going beyond one loop. The emergence of this fixed point can be traced back (i) to the competition of weak antilocalization (enhanced by delocalizing effect of repulsive Cooper-channel interaction) with the localizing Coulomb repulsion in Eq. (37), and (ii) to the competition between Cooper instability and the disorder-induced suppression of the interaction matrix element in Eq. (38). The CM phase (if indeed exists) should be separated from the I phase by a CM–I quantum phase transition fixed point which is, however, located well beyond the limit of our one-loop RG.

(5) As in other symmetry classes, we expect existence of a fixed point at $\gamma_c = -\infty$ and $t \sim 1$ (region marked by "SIT") such that the transition between superconductor and insulator occurs through the separatrix connecting this fixed point and the trivial fixed point at $t = \gamma_c = 0$. At small values of t and $\gamma_c < 0$, the separatrix is parametrized by the following equation, $t = 4\gamma_c^2$ [66].

The RG flow (and the corresponding phase diagram) for equations (37) and (38) is shown in Fig. 9. As in the case of preserved spin-rotational symmetry, we stop the RG flow when either $|\gamma_c|$ reaches the value $1/t \gg 1$ at a certain scale L_X (superconducting phase, red RG flow lines) or the resistance t reaches the value unity (insulating phase, green flow lines). In addition, we have now the critical metal phase (blue flow lines).

The dependence of t on the length scale across the consecutive SC-I-CM transitions is shown in Fig. 10. As one can see, there is a very narrow interval of t_0 values in which the insulating phase separating the SC and CM phases exists. We mention that at not too large length scales (or, equivalently, at not too low temperatures) the resistance curves for SC, I, and CM phases cross each other. As expected, the Coulomb interaction suppresses the superconductivity, so that $L_X > L_c^{\rm BCS}$, and consequently, $T_c < T_c^{\rm BCS}$ (as shown in the inset of Fig. 10).

From Eq. (27) with $n = 0$, we find the following one-loop RG result for Z_ω in the case of the Coulomb interaction:

$$\frac{d\ln Z_\omega}{dy} = \frac{t}{2}\left(\gamma_s + 2\gamma_c + 4\gamma_c^2\right). \tag{39}$$

As explained below Eq. (28), the fixed-point value of the ζ function $d\ln Z_\omega/dy$ determines the dynamical exponent controlling the temperature dependence of the specific heat. The one-loop result (39) yields for the critical metal $c_v \sim T^{2/z}$

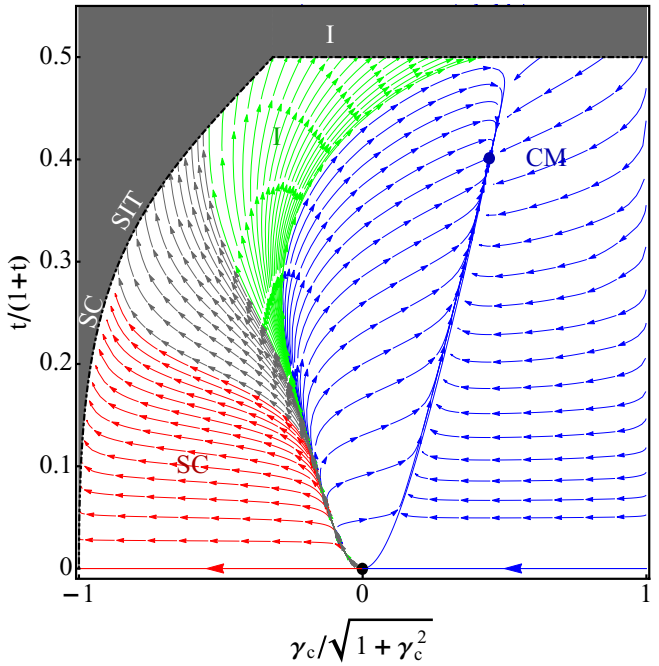

FIG. 9. (Color online) The case of broken spin-rotational symmetry with the Coulomb interaction, $\gamma_s = -1$: the RG flow obtained from numerical solutions of Eqs. (37) and (38). The arrows indicate the flow towards the infrared. The gray region indicates the part of the phase diagram that is not accessible within one-loop RG equations. The lines describing the flow to the superconducting (SC), insulating (I), and critical-metal (CM) phases are shown in red, green, and blue, correspondingly. Gray flow lines correspond to the region of superconductor-insulator transition (SIT).

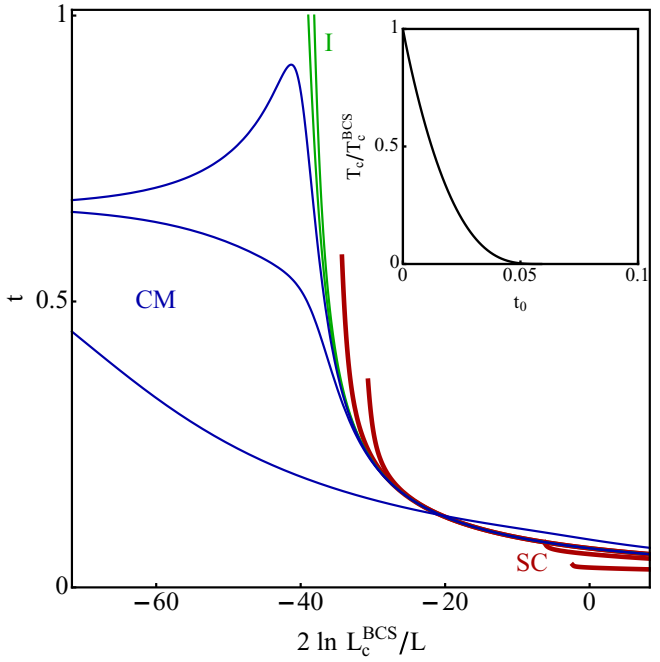

FIG. 10. (Color online) The case of broken spin-rotational symmetry with the Coulomb interaction, $\gamma_s = -1$: the dependence of t on the length scale across the transitions between superconducting (SC, red curves), insulating (I, green curves), and critical-metal (CM, blue curves) phases. The curves are obtained from numerical solutions of Eqs. (37) and (38) for $t_0 = 0.03,\ 0.05,\ 0.058039,\ 0.0580414,\ 0.0580416,\ 0.0580418,\ 0.0580419,\ 0.0580421,\ 0.07$ (from bottom to top). With further increasing the Drude resistivity t_0, the system enters again the insulating phase (not shown here), see Fig. 9. (Inset) Dependence of $T_c/T_c^{\rm BCS}$ on t_0. The value of the Cooper-channel attraction is $\gamma_{c0} = -0.12$.

with $z = 7/3$. Since $z > 2$, the CM phase is stable with respect to the deviations of γ_s from $\gamma_s = -1$.

2. Short-ranged interaction

In the case of short-ranged interaction, RG equations (23)–(26) with $n = 0$ take the form

$$\frac{dt}{dy} = t^2\left[-\frac{1}{2} + f(\gamma_s) - \gamma_c\right], \tag{40}$$

$$\frac{d\gamma_s}{dy} = -\frac{t}{2}(1+\gamma_s)\left(\gamma_s + 2\gamma_c + 4\gamma_c^2\right), \tag{41}$$

$$\frac{d\gamma_c}{dy} = -2\gamma_c^2 + \frac{t}{2}\left[-(1+\gamma_c)\gamma_s + 2\gamma_c^2(1-2\gamma_c)\right]. \tag{42}$$

These RG equations are richer than Eqs. (33)–(36) and describe the RG flow in a three-dimensional space of t, γ_s, and γ_c. (1) There is a line of clean-Fermi-liquid fixed points at $t = \gamma_c = 0$ and arbitrary γ_s. The peculiarity of the present symmetry class is that the clean noninteracting fixed point $t = \gamma_c = \gamma_s = 0$ is attractive. It corresponds to a *supermetal* (SM) phase. (2) The line of fixed points at $t = 0$ and $\gamma_c = -\infty$ corresponds to the superconducting phase. (3) As in all other symmetry classes, there is the insulating (I) phase with $t = \infty$ not reachable within the one-loop RG equations. (4) In addition to the critical metal phase at $\gamma_c^* = 1/2$, $\gamma_s^* = -1$, and $t^* = 2/3$, there is a second fully attractive fixed point at intermediate resistivity (i.e., on the border of applicability of one-loop RG equations): $\gamma_c^{**} = -1/2$, $\gamma_s^{**} = 0$, and $t^{**} = 1$. So, one-loop RG equations suggest a possibility of two different CM phases. (5) As in other symmetry classes, we expect existence of a fixed point $t \sim 1$ controlling the transition between superconductor and insulator phases. Further intermediate-coupling ($t \sim 1$) fixed points control other emerging quantum phase transitions (SM–I, SC–SM, SM–CM, and CM–I).

The phase diagram expected on the basis of RG equations (40)–(42) is shown in Fig. 11. For $\gamma_{c0} < 0$, a superconducting phase exists at small values of t_0. With increase of t_0, the QPT to insulator or supermetal occurs for given values of γ_{c0} and γ_{s0}. With increase of γ_{s0}, the superconducting phase proliferates. In the biggest part of the phase diagram, the transition between superconductor and insulator occurs at $t_0 \sim 1$. Interestingly, there is a region of the phase diagram in which a sequence of quantum phase transitions, SC–SM–I, SC–SM–CM–I, or SC–I–SM–I, occurs as t_0 grows (see Fig. 11). The dashed curve separating the region with multiple quantum phase transitions is parametrized by the condition $\gamma_{s0} = 2\gamma_{c0}$, see Appendix B.

A typical dependence of t on the length scale L across the SC-SM transition governed by increase of disorder (t_0) is illustrated in Fig. 12 for some initial values of γ_{s0} and γ_{c0}. As

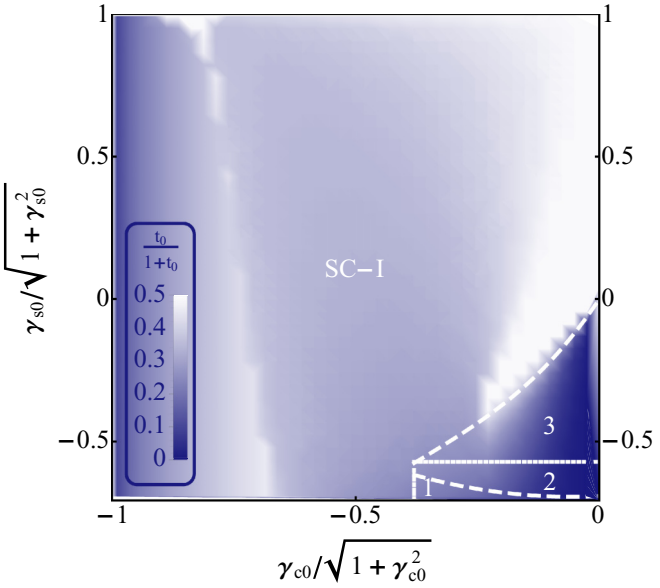

FIG. 11. (Color online) The case of broken spin-rotational symmetry with short-ranged interaction: a projection of the phase diagram on the plane $\gamma_{c0} - \gamma_{s0}$. The color indicates the value of t_0 at which the QPT from SC to SM or I occurs. In regions 1, 2, and 3, the increase of t_0 drives a sequence of QPTs: in 1—SC-SM-I, in 2—SC-SM-CM-I, and in 3—SC-I-SM-I. The figure is obtained from numerical solutions of RG equations (40)–(42).

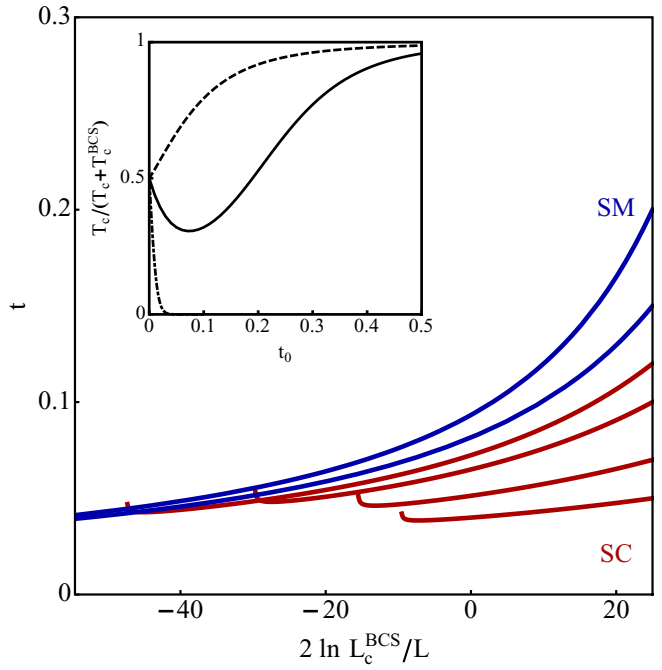

FIG. 12. (Color online) The case of broken spin-rotational symmetry with short-ranged interaction: dependence of t on the length scale across the QPT between superconducting and supermetallic phases. The curves are obtained from numerical solutions of RG equations (40)–(42) for $\gamma_{c0} = -0.04$, $\gamma_{s0} = -0.1$, and $t_0 = 0.05, 0.07, 0.1, 0.12, 0.15, 0.2$ (from bottom to top). (Inset) Dependencies of $T_c/(T_c + T_c^{BCS})$ on t_0 for $\gamma_{c0} = -0.04$ and $\gamma_{s0} = -0.005$ (solid curve), for $\gamma_{c0} = -\gamma_{s0} = -0.05$ (dashed curve) and for $\gamma_{c0} = -0.04$ and $\gamma_{s0} = -0.1$ (dot-dashed curve) are shown in the inset.

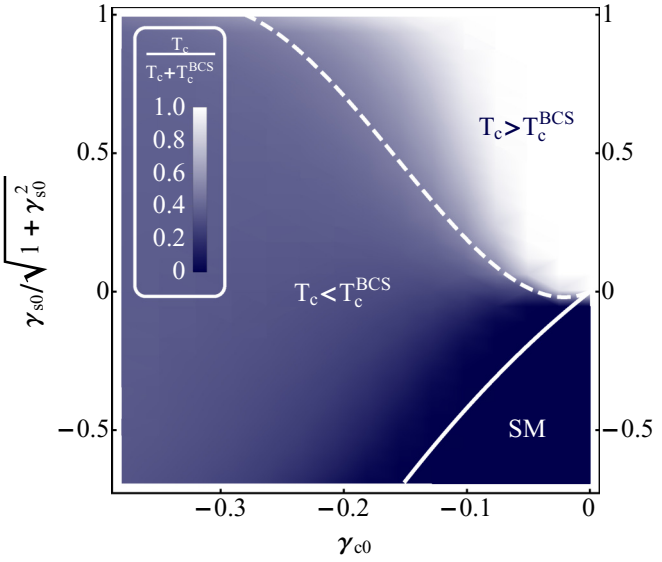

FIG. 13. (Color online) The case of broken spin-rotational symmetry with the short-ranged interaction: the color plot for the ratio $T_c/(T_c + T_c^{BCS})$ for $t_0 = 0.11$. The dashed curve separates the regions with $T_c < T_c^{BCS}$ and with $T_c > T_c^{BCS}$. The solid line indicates the boundary between superconductor and supermetal. The figure is obtained from numerical solutions of RG equations (40)–(42).

shown in the inset, in this case (dot-dashed line), the disorder suppresses the transition temperature. However, with increase of γ_{s0}, one finds a nonmonotonous dependence of T_c on t_0: at weak disorder, T_c is reduced in comparison with T_c^{BCS} whereas at intermediate disorder T_c is larger than T_c^{BCS}. There is a region in the phase diagram with small values of $\gamma_{c0} < 0$ and $\gamma_{s0} < 0$ in which $T_c > T_c^{BCS}$ (or more precisely, $L_X < L_c^{BCS}$). The enhancement of T_c in a certain range of bare couplings is in agreement with the conclusions of our work [37] where the renormalization group equations (40)–(42) with the right-hand sides expanded to the lowest nontrivial order in γ_s and γ_c were analyzed. In fact, for attraction in the particle-hole channel, $\gamma_{s0} > 0$, a significant part of the phase diagram is occupied by the superconducting phase with $T_c > T_c^{BCS}$, see Fig. 13.

The mechanism of enhancement of the transition temperature is similar to one for the case of preserved spin-rotational symmetry. For small initial values of γ_{c0} and γ_{s0}, the renormalization of the Cooper interaction amplitude occurs in two distinct steps. At the first step of RG flow, the interaction is renormalized due to the presence of disorder (the terms proportional to t), while at the second step the standard BCS-type renormalization (the term $2\gamma_c^2$) takes place. In the case $|\gamma_{s0}|, |\gamma_{c0}| \ll t_0 \ll 1$ at the first step of renormalization, we can linearize the RG equations (40)–(42) in the interaction parameters and neglect the term $-2\gamma_c^2$. Then, for $\gamma_{c0} < \gamma_{s0}/2$, in the course of RG flow, the interaction amplitudes approach the BCS line $\gamma_s = -\gamma_c$, thus converting the repulsion in the singlet particle-hole channel into attraction. This is a consequence of the (weak) multifractality of the noninteracting fixed point.

At some scale L_1 such that $\ln L_1/l = 2/t - 2/t_0$, the interaction couplings become of the order of the resistance: $|\gamma_{s,c}| \sim t$. The resistance at this scale is

$t(L_1) \sim [t_0(\gamma_{s0} - 2\gamma_{c0})]^{1/2} \ll t_0$. We note that if the length scale L_X is reached before L_1, which is typical for $t_0 \lesssim \max\{|\gamma_{c0}|, |\gamma_{s0}|\}$, one can find suppression of the transition temperature instead of enhancement (see solid curve in the inset to Fig. 12). After the length scale L_1, the second step of RG flow starts, where in Eq. (42) one can neglect terms proportional to t compared to the disorder-independent term $-2\gamma_c^2$. Thus the Cooper interaction γ_c flows according to the standard BCS RG equation for a clean system with the initial value $\gamma_c(L_1) \sim t(L_1)$ rather than γ_{c0}. Hence we find the following rough estimate for the transition temperature: $\ln 1/(T_c\tau) \sim 2\ln L_1/l + 1/|\gamma_c(L_1)| \sim [t_0(\gamma_{s0} - 2\gamma_{c0})]^{1/2} \gg \ln 1/(T_c^{\rm BCS}\tau)$, see Appendix B for details.

In full analogy with the case of preserved spin-rotation invariance, if the disorder scattering rate $1/\tau$ exceeds the Debye frequency ω_D, the starting point of the RG flow will be likely located not far from the BCS line, $\gamma_{s0} = -\gamma_{t0} = -\gamma_{c0}$ (see Sec. II C). For such initial conditions, the dependence of $T_c/(T_c + T_c^{\rm BSC})$ on t_0 is shown in the inset to Fig. 12 by the dashed curve. As in the case of preserved spin invariance, for bare interaction parameters on the BCS line, there is no initial decrease of transition temperature with increase of t_0. For a given γ_{c0}, a deviation from the BCS line in the initial conditions towards larger (smaller) values of γ_{s0} increases (decreases) the relative enhancement of the transition temperature, $T_c/T_c^{\rm BSC}$. We emphasize that inspite of the antilocalization at the noninteracting fixed point the multifractality enhances the interaction in the Cooper channel.

V. RESISTANCE IN ZERO MAGNETIC FIELD

Within the NLSM approach, physical observables can be written as correlation functions of the matrix field Q. In particular, the conductivity obtained by evaluating a linear response to an electromagnetic field in the framework of the NLSM theory with the action (1) can be expressed in the following way:

$$\sigma(i\omega_n) = -\frac{g}{16n}\left\langle \mathrm{Tr}\left[J_n^\alpha, Q(\boldsymbol{r})\right]\left[J_{-n}^\alpha, Q(\boldsymbol{r})\right]\right\rangle + \frac{g^2}{128n} \times \int d\boldsymbol{r}' \left\langle \mathrm{Tr}\, J_n^\alpha Q(\boldsymbol{r})\nabla Q(\boldsymbol{r})\, \mathrm{Tr}\, J_{-n}^\alpha Q(\boldsymbol{r}')\nabla Q(\boldsymbol{r}')\right\rangle. \tag{43}$$

Here, $\omega_n = 2\pi T n$ is a Matsubara frequency, the expectation values are defined with respect to the action (1), and

$$J_n^\alpha = \frac{t_{30} - t_{00}}{2} I_n^\alpha + \frac{t_{30} + t_{00}}{2} I_{-n}^\alpha. \tag{44}$$

As usual, the static conductivity σ can be obtained after the analytic continuation of Eq. (43) to real frequencies: $i\omega_n \to \omega + i0^+$ and, then, taking the limit $\omega \to 0$. At the classical level, $Q = \Lambda$, one finds $\sigma = g$.

The RG equations derived in this work describe the renormalization of the couplings in the NLSM action with the running spatial scale L. As such, these equations yield physical observables (e.g., the resistivity) of a finite size sample at $T = 0$. At finite temperature T, the conductivity can be evaluated in two steps. At the first step, the action (1) is renormalized from the energy scale $1/\tau$ down to T. Thus the bare parameters in the action (1) are substituted by the parameters at the length scale L_T: $g \to 2/[\pi t(L_T)]$, $\gamma_{s,t,c} \to \gamma_{s,t,c}(L_T)$, and $Z_\omega \to Z_\omega(L_T)$. Their dependence on L_T is governed by RG equations (23)–(27). At the second step, the Kubo formula (43) is evaluated under the assumption that in the NLSM action (1) Q fields are restricted by the temperature in the ultraviolet. We assume L_T to be such that $t(L_T) \ll 1$ and $|\gamma_c(L_T)| \gg 1$. Then, the conductivity can be written as

$$\sigma(T) \simeq \frac{2}{\pi t(L_T)} - \frac{\pi}{2}\gamma_c(L_T)\ln\frac{L_\phi}{L_T}. \tag{45}$$

This result illustrates the fact that at finite temperature there is always a difference between the physical resistance $\rho = 1/\sigma$ and the coupling parameter t in the NLSM action. The second term in Eq. (45) is the Maki-Thompson contribution [68–71], which is the dominant inelastic contribution to the resistivity. (We neglect the smaller Aslamazov-Larkin contribution [67].)

Comparing the two terms in Eq. (45), we find that the inelastic contribution becomes of the same order as the renormalized impurity-scattering conductivity (given by the NLSM coupling) at the scale L_X determined by the condition $t(L)|\gamma_c(L)| = 1$. Remarkably, this is the same scale as is found from the condition of validity of the one-loop RG, see Sec. III. Thus, at scales shorter than L_X, or, equivalently, at temperatures larger than T_X, the temperature dependence of the physical resistivity is dominated by the RG behavior of $t(L)$. Upon approaching the transition temperature, the role of the inelastic contribution controlled by $\gamma_c(L)$ increases. In the narrow temperature interval $T_c < T < T_X$ the conductivity is dominated by the inelastic contribution. As we have already discussed in Sec. IV, the width of this interval is

$$(T_X - T_c)/T_c \sim t(T_X). \tag{46}$$

At the transition point T_c, the running coupling γ_c diverges, $|\gamma_c(T_c)| = \infty$ and Eq. (45) formally yields $\rho(T_c) = 0$.

In fact, the behavior of the conductivity in the fluctuation region, $|T - T_c|/T_c \sim t(T_X)$, is additionally affected by superconducting phase fluctuations. These fluctuations lead to the BKT character of the actual superconducting phase transition. The corresponding shift of the transition temperature is, however, small (as has been already mentioned in the end of Sec. IV A 1) and is not important for our results. More specifically, as was argued by Beasley, Mooij, and Orlando [80], the shift is determined by disorder strength, $(T_c - T_{\rm BKT})/T_c \sim t$, for $t \ll 1$, see also Refs. [81,82]. The behavior of the true $\rho(T)$ in the fluctuation (BKT) region will be addressed elsewhere [54]. Let us only mention here that the value of the NLSM coupling $t(T_X)$ at the entrance to the fluctuating region determines [54] the stiffness of the phase fluctuations in the BKT region $T_{\rm BKT} < T < T_X$ and the relevant value of t in the shift of $T_{\rm BKT}$ with respect to T_c. Because of the renormalization of t, this value may strongly differ from the bare (high temperature) Drude value of the resistance t_0 (cf. Ref. [14]).

Ignoring the above mentioned subtleties of the behavior of $\rho(T)$ in the narrow fluctuation region $|T - T_c|/T_c \sim t(T_X)$ around the mean-field T_c, the behavior of the electrical resistance in the whole range of temperatures is well described by $\rho(T) = 1/\sigma(T)$ with $\sigma(T)$ given by Eq. (45). To relate the length scale L_c with the transition temperature T_c, one

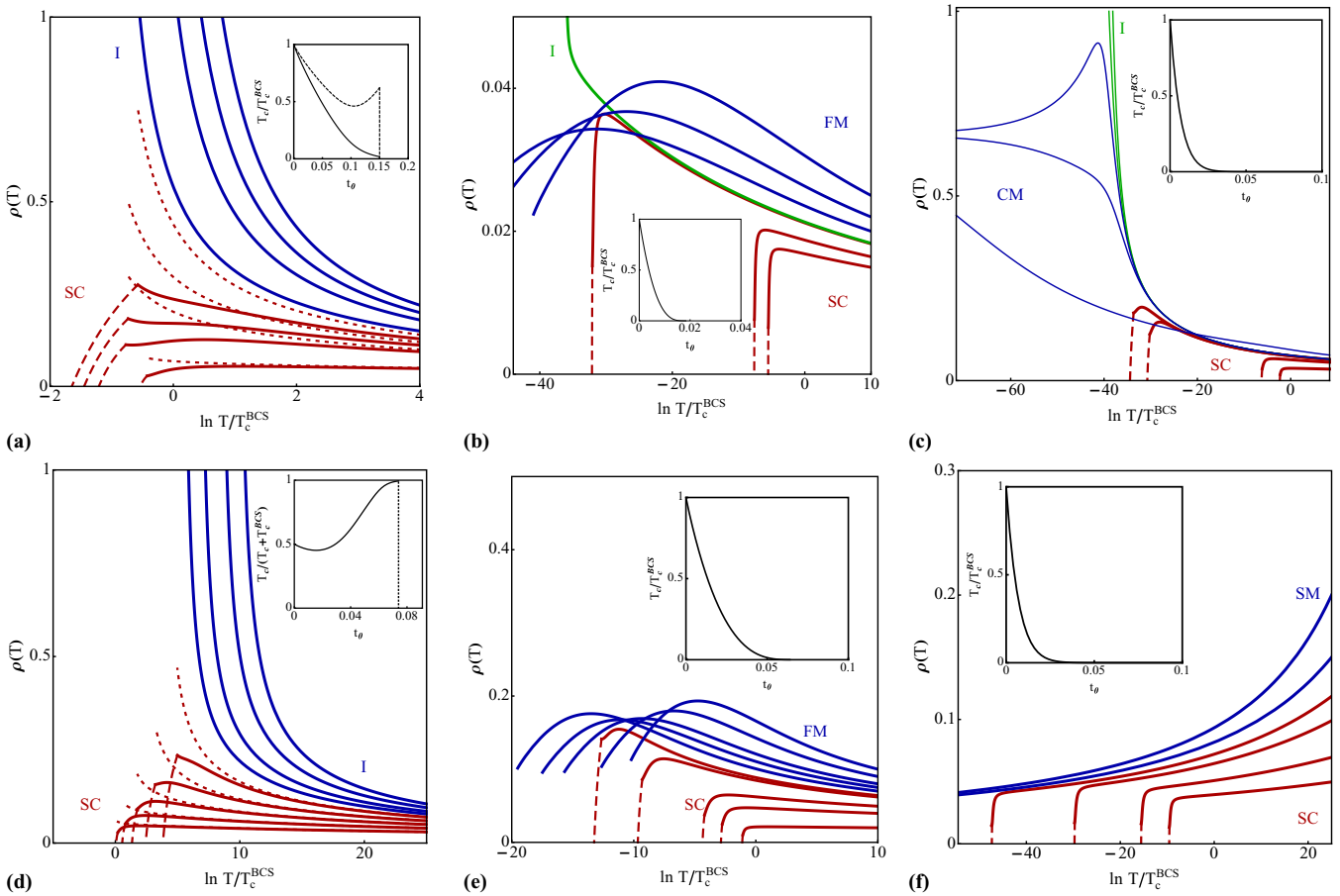

FIG. 14. (Color online) Dependence of the resistance ρ on temperature T and T_c on t_0 for the cases of the Coulomb [(a)–(c)] and short-ranged [(d)–(f)] interactions. Parameters are the same as in Figs. 3, 4, 6, 10, 8, and 12, respectively. (a), (b), (d), and (e) correspond to the case of preserved spin-rotational symmetry, (c) and (f) to the broken spin-rotational symmetry calculated from Eq. (45). The dashed parts of the curves correspond to the "fluctuation" region $T < T_X$. Dotted red curves in panels (a) and (d) show temperature dependencies of t for $T > T_X$. The dependence of T_c on t_0 is shown in the insets (solid curve). The dependence of T_X on t_0 is shown by the dashed line in the inset to (a). For all other insets T_X coincides with T_c within our accuracy.

needs to know the relevant value D_c of the diffusive coefficient $D \sim 1/(tZ_\omega)$. It is obtained by using the values for t and Z_ω at the scale L_X (which is the border of validity of the one-loop RG and simultaneously is the beginning of the fluctuation region). The transition temperature is given by $T_c \sim D_c L_c^{-2}$, see Eq. (29).

We present the dependence of $\rho(T)$ obtained in accordance with Eq. (45) (for simplicity, we dropped the logarithmic factor in the inelastic term; this does not qualitatively affect the plots) for the cases of preserved and broken spin-rotational symmetry and Coulomb and short-ranged interactions in Fig. 14. We mention that due to Maki-Thompson correction the resistance drops very fast (dashed curves in Fig. 14) since $|\gamma_c(L_X)| \gg 1$ and, consequently, $(T_c - T_X)/T_X \sim \rho(T_X) \ll 1$. Therefore the temperature T_X, at which resistivity has the maximum, can be used as an estimate of the superconducting transition temperature. In order to plot $\rho(T)$ in the fluctuation region $T < T_X$ where the one-loop RG becomes insufficient, we evaluated $\gamma_c(T)$ near T_c keeping only the BCS term $-2\gamma_c^2$ in the RG equation for γ_c.

We note that our approach for evaluating the temperature dependence of resistivity is different from that of Refs. [72,73]. In these works, the full set of the first-order perturbative quantum corrections to the conductivity was computed at finite temperature in the presence magnetic field. However, such approach assumes that the T- and H-dependent corrections to the bare Drude conductivity $1/t_0$ are small. In our approach, we split the effects leading to temperature variation of the conductivity into two parts: those related to virtual and real processes. Then virtual processes are taken into account within the RG formalism (they are included in the renormalization of t). This allows us to consider also situations with strong renormalization, $t(L_T) \gg t_0$, i.e., cases in which "quantum corrections" are large in comparison with $1/t_0$.

VI. MAGNETORESISTANCE

A transverse magnetic field introduces an additional length scale l_H (magnetic length) into the problem. In what follows, we assume that it is larger than the mean free path, $l < l_H$. Let us start from $T = 0$. In case of weak magnetic field, $l_H \gg L_c$, the superconducting instability at $L = L_c$ remains unaffected. For strong magnetic fields, $l_H \ll L_c$, the superconducting phase is destroyed by the magnetic field since the growth

of $|\gamma_c|$ within RG equations is stopped at the length scale l_H. Then the critical magnetic field can be estimated as $l_{H_c} = L_c$. This results in the standard relation, $H_c \sim T_c/D_c$. At $H < H_c$, the physical resistance ρ should vanish in the infinite system, $L = \infty$. For systems of finite size $L > L_c$, the resistance is not zero and is determined by the nontrivial configurations of the order parameter in the presence of a magnetic field.

At finite temperature, the critical magnetic field is a function of temperature. However, at $T \ll T_c$, this effect is small and can be neglected. In order to evaluate the magnetoresistance at $T \ll T_c$ and for $H > H_c$, we use a two-step RG procedure. At the first step of RG, the interaction in the Cooper channel grows towards instability. The first step ends at the length scale l_H with some values $t(l_H)$ and $\gamma_{s,t,c}(l_H)$. At $L > l_H$, the cooperon modes become ineffective and the second step of the RG procedure starts. For length scales $l_H < L < L_T$, RG equations do not contain cooperon contributions:

$$\frac{dt}{dy} = t^2[f(\gamma_s) + nf(\gamma_t)], \tag{47}$$

$$\frac{d\gamma_s}{dy} = -\frac{t}{2}(1+\gamma_s)(\gamma_s + n\gamma_t), \tag{48}$$

$$\frac{d\gamma_t}{dy} = -\frac{t}{2}(1+\gamma_t)[\gamma_s - (n-2)\gamma_t], \tag{49}$$

$$\frac{d\ln Z_\omega}{dy} = \frac{t}{2}(\gamma_s + n\gamma_t). \tag{50}$$

Here, $y = \ln L/l_H$ and the initial values of couplings in Eqs. (47)–(50) are given by $t(l_H)$ and $\gamma_{s,t,c}(l_H)$. Similarly to the case of zero magnetic field, in order to find the physical resistance $\rho(T,H)$, one needs to take into account non-RG corrections to conductivity due to superconducting

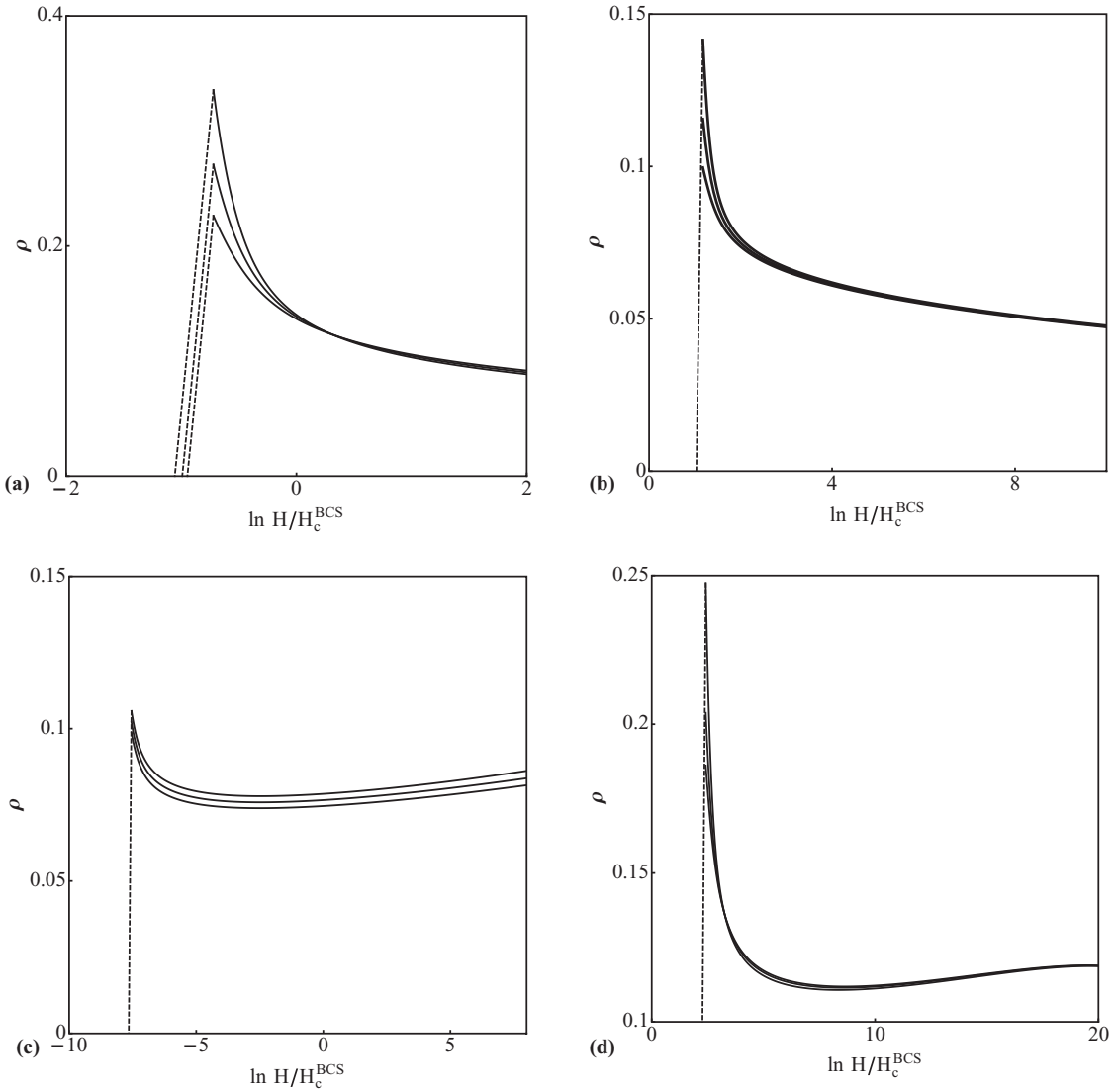

FIG. 15. Dependence of the resistance ρ on the perpendicular magnetic field H for the cases of preserved [(a) and (b)] and broken [(c) and (d)] spin-rotational symmetries. (a) and (c) correspond to the case of the Coulomb interaction, (c) and (d) to the short-ranged interaction. Solid curves are obtained from Eq. (51). The dashed lines indicate the drop of magnetoresistance to zero at $H = H_c$. The parameters used are as follows: (a) $\gamma_s = -1$, $\gamma_{c0} = -0.45$, $\gamma_t = 1$, $t_0 = 0.1$, $T = T_c/2$, $T_c/4$, $T_c/8$, (b) $\gamma_{s0} = 0.1$, $\gamma_{c0} = -0.1$, $\gamma_{t0} = -0.1$, $t_0 = 0.05$, $T = T_c/2$, $T_c/4$, $T_c/16$ (c) $\gamma_s = -1$, $\gamma_{c0} = -0.12$, $t_0 = 0.053$, $T = T_c/2$, $T_c/4$, $T_c/8$, and (d) $\gamma_{s0} = 0.05$, $\gamma_{c0} = -0.05$, $t_0 = 0.2$, $T = T_c/2$, $T_c/16$, $T_c/256$.

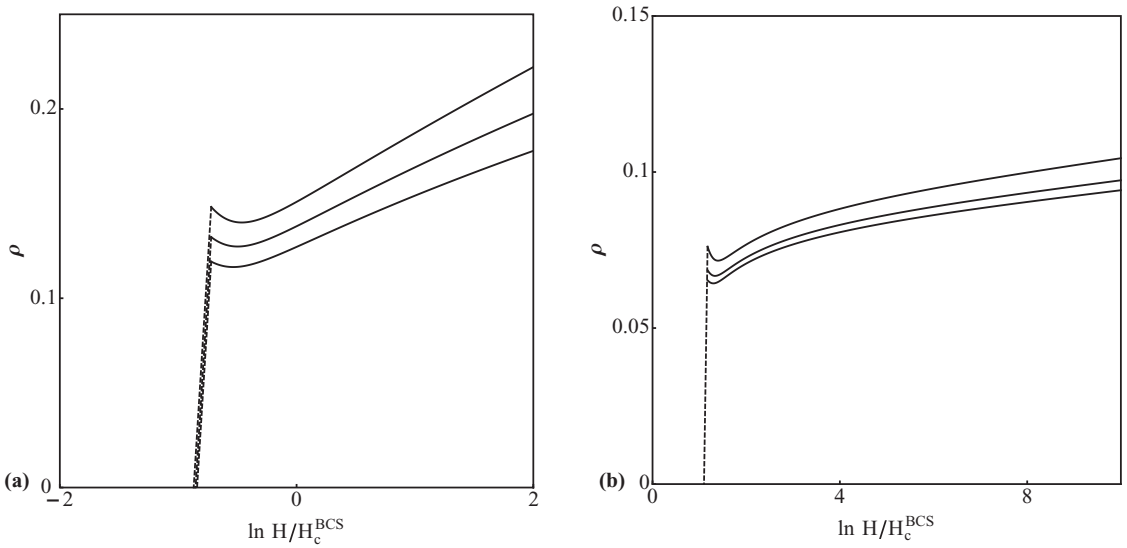

FIG. 16. Dependence of the resistance ρ on parallel magnetic field H for the case of preserved spin-rotational symmetry for the case of the Coulomb (a) and short-ranged (b) interactions. Solid curves are obtained from Eq. (56). The dashed lines indicate the drop of magnetoresistance to zero at $H = H_{cZ}$. The parameters used are as follows: (a) $\gamma_s = -1$, $\gamma_{c0} = -0.45$, $\gamma_t = 1$, $t_0 = 0.1$, $T = T_c/2$, $T_c/4$, $T_c/8$ and (b) $\gamma_{s0} = 0.1$, $\gamma_{c0} = -0.1$, $\gamma_{t0} = -0.1$, $t_0 = 0.05$, $T = T_c/2$, $T_c/4$, $T_c/16$.

fluctuations. In particular, for $|\gamma_c(l_H)| \gg 1$, the leading-order correction (which is the dominant one for magnetic fields not too close to the critical field H_c) [74] yields:

$$\sigma(T,H) = \frac{2}{\pi t(L_T)} - \frac{4}{3\pi} \ln|\gamma_c(l_H)|. \tag{51}$$

It should be emphasized that $t(L_T)$ in Eq. (51) in fact depends on the magnetic field via the two-step RG procedure. At $H = H_c$, the physical resistivity $\rho(T,H)$ should vanish. This happens due to higher-order Cooper-channel corrections of non-RG type in Eq. (51), which become important in the fluctuation region (i.e., near H_c) and make $\rho(T,H_c) = 0$ in spite of the finite value $t(L_T)$.

Let us mention that, due to renormalization on ballistic scales, $L < l$, [75], one can also expect an effect of the magnetic field on the initial values of parameters (t_0, γ_{c0}, γ_{t0}, and γ_{s0}) for RG equations (23)–(27). This leads to a shift of the length scale at which γ_c diverges. As a consequence, an additional dependence of the transition temperature on H appears. We do not take this effect into account.

The dependence of the resistivity on the perpendicular magnetic field H at different temperatures below T_c is illustrated in Fig. 15. The H dependence of resistivity at fixed $T < T_c$ is qualitatively similar to the $\rho(T)$ dependence at zero magnetic field. For all four symmetry classes, the magnetoresistance shows a maximum that grows with decreasing temperature. It is worth mentioning that the maximum should become arbitrarily high as $T \to 0$, yielding a giant magnetoresistance in agreement with experimental observations. We do not plot these curves here since we cannot controllably evaluate the resistance for $t \gtrsim 1$ within the one-loop RG.

In addition to l_H, the perpendicular magnetic field induces another length scale l_Z related to the Zeeman splitting. Usually, one expects that $l_H \ll l_Z$ since the latter can be estimated as $l_Z \sim l_H/\sqrt{(1+\gamma_t(l_Z))t(l_Z)g_L}$. Here, g_L stands for the Landé g factor. Due to Zeeman splitting, the magnetic field suppresses the triplet diffuson modes with $S_z = \pm 1$ and singlet and triplet cooperon modes with $S_z = 0$ at length scales $L > l_Z$.

In the case of fully broken spin-rotational symmetry, there is no triplet modes, and thus the orbital and Zeeman effects of the magnetic field on RG equations are the same. Therefore there is in fact only one length scale associated with the magnetic field $l_{HZ} = \min\{l_H, l_Z\}$. A similar conclusion holds for the case of partially broken spin-rotational symmetry, $n = 1$. Therefore, in the absence of spin-rotational symmetry, we do not need to consider the effect of the Zeeman splitting separately.

For the case of preserved spin-rotational symmetry, the orbital and Zeeman effects are different. For $l_H \ll l_Z$, the RG equations (47)–(50) should be modified at length scales $L > l_Z$ since two out of three triplet diffusive modes becomes massive and do not lead to infrared divergences:

$$\frac{dt}{dy} = t^2[f(\gamma_s) + f(\gamma_t)], \tag{52}$$

$$\frac{d\gamma_s}{dy} = -\frac{t}{2}(1+\gamma_s)(\gamma_s+\gamma_t), \tag{53}$$

$$\frac{d\gamma_t}{dy} = -\frac{t}{2}(1+\gamma_t)[\gamma_s+\gamma_t], \tag{54}$$

$$\frac{d\ln Z_\omega}{dy} = \frac{t}{2}(\gamma_s+\gamma_t). \tag{55}$$

Here, $y = \ln L/l_Z$ and the initial values of couplings in Eqs. (52)–(55) are given by $t(l_Z)$ and $\gamma_{s,t,c}(l_Z)$. Therefore, in this case, a three-step RG scenario is realized.

In the opposite case, $l_H \gg l_Z$, the system at length scales $l < L < l_Z$ is described by RG equations (23)–(27) (with $n = 3$). Then, for $l_Z < L < l_H$, RG equations transform into Eqs. (52)–(55) with $f(\gamma_s)$ substituted by $1 + f(\gamma_s)$ (weak-localization correction remains intact in the presence of Zeeman splitting only). For larger length scales, $L > l_H$, the system is governed by RG Eqs. (52)–(55). The suppression of

weak-localization correction does not change the qualitative behavior of the RG flow.

In the case of a parallel magnetic field, the scale l_H does not appear since the orbital effect of the magnetic field can be neglected provided $l_Z \ll L_T \ll l_H^2/d$, where d is the typical width of the film. We thus obtain a two-step RG scenario in which RG equations are modified at the length scale l_Z. As before, in order to find the physical resistance $\rho(T,H)$, one needs to take into account non-RG corrections to the conductivity due to superconducting fluctuations. For $|\gamma_c(l_H)| \gg 1$, we get [76]

$$\sigma(T,H) = \frac{2}{\pi t(L_T)} + \frac{4}{\pi} \ln|\gamma_c(l_Z)|. \tag{56}$$

The parallel-field magnetoresistance for the case of preserved spin-rotational symmetry is illustrated in Fig. 16 for several values of temperature below T_c. The dependence of the resistivity on the parallel magnetic field at fixed temperate below T_c is essentially different from the $\rho(H)$ dependence in the case of a transverse field. First, the maximum at an intermediate field is much less pronounced in the case of a parallel field. Second, the parallel-field resistivity increases with H in strong fields, contrary to the case of a transverse magnetic field.

VII. DISCUSSION

In this section, we discuss our results and their implications (in particular, for the phase diagrams of SITs), the relation to previous works, as well as limitations and possible generalizations of the RG scheme used.

A. Relevant superconducting systems

1. Symmetry of the order parameter

First of all, we note that our theory is derived for conventional (BCS) s-wave superconductors, where the effect of s-wave nonmagnetic impurities on the superconducting gap and T_c is absent at the semiclassical level ("Anderson theorem"). Our theory can be generalized to describe the multiband case with s-wave (or $s_\pm$-wave) pairing. On the other hand, in unconventional (p-wave or d-wave) superconductors, impurities do suppress the superconductivity. As a result, the diffusion regime does not develop there: either the pairing is so strong that the superconductivity is established already on the ballistic scales, or disorder kills the superconductivity. Therefore, in such systems, the enhancement of superconductivity by localization (which occurs on the diffusive scales in s-wave superconductors) is impossible.

However, in such superconductors, a secondary superconducting transition due to the pairing of Dirac quasiparticles is possible (which may change the true gap symmetry as, e.g., $d \to d + is$, thus opening the superconducting gap at the nodal points of the spectrum), see e.g., Ref. [77] for review. This transition can be described by the RG equations generalized for the novel symmetry classes (see Refs. [43,78]). Furthermore, the peculiar form of the Fermi surface near half-filling (nesting) may lead to additional emergent symmetries specific to this problem [79]. In particular, various novel interaction couplings would be possible by the enhanced symmetry. Importantly, the Coulomb interaction between the quasiparticles in this system is screened by the d-wave condensate. Thus one can expect a disorder-induced enhancement of the critical temperature for the secondary superconducting transition.

2. Macroscopic homogeneity vs granularity

In this paper, we assume that the system is macroscopically homogeneous and do not discuss granulated superconductors characterized by weak (Josephson) tunneling between macroscopic superconducting islands. In granular systems, additional energy scales appear such as Josephson and charging energies. We expect, however, that the peculiarities of inhomogeneous superconductors, while leading to the emergence of intermediate crossover regimes, do not affect the universality of the (zero-T) SIT governed by the symmetries of the system. The situation resembles the problem of Anderson metal-insulator transition, which is believed to be universal independently of whether the microscopic disorder model is "homogeneous" (e.g., white-noise disorder) or inhomogeneous (tunnel-coupled grains).

At the same time, the finite-T behavior of the resistivity in granular systems will be influenced by the presence of additional energy scales and thus differ from that of a homogeneous system. On the other hand, the behavior close to the transition will be governed by a similar BKT physics both for granular and homogeneous systems, see the discussion in Sec. V.

B. Screening of long-ranged Coulomb interaction

Above, we have considered separately the two models of electron-electron interaction: the long-range Coulomb interaction and short-ranged interaction. In the latter case, the superconductivity was shown to be enhanced by Anderson localization in a wide parametric range. In realistic electronic systems, there are two mechanisms that can suppress the Coulomb interaction and make it effectively short-range in a certain interval of length scales: (i) large dielectric constant of the medium, and (ii) screening by a nearby external metallic layer, which results in a less singular dipole-dipole type interaction at scales larger than the distance to the gate.

In the presence of a dielectric medium, the interaction constant in the singlet channel acquires a momentum dependence:

$$\gamma_s(q) = \tilde{\gamma}_s - (1+\tilde{\gamma}_s)\frac{\varkappa}{\varkappa+q}, \quad \varkappa = \frac{2\pi e^2}{\varepsilon}\frac{\partial n}{\partial \mu}. \tag{57}$$

Here, $\tilde{\gamma}_s$ is the irreducible short-ranged part of the singlet interaction amplitude, ε is the dielectric constant of the medium, $\varkappa$ is the inverse screening length, and $\partial n/\partial\mu$ is the thermodynamic density of states (which is not renormalized by the interplay of disorder and interaction).

Usually, the condition $\varkappa^{-1} \ll l$ (the screening radius is smaller than the mean free path) is fulfilled, and for length scales $L \geqslant l$, one finds $\gamma_s = -1$, which is a hallmark of long-ranged Coulomb interaction. However, for a large dielectric constant the opposite relation, $l \ll \varkappa^{-1}$, is possible. In this case, at length scales $l \leqslant L \leqslant \varkappa^{-1}$, the long-ranged Coulomb interaction provides a small contribution to γ_s and is indistinguishable from the short-ranged interaction within the

RG. If the scale L_c is smaller than $\varkappa^{-1}$, then the long-ranged Coulomb interaction does not affect the transition temperature. Therefore, for a large dielectric constant such that $\varkappa l \ll 1$, the long-range Coulomb interaction does not influence the superconducting temperature provided the following condition holds:

$$e^2\varkappa/t_0 \lesssim T_c. \tag{58}$$

When the condition (58) is not fulfilled, the long-ranged nature of Coulomb interaction screened by a high dielectric constant becomes effective at large scales $L \gtrsim \varkappa^{-1}$ before the superconductivity occurs. While for scales shorter than the screening radius the coupling constant γ_c is enhanced by short-range interaction as compared to the BCS result, at larger scales, the Coulomb repulsion starts working in the opposite direction. As a result, one encounters the competition between the enhancement and suppression of the superconductivity. In this situation, a more general scheme of including the Coulomb repulsion is necessary.

The simplest generalization of the RG procedure would be then a two-step RG. At the first step, for $L \lesssim \varkappa^{-1}$, one uses the short-ranged RG with the initial values of all interaction couplings determined by the short-range attraction (BCS line). At the second step, for $L \gtrsim \varkappa^{-1}$, the RG equations are switched to the Coulomb case with $\gamma_s = -1$ and the initial values of other couplings given by the outcome of the first step. However, within this two-step procedure, the singlet amplitude γ_s is instantly switched at $L \sim \varkappa^{-1}$ from the value dominated by the phonon-induced attraction, $\tilde{\gamma}_s(L)$, to the Coulomb dominated value $\gamma_s = -1$, implying the change of its sign.

In order to smoothly describe the crossover regime, an interpolating flow equation for the coupling γ_s defined in Eq. (57) can be derived by replacing the momentum by L^{-1}. In particular, for the case of preserved time and spin-rotational symmetries, this yields [cf. Eq. (19)]

$$\frac{\partial\gamma_s}{\partial y} = -\frac{t}{2}(1+\gamma_s)\left(\gamma_s + 3\gamma_t + 2\gamma_c + 4\gamma_c^2\right)\frac{1}{Z_L+1} - (1+\gamma_s)\frac{Z_L}{Z_L+1}. \tag{59}$$

In this flow equation, we have introduced the new coupling $Z_L = \varkappa L$ satisfying

$$\frac{\partial Z_L}{\partial y} = Z_L. \tag{60}$$

In Eq. (60), we have used the fact that $\varkappa$ is not renormalized by interactions, since it is determined by the electron charge and the thermodynamic density of states $\partial n/\partial\mu$ [32]. If the background medium is characterized by a momentum-dependent dielectric function $\epsilon(q)$, this would modify Eq. (60) accordingly. The RG flow governed by Eqs. (59) and (60) can be viewed as a two-step RG procedure with a short-ranged singlet amplitude $\gamma_s \simeq \tilde{\gamma}_s(1+Z_L) - Z_L$ at the first step.

We plot the results of the numerical evaluation of the renormalization of the Cooper-channel coupling γ_c for $\ln(1/\varkappa l) = 2$ using the two-step and interpolating RG procedures in Fig. 17. One can see that the enhancement of the superconductivity at the first (short-ranged) step of the RG is more important than the suppression at the second (long-ranged) step. As shown in the inset, the overall enhancement of the superconductivity takes place (for chosen values of the bare interactions and resistivity) for $(\varkappa l)^{-1} \gtrsim 3 \div 4$. For larger screening lengths, both the two-step and interpolating RG procedures yield close results for the enhancement of T_c.

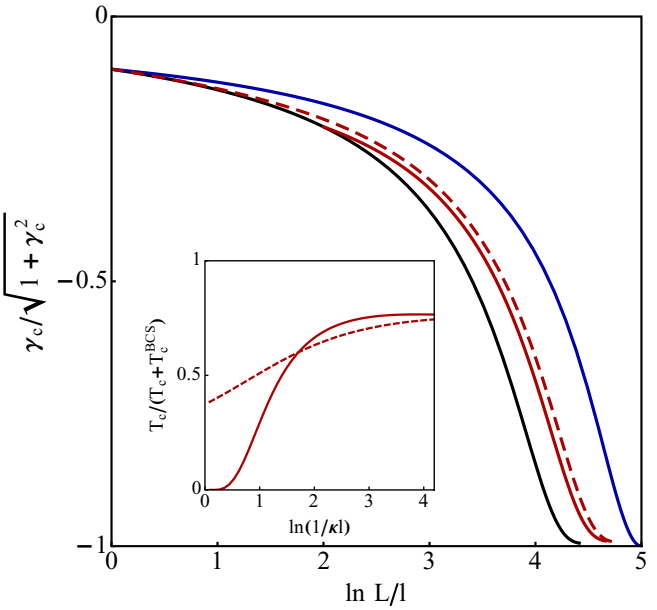

FIG. 17. (Color online) Effect of a high dielectric constant on the renormalization of Cooper-channel coupling γ_c. Black curve corresponds to the solution of RG equations (33)–(36) for $\gamma_{c0} = \gamma_{t0} = -\gamma_{s0} = -0.1$, and $t_0 = 0.05$. Blue curve corresponds to the behavior of γ_c on L for the clean BCS case. Red curve is obtained from the numerical solution of the two-step RG equations for $\ln(1/\varkappa l) = 2$. Red dashed curve is obtained from the numerical solution of the crossover RG equations (59) and (60). (Inset) Dependence of $T_c/(T_c + T_c^{\mathrm{BCS}})$ on $\ln(1/\varkappa l)$ for two-step (solid) and crossover (dashed) RG equations.

The long-range Coulomb repulsion can also be screened by a nearby metallic layer. Specifically, the electron-electron repulsion can be considered as short-ranged on scales L larger than the spacer width w_s. When the mean-free path is larger than w_s, we have the short-range case from the very beginning. In the opposite case $w_s \gg l$, without additional screening by the dielectric medium (i.e., for $\varkappa L \gg 1$) the RG procedure corresponds to the Coulomb case $\gamma_s = -1$ [up to small corrections of the order of $(\varkappa w_s)^{-1} \ll 1$] for scales $L \lesssim w_s$. For larger scales, the interaction becomes of the dipole-dipole type, but the singlet interaction constant inherited from the first step remains Coulomb-like, $\gamma_s \simeq -1$. Therefore a metallic layer placed at the distance $w_s \gg l$ is not sufficient to screen the Coulomb repulsion such that the superconductivity would be enhanced. However, the combination of the screening by a medium with a large dielectric constant (see above) and by the metallic layer does lead to the enhancement of the superconductivity as compared to the cases when these screening mechanisms are considered separately. Indeed, these two mechanisms make the interaction effectively short-ranged (with $|\gamma_s| < 1$) for short and large scales, respectively. In particular, for $\varkappa w_s \ll 1$, there is no room for the Coulomb regime at all.

C. Enhancement of superconductivity for short-range repulsion

Most of experiments on the superconducting transition in 2D films have been performed without screening the long-range component of the interaction. It is desirable to explore whether the mechanism of the enhancement of superconductivity addressed in the present work may be employed in practice to obtain structures with substantially enhanced T_c. The key condition is a suppression of the long-range component of the Coulomb interaction [37,38]. This opens a new way for searching novel materials exhibiting high-temperature superconductivity: one needs the combination of a large dielectric background constant and disorder in layered structures.

As mentioned in Introduction, 2D superconductivity has been recently realized in interfaces between two oxides, in particular, in $LaAlO_3/SrTiO_3$ interfaces [16,17]. These systems possess unique electrostatic properties owing to the giant dielectric constant of $SrTiO_3$. In particular, the long-range component of the Coulomb interaction is expected to be strongly screened in such materials. Although currently, the highest T_c reached in such materials is rather low as compared to high-T_c materials, the dependence of T_c on the conductivity of a normal state is nonmonotonic, which agrees with the localization-induced mechanism of the superconductivity enhancement. Further investigations are required to identify the ways for increasing T_c in strongly screened oxide interfaces, and to analyze optimal materials, structure design, and operation regimes, depending on the microscopic details.

A possible route for increasing the superconducting transition temperature in these materials is based on further suppression of the long-range Coulomb interaction by designing a double-interface structure with a $LaAlO_3$ layer sandwiched between two $SrTiO_3$ oxides. In such a setup, already ten atomic layers of $LaAlO_3$ are sufficient, so that the screening properties of the sample would be fully determined by the giant dielectric constant of $SrTiO_3$. At the same time, the two interfaces would be coupled by the interlayer interaction, similarly to the Coulomb drag problem in double-layer structures. The corresponding generalization of the sigma model would include an additional degree of freedom (a pseudospin in the interface space). Furthermore, the doping of $SrTiO_3$ layers away from the interfaces can produce an effective metallic gate made of the same material.

A simpler setup would involve an amorphous superconducting film placed on a $SrTiO_3$ substrate (again possibly doped away from the interface) with high dielectric constant instead of more conventional SiO_2 or Al_2O_3 insulating substrates[1] typically used in experiments on the SIT. On the other side of the substrate, one can place a metallic gate, thus realizing both mechanisms of screening discussed above. An interesting possibility of arranging a closely located metallic layer is provided by BN-graphene heterostructures [83] with gated graphene layer serving as a metallic gate and BN playing a role of a thin spacer. In this situation, a generalization of the RG equations (23)–(27) to the case of two layers (similar to Ref. [59]) needs to be done.

Recently, the superconductivity has been studied in layered material Li_xZrNCl [24]. It was found that with increase of doping level x the transition from insulator to superconductor occurs at $x \approx 0.05$. The critical resistance is close to $h/2e^2$. The temperature dependence of the resistivity, $\rho(T)$, measured across the transition is qualitatively similar to the one shown in Fig. 14(b). Near the SIT, the superconducting transition temperature increases with decrease of doping level: from $T_c(x \approx 0.12) \approx 11$ K to $T_c(x \approx 0.05) \approx 16$ K. Such behavior of superconducting temperature is in suit with the dependence $T_c(t_0)$ on BCS line predicted by our theory (see the inset to Figs. 6 and 7). Similar nonmonotonous dependence of T_c on disorder was measured in W and Mo based films (for an overview, see Ref. [84]).

In the case of repulsion in the particle-hole channel, the enhancement of superconductivity by Anderson localization (in comparison with the corresponding clean system) occurs in a certain range of (not too strong) interaction and (not too weak) disorder, see Figs. 5, 7, and 13. It should be stressed, however, that the critical temperature for short-range interaction is predicted to be always higher than T_c for unscreened Coulomb interaction when other parameters are kept fixed, see, e.g., the inset to Fig. 17. Therefore we propose to perform benchmarking experiments, measuring T_c in the same superconducting film placed on the substrate with a high dielectric constant (say, STO-material that screens the long-range Coulomb repulsion) and on the reference substrate with a not too high ε (say, SiO_2 or Al_2O_3). The experiments should be performed for sufficiently dirty samples (but still on superconducting side of the SIT), since the stronger disorder leads to a stronger difference between the critical temperatures in the two cases, see Fig. 18.

D. Relation to numerical results

Recent numerical calculations [85,86] demonstrate that disorder may indeed enhance the superconductivity in a certain range of parameters. These results should be contrasted with numerical simulations of a two-dimensional disordered Hubbard model with strong on-site attraction in small-size systems that yielded a monotonous suppression of T_c with increasing disorder [87]. The physics behind the results of our work develops for not too strong disorder and interaction, whereas Ref. [87] focused on the opposite limit. Specifically, we predict the enhancement of T_c by the Anderson localization in 2D when both disorder and interaction are weak: $|\gamma_{c0}| \ll t_0 \ll \sqrt{|\gamma_{c0}|} \ll 1$. In terms of the disordered Hubbard model used in numerical simulations [87], this regime corresponds to the following range of parameters: $|U| \ll V \ll \sqrt{|U|} \ll 1$, where U and V stand for dimensionless interaction and disorder.

It is the strong interaction U that allowed the authors of Ref. [87] to extract the information on superconducting properties from the simulation on a rather small system of 8×8 sites. As seen from Fig. 7, in the strong-coupling regime, our theory agrees with the numerics of Ref. [87]. Indeed, for strong attraction and strong disorder, our theory predicts a suppression of the mean-field T_c (and hence a suppression of the true critical temperature). The point is that, in realistic systems, the

[1]Recently, evidence for an order-of-magnitude increase of T_c in single-layer FeSe films placed on the $SrTiO_3$ substrate as compared to thicker FeSe films on conventional insulating substrates [22] has been reported in Ref. [89]. One might expect that, among other possible factors, the screening of the Coulomb interaction by the $SrTiO_3$ substrate plays an important role in this observation.

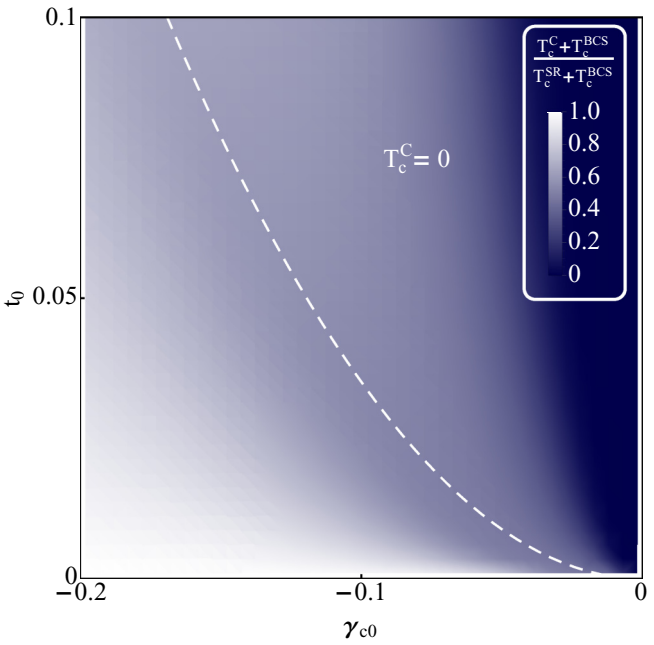

FIG. 18. (Color online) The case of broken spin-rotational symmetry. Comparison of superconducting transition temperature for the Coulomb interaction (T_c^C) and for the short-ranged interaction on the BCS line ($T_c^{\rm SR}$). The color indicates the ratio $(T_c^C + T_c^{\rm BCS})/(T_c^{\rm SR} + T_c^{\rm BCS})$. The dashed curve corresponds to the boundary of SC phase in the case of the Coulomb interaction.

attraction is normally considerably weaker (otherwise T_c would be given by the Debye energy and no challenge of obtaining high-temperature superconductivity existed) and this is precisely the range of γ_c where the enhancement of superconductivity is expected according to our predictions. The results of Ref. [87] may in addition reflect the difference between T_c and $T_{\rm BKT}$ in the strongly disordered case, see Sec. V. If one extrapolates the Beasley-Mooij-Orlando estimate [80] to the regime of strong disorder, $t_m \sim 1$, one gets $(T_c - T_{\rm BKT})/T_c \sim 1$. This correlates with the numerical findings of Ref. [87]: for strong disorder, $T_{\rm BKT}$ may be significantly lower than the mean-field T_c (this difference might be important near the SIT).

In fact, the disordered Hubbard model contains all the ingredients required for the enhancement of superconductivity by multifractality, but the range of optimal parameters requires large system sizes. To verify our prediction numerically within the disordered Hubbard model, one has to use weaker interaction and disorder and hence larger system sizes of $N \times N$ sites, where due to the logarithmic renormalization of couplings in 2D, N depends exponentially on the inverse disorder strength. Rough estimates yield at least $N \sim 30$–50 for the minimal system size where the enhancement can be detected. Indeed, in Ref. [85], where an enhancement of the superconductivity by disorder in a honeycomb lattice was detected for a certain range of parameters, the number of sites in the attractive Hubbard model was 900–1600, in consistency with the above estimate. At the same time, such system sizes are still much smaller than the sizes of real macroscopic systems where the regime required for a strong enhancement of T_c by our mechanism can be realized.

E. Beyond one-loop RG: Structure of the phase diagram

In Sec. IV, we have analyzed the one-loop RG equations for the cases of preserved and broken spin-rotational symmetry. As we have shown, the one-loop precision is applicable for $t \max\{1, |\gamma_c|\} \lesssim 1$, and therefore some fixed points of the full phase diagram remain unaccessible at this level, see gray areas in Figs. 1 and 9. Here, we discuss an expected structure of the full phase diagram, going beyond the one-loop RG equations. We will focus on the SIT part of the phase diagram, first disregarding the complications related to the appearance of additional phases such as the ferromagnetic (FM) phase for the case of preserved spin-rotational symmetry and the critical metal (CM) for the spin-orbit case. Furthermore, for simplicity, we consider the Coulomb case, $\gamma_s = -1$, which allows us to reduce the parameter space for the RG flow. We expect that the superconductor-insulator quantum phase transition is not sensitive to details of interactions and, therefore, concentrate on the simplest case of broken spin-rotational symmetry, where we have a two-parameter RG flow (for couplings t and γ_c).

In Fig. 19(a), we plot schematically the expected phase diagram for a physical electrical resistance ρ (that can differ from the NLSM coupling t as discussed in Sec. VI) and a parameter $\tilde{\gamma}_c$ ("generalized superconducting interaction") characterizing the superconducting correlations in the system. On the mean-field level, this parameter is just equal to γ_c, but beyond the mean-field description it also reflects order-parameter fluctuations and thus characterizes the overall superconducting coherence (hence tilde), diverging when the true 2D superconductivity is established. The superconducting fixed point is then located at $\rho = 0$ and $\tilde{\gamma}_c = -\infty$. As mentioned in Sec. V above, the SIT is most likely governed by the fixed point at $\rho = \rho_* \sim 1$ and $\tilde{\gamma}_c = -\infty$, see Fig. 19(a). The existence of such fixed point is compatible with the RG flows shown in Figs. 1 and 9. The SIT occurs through the separatrix connecting this fixed point with the trivial clean noninteracting fixed point $\rho = \tilde{\gamma}_c = 0$.

Two more possibilities compatible with Figs. 1 and 9 are as follows: (i) the fixed point at $\rho = \infty$ and $\tilde{\gamma}_c = -\infty$ is unstable and the SIT fixed point is located at $\rho \sim 1$ and $|\tilde{\gamma}_c| \sim 1$, see the right panel in Fig. 19(b) and (ii) the SIT fixed point is located at $\rho = \infty$ and $\tilde{\gamma}_c = -\infty$.

In both these cases, the flow towards the superconducting fixed point would occur in the presence of strong superconducting correlations for an arbitrary high resistivity. The existence of the SIT in granular systems (or 2D Josephson-junction arrays) provides a strong evidence against such a scenario. Indeed, in such strongly inhomogeneous systems, the superconductivity is established locally, but sufficiently strong disorder prevents vanishing of the total resistance.

At the same time, our one-loop RG analysis does not exclude the possibility of existence of an intermediate metallic phase around $\rho \sim 1$ at $\tilde{\gamma}_c = -\infty$, e.g., as shown in the left panel of Fig. 19(b). This metallic phase might be governed by either a segment of fixed points or by an attractive metallic fixed point. In both cases, this intermediate metallic phase would resemble a so-called "Bose metal" mentioned in Introduction. Experimental evidence for existence of such a phase was reported in literature. In the case of preserved spin-rotation invariance, we do not see any indications for

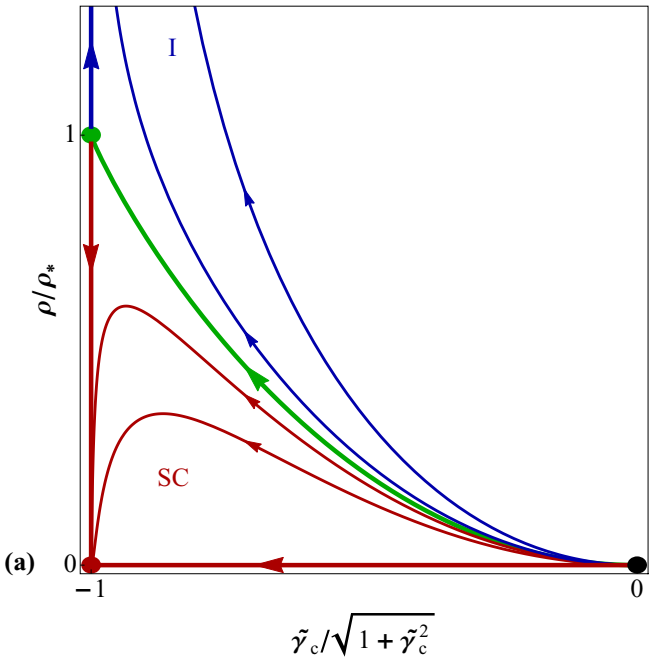

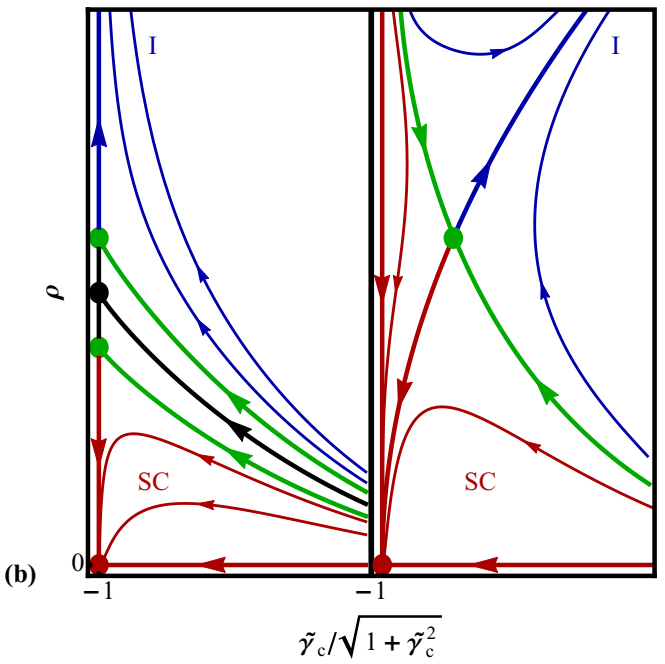

FIG. 19. (Color online) Sketch of possible RG flows for the SIT with the unstable fixed point at $\rho = \rho_*$ and $|\tilde{\gamma}_c| = \infty$ (a) and with the metallic phase at $\tilde{\gamma}_c = \infty$ [(b), left panel] or the fixed point at $\rho \sim 1$ and $|\tilde{\gamma}_c| \sim 1$ [(b), right panel].

such a scenario. For the spin-orbit class, our theory does suggest a critical-metal phase with resistivity of the order of resistance quantum, somewhat similar to the proposed "Bose metal." However, in the phase diagram this phase is separated from the superconductor by a narrow insulating region, so that the expected sequence of quantum phase transitions is SC–I–CM–I. More work is needed to prove or disprove the possibility of the intermediate metallic phase both within the NLSM formalism and experimentally.

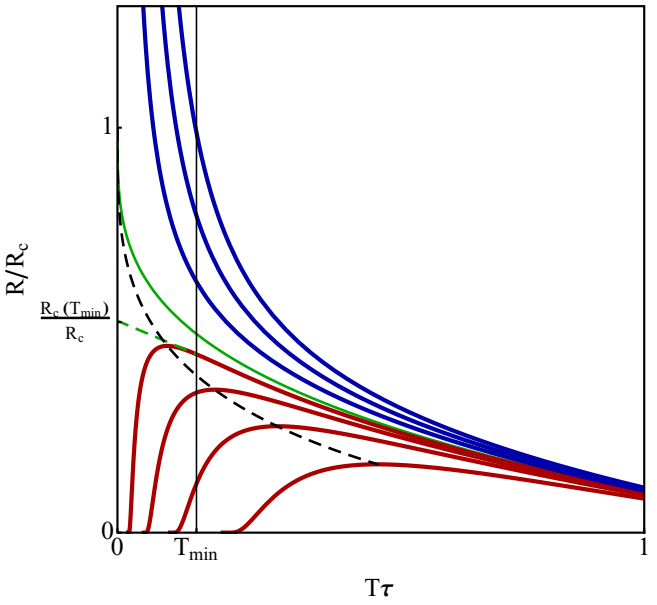

FIG. 20. (Color online) Sketch of a typical dependence $R(T)$ near the SIT. The black dashed curve demonstrates how the maximal resistance approaches the critical one with decrease of T. The solid green curve indicates the separatrix. The dashed green line demonstrates approximation to the critical resistance from the curves available for $T > T_{\min}$ (see text).

Returning to the phase diagram in Fig. 19(a), we emphasize that the SIT fixed point at $\rho_* \sim 1$ and $\tilde{\gamma}_c = -\infty$ is reached only at infinite RG scale, corresponding to exactly zero T. This implies that in realistic experiments (performed at finite temperature) the flow along the separatrix might seem as a flow towards an insulator. As a result, the critical value of resistance $R_c(T_{\min})$ inferred from the temperature dependence of the resistivity measured down to finite $T_{\min}$ might be lower than the true critical value $R_c = (h/e^2)\rho_*$, see Fig. 20. Moreover, the "critical" values $R_c(T_{\min})$ extracted in such a manner from experimental data may significantly differ for different values of $T_{\min}$. This example is typical for the two- (and more) parameter scaling and demonstrates that the "nonuniversality" of the critical resistance of the SIT might be an artifact of the interpretation of the data obtained for finite temperatures.

It is also worth noting that in the case of preserved spin-rotational symmetry (realized in many SIT experiments), the RG flow includes an extra dimension corresponding to the triplet coupling γ_t. In this situation, depending on the initial parameters, the SIT fixed point at $\rho_* \sim 1$ in the three-dimensional parameter space can be reached both from above and from below, thus leading to different conclusions on the value of R_c obtained at finite $T_{\min}$ in different samples or settings. Moreover, the extra dimension in the phase diagram in this case might result in a nonmonotonic temperature dependence of the resistivity at the SIT, as observed in some experiments.

Let us emphasize that the phase diagram in Fig. 19 is obtained within the framework of the so-called "fermionic mechanism" of the SIT (associated to the works by Finkel'stein [32,42,47]). There is a popular misconception in literature stating that, contrary to the "bosonic mechanism" [33,88]

yielding $\rho_* \sim 1$, the fermionic mechanism predicts $\rho_* \ll 1$ for a system with the Coulomb interaction. Our analysis demonstrates that this is not so: the SIT within the "fermionic mechanism" is governed by a fixed point with the critical resistivity $\rho_* \sim 1$. The confusion might arise if one neglects localization effects (due to interference and interactions) in the analysis of T_c as in Refs. [32,47]. Indeed, for very weak disorder ($t_0 \ll \gamma_{c0}^2$), the renormalization of t is negligible, see Figs. 1 and 9, where the red SC curves appear to be almost horizontal for small t_0. However, with increasing disorder and approaching the separatrix ($t_0 \propto \gamma_{c0}^2 \ll 1$), the red SC curves become more and more pushed into the region of $\rho \sim 1$ at low temperatures, and the critical resistance R_c is of the order of R_q. In other words, the temperature dependence of the resistivity for SC curves close to the transition reaches at the maximum a value $\sim R_q$ before dropping down with further lowering of the temperature. This is very well illustrated by the resistivity plots in the present paper. We thus reiterate that both fermionic and bosonic mechanisms predict the SIT governed by a fixed point at $\rho_* \sim 1$.

VIII. SUMMARY AND CONCLUSIONS

To summarize, in this paper, we have explored by means of the RG approach the interplay of superconductivity, interaction, and localization in 2D quantum systems. The focus has been put on the SIT in thin films. Our main results are as follows.

(1) Within the nonlinear sigma model formalism, we have derived the *full set of one-loop* (in disorder strength $t \ll 1$) *RG equations* for a 2D disordered interacting system, Eqs. (23)–(26). Formally, these RG equations are valid for arbitrary interaction couplings, including an arbitrary strong amplitude γ_c in the Cooper channel. The range of the applicability of one-loop RG equations has been identified as the domain $t \max\{1, |\gamma_c|\} \lesssim 1$: beyond this range, higher loops become important when approaching to the insulator $t = \infty$, or else, to the superconducting instability, $\gamma_c = -\infty$.

(2) We have employed the RG framework to explore the structure of the *phase diagram* at zero magnetic field. The analysis of RG equations has been performed for systems both with and without spin-orbit interaction (see Figs. 1, 2, 5, 7, 9, 11, and 13). Furthermore, the cases of the short-ranged and long-ranged Coulomb interactions have been investigated. In general, the phase diagram of a 2D disordered interacting system is determined by multi-parameter scaling and depends on the symmetry of the problem.

(3) The *enhancement of 2D superconductivity by the Anderson localization* [37] has been confirmed for the *short-range* case. We have identified the parameter regions where the superconductivity is enhanced by localization, both for the cases of preserved and broken spin-rotational symmetry (see Figs. 5, 7, and 13).

(4) In the case of preserved spin-rotational symmetry, the RG flow describes the three-parameter (for the Coulomb repulsion) or four-parameter (for the short-range repulsion) scaling, thus rendering the phase diagram multidimensional, with nontrivial fixed points appearing. In particular, a *ferromagnetic phase* develops with the metallic temperature behavior of the resistivity in a range of temperatures above the ferromagnetic instability (see Fig. 4). This behavior of resistivity in the ferromagnetic phase may be confused with a tendency to superconductivity in experiments.

(5) The presence of spin-orbit coupling (which removes the triplet interaction channel and converts weak localization into antilocalization) strongly affects the overall phase diagram. Two of this changes are fully expected. First, the spin-orbit coupling eliminates the ferromagnetic phase. Second, in the case of the short-range interaction, a supermetal phase emerges. What is much more intriguing, our results indicate that a *critical-metal phase* with resistivity of the order of resistance quantum R_q may arise (see Figs. 9 and 10). This phase bears certain similarity with a "Bose metal" phase, evidence for which has been found in some experiments.

(6) We have evaluated the *temperature dependence of the electrical resistivity*, $\rho(T)$, for given bare (high-temperature) couplings down to the lowest temperatures of the applicability of the one-loop RG approach. In this temperature range, the resistivity is dominated by the NLSM coupling t taken at the length scale L_T. At lower temperatures, in the close vicinity of T_c, the electric resistivity is controlled by contributions due to inelastic processes (which are not automatically included by the RG procedure but rather require an additional calculation once the RG has been stopped by temperature). These corrections lead to a strong suppression of $\rho(T)$ (see Fig. 14).

(7) We have studied the *magnetoresistance near the SIT* (Sec. VI). Both orbital and Zeeman effects of the magnetic field have been included in the unifying RG scheme complemented by the analysis of fluctuation corrections near the superconducting transition. A *nonmonotonous magnetoresistance*, see Fig. 15, has been predicted, with a maximum near the critical field H_c, in agreement with experimental observations. The magnetoresistance becomes progressively stronger with lowering temperature and becomes giant as $T \to 0$, as also seen in experiments.

(8) We have further discussed in Sec. VII the *limitations and generalizations* of our approach as well as *comparison between our theory and experiments*. In particular, we have analyzed in detail how the screening of the Coulomb interaction by substrates with high dielectric constant and by external metallic gates can be taken into account within our framework (see Fig. 17).

(9) This consideration allowed us to *propose specific sample designs for experimental observation of the superconductivity enhancement*. Also, we argued that our results for enhancement of the superconductivity are in qualitative agreement with the experimental observations in layered material Li_xZrNCl.

(10) We have discussed the possible *overall structure of a generic SIT phase diagram* (see Fig. 19) and the implications of our findings for the experimental verification of the universality of this quantum phase transition (see Fig. 20). In particular, we have shown that, in contrast to a popular belief, both "fermionic" and "bosonic" mechanisms of the SIT have to do with the *fixed point characterized by* $R \sim R_q$.

Our findings are in a qualitative agreement with most of the experiments on 2D superconductivity in disordered films. In particular, our approach explains a seemingly nonuniversal behavior of the critical resistance R_c found experimentally in different systems. Further, the analysis of the RG equations in a magnetic field is in accord with the experimentally observed

nonmonotonic behavior of the magnetoresistance near the SIT.

The detailed analysis of the temperature dependence of the resistivity in the close vicinity of the "classical" (finite-T) superconducting phase transition governed by the Berezinskii-Kosterlitz-Thouless physics is a subject of future work [54]. The effect of disorder and interaction on the topological sector of the theory (vortices in the order-parameter phase) is expected to be increasingly more pronounced upon approaching the SIT. A related line of future research [54] is devoted to the study of the zero-T resistance of a disordered superconducting film as a function of the sample size. Further, the RG approach developed here will be employed for studying the local tunneling density of states (including its mesoscopic fluctuations) in the presence of superconducting correlations [45] as well as the fluctuations of the superconducting order parameter near the SIT, as measured in experiments. Finally, the role of strong local superconducting fluctuations in the physics on the insulating side of the SIT still requires further study.

ACKNOWLEDGMENTS

We thank T. Baturina, L. Dell'Anna, M. Feigel'man, A. Finkelstein, A. Frydman, V. Gantmakher, E. König, V. Kravtsov, A. Levchenko, J. Mannhart, I. Protopopov, R. Schneider, M. Skvortsov, C. Strunk, and K. Tikhonov for discussions. The work was funded by the Russian Science Foundation under the Grant No. 14-42-00044.

APPENDIX A: BACKGROUND FIELD RENORMALIZATION OF THE NONLINEAR SIGMA-MODEL ACTION

In this Appendix, we present details of the derivation of one-loop renormalization of the NLSM action (1) with the help of the background field renormalization. Let us separate the matrix field Q into the "fast" (Q) and "slow" ($Q_0 = T_0^{-1}\Lambda T_0$) modes as

$$Q \to T_0^{-1} Q T_0. \tag{A1}$$

We assume that the "fast" matrix field Q_{nm} has a nontrivial structure in the Matsubara space for frequencies $|n|,|m| < N_{\max}$, whereas the "slow" matrix field T_0 has a nontrivial structure only for smaller frequencies:

$$(T_0)_{nm} = \begin{cases} (T_0)_{nm}, & |n| \le n_{\max} \text{ and } |m| \le n_{\max}, \\ \delta_{nm}, & |n| \le n_{\max} \text{ or } |m| \le n_{\max}. \end{cases} \tag{A2}$$

In what follows, we assume that $N_{\max} \gg n_{\max} \gg 1$.

It is convenient to rewrite the sum of interacting terms $S_{\rm int}^{(\rho)}$, $S_{\rm int}^{(\sigma)}$, and $S_{\rm int}^{(c)}$ in NLSM (1) as

$$S_{\rm int} = -\frac{\pi T}{4} \sum_{\alpha n} \sum_{r,j} \int d\boldsymbol{r}\, \Gamma_{rj}\, \mathrm{Tr}\left[J^{\alpha}_{n,rj} Q\right] \mathrm{tr}\left[J^{\alpha}_{n,rj} Q\right], \tag{A3}$$

where

$$J_{n,rj} = \begin{cases} I_n t_{rj}, & r = 0,3,\ j = 0,1,2,3, \\ L_n t_{rj}, & r = 1,2,\ j = 0,1,2,3. \end{cases} \tag{A4}$$

and

$$\Gamma_{r0} = (-1)^r \Gamma_s, \quad \Gamma_{rj} = -(-1)^r \Gamma_t, \quad r = 0,3, \quad j = 1,2,3,$$
$$\Gamma_{r0} = \Gamma_c, \quad \Gamma_{rj} = 0, \quad r = 1,2, \quad j = 1,2,3. \tag{A5}$$

The effective action for the slow Q_0 field is given by

$$S_{\rm eff}[Q_0] = \ln \int \mathcal{D}[Q] \exp S\left[T_0^{-1} Q T_0\right] \tag{A6}$$

with

$$S\left[T_0^{-1} Q T_0\right] = S[Q_0] + S[Q] + O_\sigma + O_{\rm int} + O_\eta, \tag{A7}$$

where

$$\begin{aligned} O_\sigma &= O_\sigma^{(1)} + O_\sigma^{(2),1} + O_\sigma^{(2),2}, \\ O_{\rm int} &= O_{\rm int}^{(1),1} + O_{\rm int}^{(1),2} + O_{\rm int}^{(2),1} + O_{\rm int}^{(2),2}. \end{aligned} \tag{A8}$$

Here we introduce the following terms ($\delta Q = Q - \Lambda$):

$$\begin{aligned} O_\sigma^{(1)} &= -\frac{g}{8} \int d\boldsymbol{r}\, \mathrm{Tr}\, \boldsymbol{A} \delta Q \nabla \delta Q, \\ O_\sigma^{(2),1} &= -\frac{g}{8} \int d\boldsymbol{r}\, \mathrm{Tr}\, \boldsymbol{A} \delta Q \boldsymbol{A} \Lambda, \\ O_\sigma^{(2),2} &= -\frac{g}{16} \int d\boldsymbol{r}\, \mathrm{Tr}\, \boldsymbol{A} \delta Q \boldsymbol{A} \delta Q, \\ O_{\rm int}^{(1),1} &= -\frac{\pi T}{2} \sum_{\alpha n} \sum_{r,j} \int d\boldsymbol{r}\, \Gamma_{rj}\, \mathrm{Tr}\left[J^{\alpha}_{n,rj} \delta Q\right] \mathrm{tr}\left[J^{\alpha}_{n,rj} Q_0\right], \\ O_{\rm int}^{(1),2} &= -\frac{\pi T}{2} \sum_{\alpha n} \sum_{r,j} \int d\boldsymbol{r}\, \Gamma_{rj}\, \mathrm{Tr}\left[J^{\alpha}_{n,rj} \delta Q\right] \mathrm{tr}\left[A^{\alpha}_{n,rj} \delta Q\right], \\ O_{\rm int}^{(2),1} &= -\frac{\pi T}{2} \sum_{\alpha n} \sum_{r,j} \int d\boldsymbol{r}\, \Gamma_{rj}\, \mathrm{Tr}\left[J^{\alpha}_{n,rj} Q_0\right] \mathrm{tr}\left[A^{\alpha}_{n,rj} \delta Q\right], \\ O_{\rm int}^{(2),2} &= -\frac{\pi T}{4} \sum_{\alpha n} \sum_{r,j} \int d\boldsymbol{r}\, \Gamma_{rj}\, \mathrm{Tr}\left[A^{\alpha}_{n,rj} \delta Q\right] \mathrm{tr}\left[A^{\alpha}_{n,rj} \delta Q\right], \\ O_\eta &= 4\pi T Z_\omega \int d\boldsymbol{r}\, \mathrm{tr}\, A_\eta \delta Q, \end{aligned} \tag{A9}$$

where

$$\boldsymbol{A} = T_0 \nabla T_0^{-1}, \quad A_\eta = T_0[\eta, T_0^{-1}], \quad A^{\alpha}_{n,rj} = T_0\left[J^{\alpha}_{n,rj}, T_0^{-1}\right]. \tag{A10}$$

In the one-loop approximation, the effective action $S_{\rm eff}[Q_0]$ can be obtained by expansion of $S[T_0^{-1} Q T_0]$ to the second order in A_η and $A^{\alpha}_{n;rj}$. Then, we find

$$\begin{aligned} S_{\rm eff}[Q_0] = S[Q_0] &+ \langle O_\sigma \rangle + \langle O_{\rm int} \rangle + \langle O_\eta \rangle \\ &+ \tfrac{1}{2} \langle (O_\sigma + O_{\rm int} + O_\eta)^2 \rangle, \end{aligned} \tag{A11}$$

where the average $\langle \dots \rangle$ is taken with respect to action (1).

For the perturbative (in $1/g$) treatment of the correlations of the fast fields in Eq. (A11), we shall use the square-root parametrization of the fast fields:

$$Q = W + \Lambda \sqrt{1 - W^2}, \quad W = \begin{pmatrix} 0 & w \\ \bar{w} & 0 \end{pmatrix}. \tag{A12}$$

We adopt the following notations: $W_{n_1 n_2} = w_{n_1 n_2}$ and $W_{n_2 n_1} = \bar{w}_{n_2 n_1}$ with $n_1 \ge 0$ and $n_2 < 0$. The blocks w and $\bar{w}$ (in

Matsubara space) obey

$$\bar{w} = -Cw^T C, \quad w = -Cw^* C. \tag{A13}$$

The second equality here implies that in the expansion $w^{\alpha\beta}_{n_1 n_2} = \sum_{rj} (w^{\alpha\beta}_{n_1 n_2})_{rj} t_{rj}$ some of the elements $(w^{\alpha\beta}_{n_1 n_2})_{rj}$ are real and some are purely imaginary.

Expanding the NLSM action (1) to the second order in W, we find the following propagators for diffusive modes. The propagators of diffusons ($r = 0,3$ and $j = 0,1,2,3$) read

$$\left\langle [w_{rj}(\boldsymbol{q})]^{\alpha_1\beta_1}_{n_1 n_2} [\bar{w}_{rj}(-\boldsymbol{q})]^{\beta_2\alpha_2}_{n_4 n_3} \right\rangle = \frac{2}{g} \delta^{\alpha_1\alpha_2} \delta^{\beta_1\beta_2} \delta_{n_{12},n_{34}} \mathcal{D}_q(i\Omega^{\varepsilon}_{12}) \left[\delta_{n_1 n_3} - \frac{32\pi T \Gamma_j}{g} \delta^{\alpha_1\beta_1} \mathcal{D}^{(j)}_q(i\Omega^{\varepsilon}_{12}) \right], \tag{A14}$$

where $\Omega^{\varepsilon}_{12} = \varepsilon_{n_1} - \varepsilon_{n_2} = 2\pi T n_{12} = 2\pi T(n_1 - n_2)$. The standard diffuson propagator is given as

$$\mathcal{D}^{-1}_q(i\omega_n) = q^2 + 16 Z_\omega |\omega_n|/g. \tag{A15}$$

The diffusons renormalized by interaction in the singlet [$\mathcal{D}^{(0)}_q(\omega) \equiv \mathcal{D}^s_q(\omega)$] and triplet [$\mathcal{D}^{(1)}_q(\omega) = \mathcal{D}^{(2)}_q(\omega) = \mathcal{D}^{(3)}_q(\omega) \equiv \mathcal{D}^t_q(\omega)$] particle-hole channels are as follows:

$$\begin{aligned} \left[\mathcal{D}^s_q(i\omega_n)\right]^{-1} &= q^2 + 16(Z_\omega + \Gamma_s)|\omega_n|/g, \\ \left[\mathcal{D}^t_q(i\omega_n)\right]^{-1} &= q^2 + 16(Z_\omega + \Gamma_t)|\omega_n|/g. \end{aligned} \tag{A16}$$

The propagators of singlet cooperon modes ($r = 1,2$ and $j = 0$) can be written as

$$\left\langle [w_{r0}(\boldsymbol{q})]^{\alpha_1\beta_1}_{n_1 n_2} [\bar{w}_{r0}(-\boldsymbol{q})]^{\beta_2\alpha_2}_{n_4 n_3} \right\rangle = \frac{2}{g} \delta^{\alpha_1\alpha_2} \delta^{\beta_1\beta_2} \delta_{n_{14},n_{32}} \mathcal{C}_q\left(i\Omega^{\varepsilon}_{12}\right) \left[\delta_{n_1 n_3} - \frac{64\pi T z}{g} \delta^{\alpha_1\beta_1} \mathcal{C}_q\left(i\Omega^{\varepsilon}_{34}\right) \mathcal{L}_q(i\mathcal{E}_{12}) \right], \tag{A17}$$

where $\mathcal{E}_{12} = \varepsilon_{n_1} + \varepsilon_{n_2}$, $\mathcal{C}_q(i\omega_n) \equiv \mathcal{D}_q(i\omega_n)$, and the fluctuation propagator ($\gamma_c = \Gamma_c/Z_\omega$)

$$\mathcal{L}^{-1}_q(i\omega_n) = \gamma_c^{-1} + \ln\frac{\Lambda}{4\pi T} - \psi\left(\frac{Dq^2 + |\omega_n| + \Lambda'}{4\pi T} + \frac{1}{2}\right) + \psi\left(\frac{1}{2}\right). \tag{A18}$$

Here, $D = g/(16Z_\omega)$ stands for the diffusion coefficient, $\psi(z)$ denotes the digamma function, and $\Lambda = 4\pi T N_{\max}$ ($\Lambda' = 4\pi T n_{\max}$) determines the ultraviolet (infrared) for the fast modes. The propagators of triplet cooperons ($r = 1,2$ and $j = 1,2,3$) are insensitive to the interaction and are as follows:

$$\left\langle [w_{rj}(\boldsymbol{q})]^{\alpha_1\beta_1}_{n_1 n_2} [\bar{w}_{rj}(-\boldsymbol{q})]^{\beta_2\alpha_2}_{n_4 n_3} \right\rangle = \frac{2}{g} \delta^{\alpha_1\alpha_2} \delta^{\beta_1\beta_2} \delta_{n_1 n_3} \delta_{n_2 n_4} \mathcal{C}_q\left(i\Omega^{\varepsilon}_{12}\right). \tag{A19}$$

In general, each term in the right-hand side of Eq. (A11) produces contributions that cannot be expressed in terms of Q_0 only. However, all such contributions cancel in the total expression (A11). Therefore we will not list them below. Expanding δQ in series of W according to Eq. (A12) and performing averaging with the help of Eqs. (A14) and (A17), we obtain the action (1) for the slow field Q_0 but with

$$\begin{aligned} g(\Lambda) &\to g(\Lambda') = g(\Lambda) + \delta g, \\ \Gamma_{s,t,c}(\Lambda) &\to \Gamma_{s,t,c}(\Lambda') = \Gamma_{s,t,c}(\Lambda) + \delta\Gamma_{s,t,c}, \\ Z_\omega(\Lambda) &\to Z_\omega(\Lambda') = Z_\omega(\Lambda) + \delta Z_\omega. \end{aligned} \tag{A20}$$

The contributions $\delta g, \delta\Gamma_{s,t,c}$, and δZ_ω take into account the effect of integration over the fast modes from the ultraviolet energy scale Λ down to new ultraviolet scale Λ'.

Below we list the different nonzero contributions to $\delta g, \delta\Gamma_{s,t,c}$, and δZ_ω from each term in the right-hand side of Eq. (A11). We start from corrections to the conductance:

$$\left\langle O^{(2),1}_\sigma \right\rangle \to \delta g^{(2),1}_\sigma = 2 \int_{q,\omega_n} \left[2\mathcal{C}^2_q(i\omega_n)\mathcal{L}_q(i\omega_n) + \sum_{j=0}^{3} \gamma_j \mathcal{D}_q(i\omega_n)\mathcal{D}^{(j)}_q(i\omega_n) \right] \tag{A21}$$

and

$$\left\langle O^{(2),2}_\sigma \right\rangle \to \delta g^{(2),2}_\sigma = -4 \int_q \mathcal{C}_q(0). \tag{A22}$$

Here we use the following notation:

$$\int_{q,\omega_n} \equiv \frac{2\pi T}{D} \sum_{n>0} \int \frac{d^2\boldsymbol{q}}{(2\pi)^2} \Theta(\Lambda - Dq^2 - |\omega_n|)\Theta(Dq^2 + |\omega_n| - \Lambda') \tag{A23}$$

and

$$\int_q \equiv \int \frac{d^2\boldsymbol{q}}{(2\pi)^2}\Theta(\Lambda - Dq^2)\Theta(Dq^2 - \Lambda'), \tag{A24}$$

where $\Theta(x)$ stands for the Heaviside step function. Next,

$$\left\langle O_{\rm int}^{(2),2} + \frac{1}{2}\left[O_{\rm int}^{(1),2}\right]^2 \right\rangle \to \delta g_{\rm int}^{(2),2} = -2\int_{q,\omega_n}\sum_{j=0}^{3}\gamma_j \mathcal{D}_q(i\omega_n)\mathcal{D}_q^{(j)}(i\omega_n)[1-2q^2\mathcal{D}_q(i\omega_n)] - 4\int_{q,\omega_n}\mathcal{L}_q(i\omega_n)\mathcal{C}_q^2(i\omega_n)[1-2q^2\mathcal{C}_q(i\omega_n)]. \tag{A25}$$

In total, we find

$$g(\Lambda') = g(\Lambda) - 4\int_q \mathcal{C}_q(0) + 4\int_{q,\omega_n} q^2\left[2\mathcal{C}_q^3(i\omega_n)\mathcal{L}_q(i\omega_n) + \sum_{j=0}^{3}\gamma_j\mathcal{D}_q^2(i\omega_n)\mathcal{D}_q^{(j)}(i\omega_n)\right]. \tag{A26}$$

The renormalization of Z_ω is described by the following terms:

$$\langle O_\eta\rangle \to \delta Z_\omega^\eta = \frac{2}{g}Z_\omega\int_{q,\omega_n}\left[2Z_\omega\mathcal{C}_q^2(i\omega_n)\mathcal{L}_q(i\omega_n) + \sum_{j=0}^{3}\Gamma_j\mathcal{D}_q(i\omega_n)\mathcal{D}_q^{(j)}(i\omega_n)\right], \tag{A27}$$

$$\left\langle O_{\rm int}^{(2),2} + \frac{1}{2}\left[O_{\rm int}^{(1),2}\right]^2\right\rangle \to \delta Z_\omega^{(2),2} = \frac{2}{g}\int_{q,\omega_n}\left\{\sum_{j=0}^{3}\Gamma_j\left[\mathcal{D}_q^{-1}(i\omega_n)\mathcal{D}_q^{(j)}(i\omega_n) - 1\right]\partial_n D_q(i\omega_n) + 2Z_\omega\mathcal{C}_q(i\omega_n)\partial_n\mathcal{L}_q(i\omega_n)\right\}, \tag{A28}$$

where $\partial_n f(i\omega_n) \equiv (g/16)\partial f/\partial\omega_n$. Combining Eqs. (A27) and (A28) together, we obtain

$$Z_\omega(\Lambda') = Z_\omega(\Lambda) + \frac{2}{g}(\Gamma_s + 3\Gamma_t)\int_{q,\omega_n}\mathcal{D}_q^2(i\omega_n) + \frac{4}{g}Z_\omega\int_{q,\omega_n}[\mathcal{C}_q(i\omega_n)\partial_n\mathcal{L}_q(i\omega_n) - \mathcal{L}_q(i\omega_n)\partial_n\mathcal{C}_q(i\omega_n)]. \tag{A29}$$

The corrections to the interaction amplitude Γ_s are as follows:

$$\left\langle O_{\rm int}^{(2),1}\right\rangle \to \delta\Gamma_{s,\rm int}^{(2),1} = \frac{4}{g}\Gamma_s\int_{q,\omega_n}\left[2Z_\omega\mathcal{C}_q^2(i\omega_n)\mathcal{L}_q(i\omega_n) + \sum_{j=0}^{3}\Gamma_j\mathcal{D}_q(i\omega_n)\mathcal{D}_q^{(j)}(i\omega_n)\right], \tag{A30}$$

$$\left\langle O_{\rm int}^{(2),2} + \frac{1}{2}\left[O_{\rm int}^{(1),2}\right]^2\right\rangle \to \delta\Gamma_{s,\rm int}^{(2),2} = -\frac{2}{g}(\Gamma_s + 3\Gamma_t)\int_q \mathcal{D}_q(0) - \frac{4}{g}Z_\omega\int_q \mathcal{C}_q(0)\mathcal{L}_q(0) - \frac{8}{g}Z_\omega\int_{q,\omega_n}\mathcal{C}_q^2(i\omega_n)\mathcal{L}_q^2(i\omega_n), \tag{A31}$$

$$\left\langle O_{\rm int}^{(1),1}O_{\rm int}^{(1),2}\right\rangle \to \delta\Gamma_{s,\rm int}^{(1),1;(1),2} = -\frac{4}{g}\Gamma_s\int_{q,\omega_n}\left[2Z_\omega\mathcal{C}_q^2(i\omega_n)\mathcal{L}_q(i\omega_n) + \sum_{j=0}^{3}\Gamma_j\mathcal{D}_q(i\omega_n)\mathcal{D}_q^{(j)}(i\omega_n)\right]. \tag{A32}$$

In total, we find

$$\Gamma_s(\Lambda') = \Gamma_s(\Lambda) - \frac{2}{g}(\Gamma_s + 3\Gamma_t)\int_q \mathcal{D}_q(0) - \frac{4}{g}Z_\omega\int_q \mathcal{C}_q(0)\mathcal{L}_q(0) - \frac{8}{g}Z_\omega^2\int_{q,\omega_n}\mathcal{C}_q^2(i\omega_n)\mathcal{L}_q^2(i\omega_n). \tag{A33}$$

The corrections to the interaction amplitude Γ_t can be listed as follows:

$$\left\langle O_{\rm int}^{(2),1}\right\rangle \to \delta\Gamma_{t,\rm int}^{(2),1} = \frac{4}{g}\Gamma_s\int_{q,\omega_n}\left[2Z_\omega\mathcal{C}_q^2(i\omega_n)\mathcal{L}_q(i\omega_n) + \sum_{j=0}^{3}\Gamma_j\mathcal{D}_q(i\omega_n)\mathcal{D}_q^{(j)}(i\omega_n)\right], \tag{A34}$$

$$\left\langle O_{\rm int}^{(2),2} + \frac{1}{2}\left[O_{\rm int}^{(1),2}\right]^2\right\rangle \to \delta\Gamma_{t,\rm int}^{(2),2} = -\frac{2}{g}(\Gamma_s - \Gamma_t)\int_q \mathcal{D}_q(0) + \frac{4}{g}Z_\omega\int_q \mathcal{C}_q(0)\mathcal{L}_q(0) - \frac{8}{g}\Gamma_t^2\int_{q,\omega_n}\mathcal{D}_q^{t2}(i\omega_n), \tag{A35}$$

$$\frac{1}{2}\left\langle\left[O_{\rm int}^{(1),1}\right]^2\right\rangle \to \delta\Gamma_{t,\rm int}^{(1),1;(1),1} = \frac{8}{g}\Gamma_t^2\int_{q,\omega_n}\left[\mathcal{D}_q^2(i\omega_n) - \mathcal{D}_q^{t2}(i\omega_n)\right] - \frac{8}{g}\Gamma_t^2\left(\frac{D}{4\pi T}\right)^2\int_{q,\omega_n}\mathcal{L}_q(i\omega_n)\psi''(\mathcal{X}_{q,i|\omega_n|}), \tag{A36}$$

$$\left\langle O_{\rm int}^{(1),1}O_{\rm int}^{(1),2}\right\rangle \to \delta\Gamma_{t,\rm int}^{(1),1;(1),2} = \frac{4}{g}\Gamma_t\int_{q,\omega_n}\left[2Z_\omega\mathcal{C}_q^2(i\omega_n)\mathcal{L}_q(i\omega_n) - \sum_{j=0}^{3}\Gamma_j\mathcal{D}_q(i\omega_n)\mathcal{D}_q^{(j)}(i\omega_n) + 4\Gamma_t\mathcal{D}_q^{t2}(i\omega_n)\right]. \tag{A37}$$

Here, $\mathcal{X}_{q,i|\omega_n|} = (Dq^2 + |\omega_n| + \Lambda')/(4\pi T) + 1/2$. In total, we obtain

$$\Gamma_t(\Lambda') = \Gamma_t(\Lambda) - \frac{2}{g}(\Gamma_s - \Gamma_t)\int_q \mathcal{D}_q(0) + \frac{8}{g}\Gamma_t^2\int_{q,\omega_n}\mathcal{D}_q^2(i\omega_n) + \frac{4}{g}Z_\omega\int_q \mathcal{C}_q(0)\mathcal{L}_q(0)$$
$$+ \frac{16}{g}\Gamma_t Z_\omega\int_{q,\omega_n}\mathcal{L}_q(i\omega_n)\left[\mathcal{C}_q^2(i\omega_n) - \frac{\Gamma_t}{2z}\left(\frac{D}{4\pi T}\right)^2\psi''(\mathcal{X}_{q,i|\omega_n|})\right]. \tag{A38}$$

Finally, the corrections to the Cooper channel interaction amplitude Γ_c are given as

$$\left\langle O_{\rm int}^{(2),1}\right\rangle \to \delta\Gamma_{c,\rm int}^{(2),1} = \frac{4}{g}\Gamma_c\int_{q,\omega_n}\left[2Z_\omega\mathcal{C}_q^2(i\omega_n)\mathcal{L}_q(i\omega_n) + \sum_{j=0}^{3}\Gamma_j\mathcal{D}_q(i\omega_n)\mathcal{D}_q^{(j)}(i\omega_n)\right], \tag{A39}$$

$$\left\langle O_{\rm int}^{(2),2} + \frac{1}{2}\left[O_{\rm int}^{(1),2}\right]^2\right\rangle \to \delta\Gamma_{c,\rm int}^{(2),2} = -\frac{2}{g}(\Gamma_s - 3\Gamma_t)\int_q \mathcal{D}_q(0) - \frac{2}{g}\Gamma_s Z_\omega\int_{q,\omega_n}\mathcal{D}_q^{-1}(i\omega_n)\mathcal{D}_q^{(s)}(i\omega_n)\mathcal{L}_q(i\omega_n)\left[\mathcal{D}_q^2(i\omega_n) + \mathcal{C}_q^2(i\omega_n)\right], \tag{A40}$$

$$\frac{1}{2}\left\langle\left[O_{\rm int}^{(1),1}\right]^2\right\rangle \to \delta\Gamma_{c,\rm int}^{(1),1;(1),1} = -\Gamma_c\mathcal{L}_{q=0}(i\omega_n = 0)\int_{\omega_m}\mathcal{C}_{q=0}(i\omega_m), \tag{A41}$$

$$\left\langle O_{\rm int}^{(1),1}O_{\rm int}^{(1),2}\right\rangle \to \delta\Gamma_{c,\rm int}^{(1),1;(1),2} = \frac{4}{g}\Gamma_c\left[-\mathcal{L}_{q=0}(i\omega_n = 0)\int_{\omega_m}\mathcal{C}_{q=0}(i\omega_m)\right]$$
$$\times\int_{q,\omega_n}\left[2Z_\omega\mathcal{C}_q^2(i\omega_n)\mathcal{L}_q(i\omega_n) + \sum_{j=0}^{3}\Gamma_j\mathcal{D}_q(i\omega_n)\mathcal{D}_q^{(j)}(i\omega_n)\right]. \tag{A42}$$

Here we introduce

$$\int_{\omega_n} \equiv \frac{2\pi T}{D}\sum_{n>0}\Theta(\Lambda - Dq^2 - |\omega_n|)\Theta(Dq^2 + |\omega_n| - \Lambda'). \tag{A43}$$

In total, we obtain

$$\Gamma_c(\Lambda') = \Gamma_c(\Lambda) + \Gamma_c\left[-\mathcal{L}_{q=0}(i\omega_n = 0)\int_{\omega_m}\mathcal{C}_{q=0}(i\omega_m)\right]\frac{4}{g}\int_{q,\omega_n}\left[2Z_\omega\mathcal{C}_q^2(i\omega_n)\mathcal{L}_q(i\omega_n) + \sum_{j=0}^{3}\Gamma_j\mathcal{D}_q(i\omega_n)\mathcal{D}_q^{(j)}(i\omega_n)\right]$$
$$- \frac{2}{g}(\Gamma_s - 3\Gamma_t)\int_q \mathcal{D}_q(0) - \frac{2}{g}\Gamma_s Z_\omega\int_{q,\omega_n}\mathcal{D}_q^{-1}(i\omega_n)\mathcal{D}_q^{(s)}(i\omega_n)\mathcal{L}_q(i\omega_n)\left[\mathcal{D}_q^2(i\omega_n) + \mathcal{C}_q^2(i\omega_n)\right]. \tag{A44}$$

We emphasize that Eqs. (A29) and (A33) implies that

$$Z_\omega(\Lambda') + \Gamma_s(\Lambda') = Z_\omega(\Lambda) + \Gamma_s(\Lambda) + \frac{4}{g}Z_\omega\int_{q,\omega_n}\mathcal{C}_q(i\omega_n)\mathcal{L}_q^2(i\omega_n)\left[\psi'(\mathcal{X}_{q,i|\omega_n|}) - \frac{4\pi T}{D}\mathcal{C}_q(i\omega_n)\right] = Z_\omega(\Lambda) + \Gamma_s(\Lambda). \tag{A45}$$

Here we employ the following relation: $\partial_n\mathcal{L}_q(i\omega_n) = [D/(4\pi T)]\mathcal{L}_q^2(i\omega_n)\psi'(\mathcal{X}_{q,i|\omega_n|})$. Also since $\Lambda' \gg 4\pi T$, we use that $\psi'(\mathcal{X}_{q,i|\omega_n|}) \approx (4\pi T/D)\mathcal{C}_q(i\omega_n)$.

The one-loop renormalization of the parameters of the NLSM action obtained from the background field procedure can be summarized as follows:

$$g(\Lambda') = g(\Lambda) - 4\int_q \mathcal{C}_q(0) + 4\int_{q,\omega_n} q^2\left[2\mathcal{C}_q^3(i\omega_n)\mathcal{L}_q(i\omega_n) + \sum_{j=0}^{3}\gamma_j\mathcal{D}_q^2(i\omega_n)\mathcal{D}_q^{(j)}(i\omega_n)\right], \tag{A46}$$

$$Z_\omega(\Lambda') = Z_\omega(\Lambda) + \frac{2}{g}(\Gamma_s + 3\Gamma_t)\int_{q,\omega_n}\mathcal{D}_q^2(i\omega) + \frac{4Z_\omega}{g}\int_{q,\omega_n}\mathcal{C}_q^2(i\omega_n)\left[\mathcal{L}_q^2(i\omega_n) + \mathcal{L}_q(i\omega_n)\right], \tag{A47}$$

$$\Gamma_s(\Lambda') = \Gamma_s(\Lambda) - \frac{2}{g}(\Gamma_s + 3\Gamma_t)\int_{q,\omega_n}\mathcal{D}_q^2(i\omega) - \frac{4Z_\omega}{g}\int_{q,\omega_n}\mathcal{C}_q^2(i\omega_n)\left[\mathcal{L}_q^2(i\omega_n) + \mathcal{L}_q(i\omega_n)\right], \tag{A48}$$

$$\Gamma_t(\Lambda') = \Gamma_t(\Lambda) - \frac{2}{g}\left(\Gamma_s - \Gamma_t - 4\frac{\Gamma_t^2}{Z_\omega}\right)\int_{q,\omega_n}\mathcal{D}_q^2(i\omega_n) + \frac{4}{g}\left(Z_\omega + 4\Gamma_t + \frac{2\Gamma_t^2}{Z_\omega}\right)\int_{q,\omega_n}\mathcal{C}_q^2(i\omega + n)\mathcal{L}_q(i\omega_n)$$
$$- \frac{4}{gD}\int_{q,\omega_n}\mathcal{C}_q^2(i\omega_n)\mathcal{L}_q^2(i\omega_n), \tag{A49}$$

and

$$\Gamma_c(\Lambda')=\Gamma_c(\Lambda)-\frac{\Gamma_c^2}{Z_\omega}\int_{\omega_n}\mathcal{C}_{q=0}(i\omega_n)-\frac{2}{g}(\Gamma_s-3\Gamma_t)\int_{q,\omega_n}\mathcal{D}_q^2(i\omega_n)+\frac{8\Gamma_c}{g}\int_{q,\omega_n}\mathcal{C}_q^2(i\omega_n)\mathcal{L}_q(i\omega_n)+\frac{12\Gamma_t\Gamma_c}{gZ_\omega}\int_{q,\omega_n}\mathcal{D}_q(i\omega_n)\mathcal{D}_q^t(i\omega_n). \tag{A50}$$

To derive RG equations from Eqs. (A46)–(A50), we choose $\Lambda'=\Lambda+d\Lambda$. Then, provided $d\Lambda/\Lambda$ corresponds to $-2dL/L$ we obtain RG equations (18)–(22).

APPENDIX B: ENHANCEMENT OF T_c IN THE CASE OF WEAK SHORT-RANGED INTERACTION

1. Orthogonal symmetry class

Expanding RG equations (23)–(26) with $n=3$ to the lowest order in interactions $\gamma_{s,t,c}$, we find

$$\frac{dt}{dy}=t^2,\quad \frac{d}{dy}\begin{pmatrix}\gamma_s\\ \gamma_t\\ \gamma_c\end{pmatrix}=-\frac{t}{2}\mathcal{R}_o\begin{pmatrix}\gamma_s\\ \gamma_t\\ \gamma_c\end{pmatrix}-\begin{pmatrix}0\\ 0\\ 2\gamma_c^2\end{pmatrix}. \tag{B1}$$

Here, within our accuracy, we neglect the interaction corrections to t in comparison with weak-localization correction. The matrix

$$\mathcal{R}_o=\begin{pmatrix}1 & 3 & 2\\ 1 & -1 & -2\\ 1 & -3 & 0\end{pmatrix} \tag{B2}$$

has the following eigenvalues and eigenvectors:

$$\lambda=-4:\begin{pmatrix}-1\\ 1\\ 1\end{pmatrix};\quad \lambda'=2:\begin{pmatrix}1\\ 1\\ -1\end{pmatrix}\text{ and }\begin{pmatrix}1\\ -1\\ 2\end{pmatrix}. \tag{B3}$$

If the γ_c^2 term is neglected, the solution of the linear system (B1) approaches the eigenvector with $\lambda=-4$, i.e., interaction parameters tends to the BCS line $-\gamma_s=\gamma_t=\gamma_c$. Let us expand the vector formed by $\gamma_{s,t,c}$ in eigenvectors (B3):

$$\begin{pmatrix}\gamma_s\\ \gamma_t\\ \gamma_c\end{pmatrix}=\begin{pmatrix}-1 & 1 & 1\\ 1 & 1 & -1\\ 1 & -1 & 2\end{pmatrix}\begin{pmatrix}a\\ b\\ c\end{pmatrix}. \tag{B4}$$

Transforming the set of equations (B1) to the new variables a,b, and c, we get

$$\begin{aligned}\frac{dt}{dy}&=t^2,\\ \frac{da}{dy}&=2ta-\frac{2}{3}(a-b+2c)^2,\\ \frac{db}{dy}&=-tb,\\ \frac{dc}{dy}&=-tc-\frac{2}{3}(a-b+2c)^2.\end{aligned} \tag{B5}$$

Equations (B5) are supplemented by the following initial conditions: $t(0)=t_0$, $a(0)=a_0$, $b(0)=b_0$, and $c(0)=c_0$, where

$$\begin{pmatrix}a_0\\ b_0\\ c_0\end{pmatrix}=\begin{pmatrix}-1/6 & 1/2 & 1/3\\ 1/2 & 1/2 & 0\\ 1/3 & 0 & 1/3\end{pmatrix}\begin{pmatrix}\gamma_{s,0}\\ \gamma_{t,0}\\ \gamma_{c,0}\end{pmatrix}. \tag{B6}$$

From Eq. (B5), it is easy to find

$$t(y)=\frac{t_0}{1-t_0y},\quad b(y)=b_0(1-t_0y)\equiv b_0\frac{t_0}{t}. \tag{B7}$$

Since b decreases upon RG flow, it is not important and we neglect it in the future analysis.

Equations for the remaining two variables, a and c are coupled. If the quadratic term is neglected, then a increases and c decreases. This suggests that c can be neglected. This is confirmed by a more careful analysis which shows that, although on the very last interval of RG "time" y the variable c starts to increase and becomes of the same order as a (i.e., of order unity), this weakly affect the RG scale at which this happens (i.e., the temperature of the superconducting transition). Thus we neglect c in what follows.

We can now easily solve the remaining equation for a. We assume the starting value a_0 to be negative (which means that there is attraction in the Cooper channel that is supposed to lead to the superconductivity), $a=-|a|$. This is, in particular, the case when $\gamma_{c,0}$ is the dominant coupling and $\gamma_{c,0}<0$. Then the equation reads

$$\frac{d|a|}{dy}=2t|a|+\frac{2}{3}a^2. \tag{B8}$$

Solving this equation, we obtain

$$a(y)=-\left(\frac{t_0^2}{|a_0|t^2}+\frac{2t_0}{3t^2}-\frac{2}{3t}\right)^{-1}. \tag{B9}$$

Let us analyze the result obtained. Let us first assume that $|a_0|\ll t_0$. Then the second term in brackets in the right-hand side of (B9) is small compared to the first one and can be neglected,

$$a^{-1}(y)=-\frac{1}{t}\left(\frac{t_0^2}{|a_0|t}-\frac{2}{3}\right). \tag{B10}$$

With increasing RG scale y, the resistance t increases together with the interaction a. If t reaches first unity, we get an insulator; if $a\sim 1$ happens first, we get a superconductor. It is easy to see that the second possibility (superconductivity) is realized if $|a_0|\gg t_0^2$. Then at the point of divergence of a we have a resistance $t_*\simeq 3t_0^2/(2|a_0|)\ll 1$. This occurs at $y_*\simeq\frac{1}{t_0}-\frac{1}{t_*}$, i.e., we can estimate the temperature of superconducting transition as $T_c\sim\exp(-2y_*)$ yielding

$$T_c\sim\frac{1}{\tau}\exp\left\{-\frac{2}{t_0}\left[1-\frac{t_0}{t_*}\right]\right\}. \tag{B11}$$

Here the factor 2 in the exponent originates from a translation of the length scale into energy (temperature). Under the above assumption, $|a_0|\ll t_0$, the second term in square brackets in

the exponential of (B11) is just a small correction to the first one.

The transition temperature (B11) is much higher than the BCS temperature $T_c^{\rm BCS} = (1/\tau)e^{-1/|\gamma_{c,0}|}$, so that the superconductivity is strongly enhanced by disorder. The origin of the enhanced superconductivity is in the increase of $|a|$ governed by the eigenvalue $\lambda = -4$ of matrix $\mathcal{R}_o$, which yields the eigenvalue $-(t/2)\times(-4) = 2t$ of the linear part of the system in Eq. (B1). This is nothing but the anomalous multifractal exponent $-\Delta_2$ for this symmetry class [90]. (We have in mind the "weak multifractality" in 2D.) Therefore the (multi)fractality is the source of the enhancement of the superconductivity.

By solving (B5) with $b = 0$ and a given by Eq. (B10), one finds that although $|c|$ decreases initially, eventually with increasing the RG scale towards y_* it becomes of the order of unity: $|c(y_*)| \sim 1$. Therefore, to determine a precise value of t_*, one has to solve coupled equations for a and c [with $(b = 0)$].

If $|a_0| \ll t_0^2$, the resistance reaches unity before the interaction becomes strong, and the system is an insulator. Finally, if $|a_0| \gg t_0$, the disorder is not particularly important, and the transition temperature is given by usual clean BCS $T_c^{\rm BCS}$. In the latter case, neglecting b and c is not parametrically justified and leads to an incorrect numerical factor in the exponent.

For the initial values of interaction parameters used in the inset of Fig. 6, we find that $a_0 = -0.01$. Thus we expect the regime with $T_c \approx T_c^{\rm BCS}$ for $t_0 \ll |a_0| = 0.01$. In the range of t_0 between $|a_0| = 0.01$ and $\sqrt{|a_0|} = 0.1$, the transition occurs at $T_c \gg T_c^{\rm BCS}$. At $t_0 \sim \sqrt{|a_0|} = 0.1$ the superconductor-insulator transition is expected. The above crude analysis of RG equations linearized in interactions is in good agreement with the numerical solutions of full RG equations (23)–(26).

2. Symplectic symmetry class

Now we consider the symplectic symmetry class, i.e., assume that the spin symmetry is completely broken. Expanding Eqs. (23)–(26) with $n = 0$ to the lowest order in interactions $\gamma_{s,t,c}$, we obtain

$$\frac{dt}{dy} = -\frac{t^2}{2}, \quad \frac{d}{dy}\begin{pmatrix}\gamma_s\\ \gamma_c\end{pmatrix} = -\frac{t}{2}\mathcal{R}_s\begin{pmatrix}\gamma_s\\ \gamma_c\end{pmatrix} - \begin{pmatrix}0\\ 2\gamma_c^2\end{pmatrix}. \quad \text{(B12)}$$

Here we neglect interaction corrections to t in comparison with weak antilocalization. The matrix

$$\mathcal{R}_s = \begin{pmatrix}1 & 2\\ 1 & 0\end{pmatrix} \quad \text{(B13)}$$

has the following eigenvalues and eigenvectors:

$$\lambda = -1: \quad \begin{pmatrix}-1\\ 1\end{pmatrix}; \quad \lambda' = 2: \quad \begin{pmatrix}2\\ 1\end{pmatrix}. \quad \text{(B14)}$$

If the γ_c^2 term is neglected, the solution of the linear system in Eq. (B12) approaches the eigenvector with $\lambda = -1$, i.e., interaction amplitudes approach the BCS (in the absence of γ_t) line $\gamma_s = -\gamma_c$. As in the orthogonal case, we can expand the vector formed by $\gamma_{s,c}$ in the eigenvectors

$$\begin{pmatrix}\gamma_s\\ \gamma_c\end{pmatrix} = \begin{pmatrix}-1 & 2\\ 1 & 1\end{pmatrix}\begin{pmatrix}a\\ c\end{pmatrix}. \quad \text{(B15)}$$

Transforming the set of equations (B12) to the new variables a and c, we find

$$\begin{aligned}\frac{dt}{dy} &= -\frac{t^2}{2},\\ \frac{da}{dy} &= \frac{t}{2}a - \frac{4}{3}(a+c)^2,\\ \frac{dc}{dy} &= -tc - \frac{2}{3}(a+c)^2.\end{aligned} \quad \text{(B16)}$$

Equations (B16) are supplemented by the initial conditions: $t(0) = t_0$, $a(0) = a_0$ and $c(0) = c_0$, where

$$\begin{pmatrix}a_0\\ c_0\end{pmatrix} = \begin{pmatrix}-1/3 & 2/3\\ 1/3 & 1/3\end{pmatrix}\begin{pmatrix}\gamma_{s,0}\\ \gamma_{c,0}\end{pmatrix}. \quad \text{(B17)}$$

From the first of Eqs. (B16), we find

$$t(y) = \frac{t_0}{1 + yt_0/2}. \quad \text{(B18)}$$

Equations for two variables, a and c are coupled. If the quadratic term is neglected, then a increases and c decreases. At the later stage of RG, the quadratic terms lead to an enhancement of c. This suggests that c can be neglected for a qualitative analysis of RG equations (B16). We thus neglect c and keep only a (fully analogously to what we have done in the orthogonal case). The resulting equation for a reads

$$\frac{da}{dy} = \frac{t}{2}a - \frac{4}{3}a^2. \quad \text{(B19)}$$

We solve this equation with the result

$$a = \frac{1}{t}\left(\frac{1}{a_0 t_0} + \frac{4}{3t^2} - \frac{4}{3t_0^2}\right)^{-1}. \quad \text{(B20)}$$

Provided $a_0 < 0$, the superconducting instability is possible. The new, different from standard clean BCS behavior, emerges under the condition $|a_0| \ll t_0$. Then the condition $a \sim 1$ yields

$$t_* \simeq 2(|a_0|t_0/3)^{1/2} \ll t_0. \quad \text{(B21)}$$

By solving Eq. (B16) with a given by Eq. (B20), we find that although $|c|$ decreases initially, eventually with increasing RG scale it reaches a: $c \sim a$ at $t = t_*$. Therefore, to determine the precise value of t_*, one has to solve coupled equations for a and c.

Equation (B21) yields the following estimate for the transition temperature:

$$T_c \sim \frac{1}{\tau}e^{-2y_*} \sim e^{-4/t_*} \sim \exp\left(-\frac{\mathcal{C}}{\sqrt{|a_0|t_0}}\right) \gg T_c^{\rm BCS}. \quad \text{(B22)}$$

The constant $\mathcal{C}$ is of the order of unity and depends on ratio c_0/a_0. The clean BCS result is restored (up to small corrections) at $|a_0| \gg t_0$. For $a_0 < 0$ (or, equivalently, $\gamma_{c,0} < \gamma_{s,0}/2$), there is no transition to the supermetallic phase with increase of t_0.

As in the orthogonal case, the source of the enhancement of the superconducting temperature is in the first term on the right-hand side of Eq. (B19). The eigenvalue $t/2$ is the anomalous multifractal exponent $-\Delta_2$ for the symplectic symmetry class. Therefore, also in this case, the (multi)fractality is

the source of the enhancement of the superconductivity. This enhancement is less efficient than in the orthogonal case for two reasons, because of antilocalizing behavior that leads to a decrease of t and therefore weakening of multifractality.

[1] H. Kamerlingh Onnes, Comm. Phys. Lab. Univ. Leiden, Report Nos. 122b and 124c, 1911.

[2] J. Bardeen, L. N. Cooper, and J. R. Schrieffer, Phys. Rev. **108**, 1175 (1957).

[3] P. W. Anderson, Phys. Rev. **109**, 1492 (1958).

[4] D. B. Haviland, Y. Liu, and A. M. Goldman, Phys. Rev. Lett. **62**, 2180 (1989).

[5] K. A. Parendo, K. H. Sarwa, B. Tan, A. Bhattacharya, M. Eblen-Zayas, N. E. Staley, and A. M. Goldman, Phys. Rev. Lett. **94**, 197004 (2005).

[6] S. J. Lee and J. B. Ketterson, Phys. Rev. Lett. **64**, 3078 (1990).

[7] A. Yazdani and A. Kapitulnik, Phys. Rev. Lett. **74**, 3037 (1995).

[8] Y. Qin, C. L. Vicente, and J. Yoon, Phys. Rev. B **73**, 100505(R) (2006).

[9] A. F. Hebard and M. A. Paalanen, Phys. Rev. Lett. **65**, 927 (1990).

[10] G. Sambandamurthy, L. W. Engel, A. Johansson, and D. Shahar, Phys. Rev. Lett. **92**, 107005 (2004); G. Sambandamurthy, L. W. Engel, A. Johansson, E. Peled, and D. Shahar, *ibid.* **94**, 017003 (2005); D. Sherman, G. Kopnov, D. Shahar, and A. Frydman, *ibid.* **108**, 177006 (2012).

[11] B. Sacépé, T. Dubouchet, C. Chapelier, M. Sanquer, M. Ovadia, D. Shahar, M. Feigel'man, and L. Ioffe, Nat. Phys. **7**, 239 (2011).

[12] M. Mondal, A. Kamlapure, M. Chand, G. Saraswat, S. Kumar, J. Jesudasan, L. Benfatto, V. Tripathi, and P. Raychaudhuri, Phys. Rev. Lett. **106**, 047001 (2011); M. Chand, G. Saraswat, A. Kamlapure, M. Mondal, S. Kumar, J. Jesudasan, V. Bagwe, L. Benfatto, V. Tripathi, and P. Raychaudhuri, Phys. Rev. B **85**, 014508 (2012); G. Lemarié, A. Kamlapure, D. Bucheli, L. Benfatto, J. Lorenzana, G. Seibold, S. C. Ganguli, P. Raychaudhuri, and C. Castellani, *ibid.* **87**, 184509 (2013).

[13] T. I. Baturina, A. Y. Mironov, V. M. Vinokur, M. R. Baklanov, and C. Strunk, Phys. Rev. Lett. **99**, 257003 (2007); B. Sacépé, C. Chapelier, T. I. Baturina, V. M. Vinokur, M. R. Baklanov, and M. Sanquer, *ibid.* **101**, 157006 (2008); Nat. Commun. **1**, 140 (2010).

[14] T. I. Baturina, S. V. Postolova, A. Yu. Mironov, A. Glatz, M. R. Baklanov, and V. M. Vinokur, Europhys. Lett. **97**, 17012 (2012).

[15] A. M. Goldman and N. Markovic, Phys. Today **51**, 39 (1998); V. F. Gantmakher and V. T. Dolgopolov, Physics-Uspekhi **53**, 3 (2010); A. M. Goldman, Int. J. Mod. Phys. B **24**, 4081 (2010).

[16] A. D. Caviglia, S. Gariglio, N. Reyren, D. Jaccard, T. Schneider, M. Gabay, S. Thiel, G. Hammerl, J. Mannhart, and J.-M. Triscone, Nature (London) **456**, 624 (2008).

[17] J. A. Sulpizio, S. Ilani, P. Irvin, and J. Levy, Annu. Rev. Mater. Res. **44**, 117 (2014).

[18] M. Kim, Y. Kozuka, C. Bell, Y. Hikita, and H. Y. Hwang, Phys. Rev. B **86**, 085121 (2012).

[19] K. Ueno, T. Nojima, S. Yonezawa, M. Kawasaki, Y. Iwasa, and Y. Maeno, Phys. Rev. B **89**, 020508(R) (2014).

[20] J. T. Ye, Y. J. Zhang, R. Akashi, M. S. Bahramy, R. Arita, and Y. Iwasa, Science **338**, 1193 (2012); J. T. Ye, Y. J. Zhang, M. Yoshida, Y. Saito, and Y. Iwasa, J. Supercond. Nov. Magn. **27**, 981 (2014).

[21] K. Taniguchi, A. Matsumoto, H. Shimotani, and H. Takagi, Appl. Phys. Lett. **101**, 042603 (2012).

[22] R. Schneider, A. G. Zaitsev, D. Fuchs, and H. von Löhneysen, Phys. Rev. Lett. **108**, 257003 (2012); J. Low Temp. Phys. **178**, 118 (2014); J. Phys.: Condens. Matter **26**, 455701 (2014); Eur. Phys. J. B **88**, 14 (2015).

[23] A. T. Bollinger, G. Dubuis, J. Yoon, D. Pavuna, J. Misewich, and I. Bozovic, Nature (London) **472**, 458 (2011).

[24] Y. Taguchi, A. Kitora, and Y. Iwasa, Phys. Rev. Lett. **97**, 107001 (2006); Y. Taguchi, T. Kawabata, T. Takano, A. Kitora, K. Kato, M. Takata, and Y. Iwasa, Phys. Rev. B **76**, 064508 (2007); Y. Kasahara, T. Kishiume, T. Takano, K. Kobayashi, E. Matsuoka, H. Onodera, K. Kuroki, Y. Taguchi, and Y. Iwasa, Phys. Rev. Lett. **103**, 077004 (2009); H. Kotegawa, S. Oshiro, Y. Shimizu, H. Tou, Y. Kasahara, T. Kishiume, Y. Taguchi, and Y. Iwasa, Phys. Rev. B **90**, 020503(R) (2014).

[25] A. A. Abrikosov and L. P. Gorkov, Sov. Phys. JETP **8**, 1090 (1959); **9**, 220 (1959).

[26] P. W. Anderson, J. Phys. Chem. Solids **11**, 26 (1959).

[27] L. N. Bulaevskii and M. V. Sadovskii, JETP Lett. **39**, 640 (1984); J. Low Temp. Phys. **59**, 89 (1985); JETP Lett. **43**, 99 (1986); L. N. Bulaevskii, S. V. Panyukov, and M. V. Sadovskii, Sov. Phys. JETP **65**, 380 (1987).

[28] A. Kapitulnik and G. Kotliar, Phys. Rev. Lett. **54**, 473 (1985); M. Ma and P. A. Lee, Phys. Rev. B **32**, 5658 (1985); G. Kotliar and A. Kapitulnik, *ibid.* **33**, 3146 (1986).

[29] S. Maekawa and H. Fukuyama, J. Phys. Soc. Jpn. **51**, 1380 (1982); S. Maekawa, H. Ebisawa, and H. Fukuyama, *ibid.* **53**, 2681 (1984).

[30] P. W. Anderson, K. A. Muttalib, and T. V. Ramakrishnan, Phys. Rev. B **28**, 117 (1983).

[31] L. Coffey, K. A. Muttalib, and K. Levin, Phys. Rev. Lett. **52**, 783 (1984).

[32] A. M. Finkel'stein, *Electron Liquid in Disordered Conductors*, edited by I. M. Khalatnikov, Soviet Scientific Reviews Vol. 14 of (Harwood Academic, London, 1990).

[33] M. P. A. Fisher, Phys. Rev. Lett. **65**, 923 (1990); M. P. A. Fisher, G. Grinstein, and S. M. Girvin, *ibid.* **64**, 587 (1990); M.-C. Cha, M. P. A. Fisher, S. M. Girvin, M. Wallin, and A. P. Young, Phys. Rev. B **44**, 6883 (1991).

[34] P. Phillips and D. Dalidovich, Science **302**, 243 (2003).

[35] M. V. Feigel'man, L. B. Ioffe, V. E. Kravtsov, and E. A. Yuzbashyan, Phys. Rev. Lett. **98**, 027001 (2007).

[36] M. V. Feigel'man, L. B. Ioffe, V. E. Kravtsov, and E. Cuevas, Ann. Phys. **325**, 1390 (2010).

[37] I. S. Burmistrov, I. V. Gornyi, and A. D. Mirlin, Phys. Rev. Lett. **108**, 017002 (2012).

[38] V. E. Kravtsov, J. Phys.: Conf. Ser. **376**, 012003 (2012).

[39] D. Belitz and T. R. Kirkpatrick, Rev. Mod. Phys. **66**, 261 (1994).

[40] A. M. M. Pruisken, M. A. Baranov, and B. Škorić, Phys. Rev. B **60**, 16807 (1999).

[41] A. Kamenev and A. Andreev, Phys. Rev. B **60**, 2218 (1999).

[42] A. M. Finkelstein, Z. Phys. B **56**, 189 (1984).

[43] L. Dell'Anna, Phys. Rev. B **88**, 195139 (2013).

[44] M. A. Skvortsov and M. V. Feigel'man, Phys. Rev. Lett. **95**, 057002 (2005).
[45] I. S. Burmistrov, I. V. Gornyi, and A. D. Mirlin (unpublished).
[46] I. S. Burmistrov, I. V. Gornyi, and A. D. Mirlin, Phys. Rev. Lett. **111**, 066601 (2013); Phys. Rev. B **91**, 085427 (2015).
[47] A. M. Finkelstein, Physica B **197**, 636 (1994).
[48] M. I. D'yakonov and V. I. Perel', Sov. Phys. JETP **33**, 1053 (1971).
[49] S. Hikami, A. I. Larkin, and Y. Nagaoka, Progr. Theor. Phys. **63**, 707 (1980).
[50] C. Castellani and C. Di Castro, Phys. Rev. B **34**, 5935 (1986).
[51] T. R. Kirkpatrick and D. Belitz, Phys. Rev. B **41**, 11082 (1990).
[52] A. Punnoose and A. M. Finkelstein, Science **310**, 289 (2005).
[53] There is a subtle difference between the scaling with temperature and with the system size. At zero T, RG equations (23)–(26) describe the behavior of the system upon changing the system size L. The divergence of γ_c indicates establishing of the absolute value of superconducting order parameter on the length scale L_c. We note that both the total electrical resistance $\rho(L_c)$ and the NLSM coupling $t(L_c)$ which, in general, are different from each other due to the contribution of inelastic processes (see discussion in Sec. V), are finite. At scales $L > L_c$, the length-scale dependence of the (four-contact) resistance of a square sample is governed by the contribution of nontrivial configurations of the order parameter [54] (similar to the "quantum phase slips" in a quasi-one-dimensional systems). The resistance becomes zero only in the thermodynamic limit, $L = \infty$.
[54] E. König *et al.* (unpublished).
[55] In addition to fixed points that describe phases and transitions between them there is a nontrivial fixed point at $\gamma_c^* \approx -0.3$, $\gamma_t^* \approx 2.5$, $\gamma_s^* = -1$, and $t^* \approx 0.03$ (stable with respect to the γ_s direction). Since t^* is a parameterless number, the one-loop approximation is, strictly speaking, not sufficient for determining the couplings at this fixed point. However, the numerical smallness of the obtained value of t^* suggests that the one-loop RG is still reasonably well controlled near this fixed point. This fixed point is unstable in two directions and is located on the critical surface separating the superconducting and ferromagnetic phases. It resembles the Nishimori point in 2D random-bond Ising model [56]. The analysis of RG equations (30)–(32) in the vicinity of this fixed point suggests that it separates two fixed points on the critical surface that control the transitions between SC and FM phases. We expect that one such fixed point is situated in the strong coupling region whereas the other corresponds to a certain clean limit (cf. discussion in Ref. [39]). We will investigate this interesting possibility elsewhere.
[56] H. Nishimori, Prog. Theor. Phys. **66**, 1169 (1981); J. Phys. Soc. Jpn. **55**, 3305 (1986); Y. Ozeki and H. Nishimori, J. Phys. A: Math. Gen. **26**, 3399 (1993).
[57] Two-dimensional systems with strong spin-orbit interaction can be topologically protected from localization, when they appear as surface states of 3D topological insulators and superconductors [58]. In terms of the NLSM, such metallic states are described by an action with an additional topological term, see, e.g., Refs. [59]. The combined effect of disorder, Coulomb interaction, and topology in such system may lead to the emergence of a novel critical point [60] with $t \sim 1$, while no insulating phase appears. In this work, we do not consider 2D surfaces of 3D topological insulators and superconductors and relegate the discussion of the full phase diagrams for topologically protected systems (including graphene with superconducting islands [61]) to future work.
[58] M. Z. Hasan and C. L. Kane, Rev. Mod. Phys. **82**, 3045 (2010); X.-L. Qi and S.-C. Zhang, *ibid.* **83**, 1057 (2011); B. A. Bernevig and T. L. Hughes, *Topological Insulators and Topological Superconductors* (Princeton University Press, Princeton, 2013).
[59] E. J. König, P. M. Ostrovsky, I. V. Protopopov, I. V. Gornyi, I. S. Burmistrov, and A. D. Mirlin, Phys. Rev. B **88**, 035106 (2013); **90**, 165435 (2014).
[60] P. M. Ostrovsky, I. V. Gornyi, and A. D. Mirlin, Phys. Rev. Lett. **105**, 036803 (2010).
[61] Z. Han, A. Allain, H. Arjmandi-Tash, K. Tikhonov, M. Feigelman, B. Sacépé, and V. Bouchiat, Nat. Phys. **10**, 380 (2014).
[62] B. N. Narozhny, I. L. Aleiner, and A. I. Larkin, Phys. Rev. B **62**, 14898 (2000).
[63] H. Fukuyama, J. Phys. Soc. J. **51**, 1105 (1982).
[64] C. Castellani, C. Di Castro, G. Forgacs, and S. Sorella, Solid Stat. Commun. **52**, 261 (1984).
[65] M. Ma and E. Fradkin, Phys. Rev. Lett. **56**, 1416 (1986).
[66] A. M. Finkelstein, JETP Lett. **45**, 46 (1987).
[67] L. G. Aslamazov and A. I. Larkin, Sov. Phys. Solid State **10**, 875 (1968).
[68] K. Maki, Progr. Theor. Phys. **39**, 897 (1968).
[69] R. S. Thompson, Phys. Rev. B **1**, 327 (1970).
[70] A. I. Larkin and Yu. N. Ovchinnikov, J. Low Temp. Phys. **10**, 407 (1973); JETP **92**, 519 (2001).
[71] A. Levchenko, Phys. Rev. B **81**, 012507 (2010).
[72] A. Glatz, A. A. Varlamov, and V. M. Vinokur, Phys. Rev. B **84**, 104510 (2011).
[73] K. S. Tikhonov, G. Schwiete, and A. M. Finkelstein, Phys. Rev. B **85**, 174527 (2012).
[74] V. M. Galitski and A. I. Larkin, Phys. Rev. B **63**, 174506 (2001).
[75] G. Zala, B. N. Narozhny, and I. L. Aleiner, Phys. Rev. B **64**, 201201(R) (2001); **65**, 020201(R) (2001).
[76] M. Khodas, A. Levchenko, and G. Catelani, Phys. Rev. Lett. **108**, 257004 (2012).
[77] S. Sachdev, *Quantum Phase Transitions* (Cambridge University Press, Cambridge, 2011); M. Vojta and S. Sachdev, Adv. Solid State Phys. **41**, 329 (2001).
[78] D. V. Khveshchenko, A. G. Yashenkin, and I. V. Gornyi, Phys. Rev. Lett. **86**, 4668 (2001); J. S. Meyer, I. V. Gornyi, and A. Altland, *ibid.* **90**, 107001 (2003); Int. J Mod. Phys. B **18**, 949 (2004); L. Dell'Anna, Nucl. Phys. B **758**, 255 (2006).
[79] A. G. Yashenkin, W. A. Atkinson, I. V. Gornyi, P. J. Hirschfeld, and D. V. Khveshchenko, Phys. Rev. Lett. **86**, 5982 (2001); A. Altland, Phys. Rev. B **65**, 104525 (2002); A. Altland, B. D. Simons, and M. R. Zirnbauer, Phys. Rep. **359**, 283 (2002).
[80] M. R. Beasley, J. E. Mooij, and T. P. Orlando, Phys. Rev. Lett. **42**, 1165 (1979).
[81] B. I. Halperin and D. R. Nelson, J. Low Temp. Phys. **36**, 599 (1979).
[82] A. T. Fiory, A. F. Hebard, and W. I. Glaberson, Phys. Rev. B **28**, 5075 (1983); A. M. Kadin, K. Epstein, and A. M. Goldman,

ibid. **27**, 6691 (1983); J. W. P. Hsu and A. Kapitulnik, *ibid.* **45**, 4819 (1992); L. Benfatto, C. Castellani, and T. Giamarchi, *ibid.* **80**, 214506 (2009).

[83] L. A. Ponomarenko, A. K. Geim, A. A. Zhukov, R. Jalil, S. V. Morozov, K. S. Novoselov, V. V. Cheianov, V. I. Fal'ko, K. Watanabe, T. Taniguchi, and R. V. Gorbachev, Nat. Phys. **7**, 958 (2011).

[84] M. S. Osofsky, R. J. Soulen, Jr., J. H. Claassen, G. Trotter, H. Kim, and J. S. Horwitz, Phys. Rev. Lett. **87**, 197004 (2001).

[85] I.-D. Potirniche, J. Maciejko, R. Nandkishore, and S. L. Sondhi, Phys. Rev. B **90**, 094516 (2014).

[86] J. Mayoh and A. M. García-García, arXiv:1412.0029.

[87] N. Trivedi, R. T. Scalletar, and M. Randeria, Phys. Rev. B **54**, R3756 (1996); K. Bouadim, Y. L. Loh, M. Randeria, and N. Trivedi, Nat. Phys. **7**, 884 (2011).

[88] C. Chamon and C. Nayak, Phys. Rev. B **66**, 094506 (2002).

[89] Wang Qing-Yan *et al.*, Chinese Phys. Lett. **29**, 037402 (2012); Defa Liu *et al.*, Nature Comm. **3**, 931 (2012); Shaolong He *et al.*, Nature Mat. **12**, 605 (2013); Shiyong Tan *et al.*, *ibid.* **12**, 634 (2013); Zhang Wen-Hao *et al.*, Chinese Phys. Lett. **31**, 017401 (2014).

[90] D. Höf and F. Wegner, Nucl. Phys. B **275**, 561 (1986); F. Wegner, *ibid.* **280**, 193 (1987); **280**, 210 (1987).